The Design, Synthesis, and Evaluation of Radiopharmaceuticals for Actinium-225

by

Victoria Brown

B.Sc., McMaster University, 2019

Thesis Submitted in Partial Fulfillment of the
Requirements for the Degree of
Master of Science

in the
Department of Chemistry
Faculty of Science

SIMON FRASER UNIVERSITY
Fall 2021

Declaration of Committee

Name:	**Victoria Brown**
Degree:	**Master of Science (Chemistry)**
Title:	**The Design, Synthesis, and Evaluation of Radiopharmaceuticals for Actinium-225**
Committee:	**Chair:** **Hua-Zhong Yu** Professor, Chemistry
	Caterina Ramogida Supervisor Assistant Professor, Chemistry
	Tim Storr Committee Member Professor, Chemistry
	Rob Britton Committee Member Professor, Chemistry
	Corina Andreoiu Examiner Professor, Chemistry

Abstract

This thesis studies the design, synthesis, and optimization of radiopharmaceuticals for targeted alpha therapy applications with actinium-225 (^{225}Ac). In Chapter 2, three novel radiopharmaceuticals - **2.1** (DOTA-CCZ-N-Me-α-CycMSH), **2.2** (Macropa-CCZ-N-Me-α-CycMSH), and **2.6** (Macropa-α-CycMSH) for malignant melanoma therapy were labeled with ^{225}Ac and evaluated. All three radiopharmaceuticals exhibited excellent *in vitro* stability, while Macropa-CCZ-N-Me-α-CycMSH showed lower tumor uptake and moderate normal tissue uptake. In Chapter 3, a total of 5 diaza-18-crown-6 macrocyclic ligands (macropa, macropaquin, macroquin-SO_3, macrohopo, and macrohopo′) as chelators for ^{225}Ac were investigated. Two of the chelators (macrohopo and macrohopo′) which contain hydroxypyridinone pendant donor arms are novel and were synthesized/characterized in this work. Macropaquin was able to quantitively radiolabel at chelator concentrations as low as 10^{-6} M at ambient temperatures within one hour, while chelator macrohopo was unable to achieve ^{225}Ac complexation under any conditions. This thesis showcases the complexity of radiopharmeticuals, in particular for ^{225}Ac.

Keywords: Actinium-225; targeted alpha therapy (TAT); α-CycMSH; hydroxypyridinone (HOPO) groups; macrocyclic ligands

Acknowledgements

First I must acknowledge my supervisor Dr. Caterina F. Ramogida for her continuous support and guidance over the course of my Masters. Thank you for your encouragement, understanding, and patience these past two years – it made a big impact on my life and made my masters more enjoyable.

I would also like to acknowledge all my group members – past and present. It has been a great pleasure to work with you. In particular, I'd like to thank Dr. Anthony W. McDonagh for your patience and eagerness to teach organic chemistry, general lab tips/tricks, and willingness to talk about mental health. To my fellow female lab mates Parmissa, Lexi, Imma, Karla, and Brooke for all your support, friendships, and guidance.

To all the collaborators who made this work possible, I'd like to say thank you. Dr. Chengcheng Zhang at BCCA for the radiotracers and peptide. Dr. Justin J. Wilson and his group at Cornell University (Aohan Hu & David J. Fiszbein) for continued collaborations. Dr. Cristina Rodríguez-Rodríguez for help and guidance with the biodistribution studies. Members of the Orvig Group at UBC (Luke Wharton, Lily Southcott, and Aidan Ingham) for support with various radiometal radiolabeling. I'd like to acknowledge the helpful staff at TRIUMF which made radiolabeling possible. Thank you to SFU for the BCGS, NSERC-CGSM, graduate fellowship, and Dupont entrance scholarship funding.

Thank you to my committee Dr. Tim Storr and Dr. Rob Britton for their time to read my thesis and attend committee meetings.

Most importantly I'd like to thank my parents for their endless love and support, without you I wouldn't be where I am today. Finally, I must thank Aidan H, your love, patience, support, and kindness made this possible.

For my biggest supporters – Mom & Dad

Table of Contents

List of Tables

List of Figures

List of Schemes

List of Symbols and Acronyms

β^+	Positron
β^-	Beta particle
% ID/g	Percent injected dose per gram
°C	Degree Celsius
3D	Three dimensional
Å	Angstrom, $1 \bullet 10^{-10}$ m
Ac	Acetate
AML	Acute Myeloid Leukemia
Aoc	8-aminooctanoic acid
BCC	Basal cell carcinoma
BFC	Bifunctional chelator
Bq	Becquerel
calcd.	Calculated
CHX-A"-DTPA	2-(p-isothiocyanatobenzyl)-cyclohexyldiethylenetriamine-pentaacetic acid
CN	Coordination number
CNL	Canadian Nuclear Laboratories
COSY	Correlation spectroscopy (^{1}H-^{1}H NMR)
CT	Computed tomography
CycMSH/αMSH	Cyclized α-Melanocyte-Stimulating Hormone
Da	Dalton
DCM	Dichloromethane
DFT	Density functional theory
DGA	N,N,N',N'-tetra-n-octyldiglycolamide
DIPEA	N-Disisopropylethylamine
DMF	Dimethylformamide
DMPS	2,3-dimercapto-1-propanesulfonic acid
DMSA	Meso-2,3-dimercaptosuccinic acid
DMSO	Dimethylsulfoxide
DOTA	1,4,7,10-tetraazacyclododecane-1,4,7,10-tetraacetic acid
DOTMP	1,4,7,10-tetraazacyclododecane-1,4,7,10-tetramethylene-phosphinic acid

DOTPA	1,4,7,10-tetraazacyclododecane-1,4,7,10-tetrapropionic acid
DTPA	Diethylenetriaminepentaacetic acid
EA	Elemental analysis
EDC	1-ethyl-3-(3-dimethylaminopropyl) carbodiimide
EDTA	Ethylenediaminetetraacetic acid
EPR	Enhanced Permeability and Retention
Eq	Equivalent(s)
EtOH	Ethanol
FDA	Food and Drug Administration (USA)
FLASH	Ultra High dose rate radiotherapy
g	grams
HEHA	1,4,7,10,13,16-hexaazacyclohexadecane-N,N',N'',N''',N'''',N'''''-hexaacetic acid
HEPES	4-(2-hydroxyethyl)-1-piperazineethanesulfonic acid
HMBC	Heteronuclear multiple bond correlation (^{1}H-^{13}C NMR)
HOPO	Hydroxypyridinone
HPGe	High purity germanium
HPLC	High performance liquid chromatography
HR-ESI-MS	High-resolution electrospray-ionization mass spectrometry
HSQC	Heteronuclear single bond correlation (^{1}H-^{13}C NMR)
Hz	Hertz
IEDDA	Inverse Electron-demand Diels-Alder
IR	Infrared spectroscopy
J	Coupling constant (NMR)
K_a	Protonation constant
LDAC	Low-dose cytarabine
LET	Linear energy transfer
M	Molar (moles/litre)
M.A.	Molar Activity
MAE	Meitner-Auger electrons
MC	Melanocortin
MC1R	Melanocortin 1 receptor
mCRPC	Metastatic castration-resistance prostate cancer
MeOH	Methanol

MRI	Magnetic resonance imaging
NaOAc	Sodium acetate
NH_4OAc	Ammonium acetate
NMR	Nuclear magnetic resonance
NOTA	1,4,7-Triazacyclononane-1,4,7-triacetic acid
NP	Nanoparticle
OC	Octreotide
p.i.	Post Injection
PBS	Phosphate buffered saline
PEG	Polyethylene glycol
PEPA	1,4,7,10,13-pentaazacyclopentadecane-*N,N',N'',N''',N''''*-pentaacetic acid
PET	Positron emission tomography
PSMA	Prostate-specific membrane antigen
PRIT	Pre-targeted radioimmunotherapy
PSA	Prostate specific antigen
RCY	Radiochemical yield
RIT	Radioimmunotherapy
RT	Room temperature
SCC	Squamous cell carcinoma
SPECT	Single-photon emission computed tomography
$t_{1/2}$	Half-life
TAT	Targeted alpha therapy
TCO	Transcyclooctene
TEA	Triethylamine
TETA	1,4,8,11-Tetraazacyclotetradecane-1,4,8,11-tetraacetic acid
TETPA	1,4,8,11-tetraazacyclotetradecane-1,4,8,11-tetrapropionic acid
TFA	Trifluoroacetic acid
THF	Tetrahydrofuran
TLC	Thin layer chromatography
TOF	Time-of-flight
TRT	Targeted radionuclide therapy
Tz	Tetrazine

US	Ultrasound
VT NMR	Variable temperature nuclear magnetic resonance
α	Alpha particle
γ	Gamma ray
μ	Micro (10^{-6})

Chapter 1.

Introduction

1.1. Motivation

Accounting for approximately 30% of Canadians deaths, cancer is the number one cause of death in Canada[1]. There have been significant improvements in early detection and treatment options, indicated by decreases of 35% and 20% in mortality rates for males and females respectively[1]. However, the Canadian Cancer Society estimates in 2021, that 1 in 2 Canadians will develop cancer in their lifetime and 1 in 4 Canadians will die from the disease[1]. As such, innovative methods for better therapeutics and early detection methods are of the utmost importance. Current detection methods include laboratory tests, biopsy, physical examinations, and image testing[2]. Therapeutic methods include chemotherapy, surgery, immunotherapy, radiation therapy, targeted drug therapy, and more[2]. This thesis focuses on the use of nuclear medicine for the diagnosis and selective treatment of cancers.

1.2. Nuclear Medicine

Nuclear medicine has become a formidable tool for various medicinal fields (cancer, heart disease, neurological disorders, etc.) which relies on the use of radioactive nuclides for diagnostic imaging and treatment of diseases. Diagnostic methods use positron (β^+) emitters and gamma ray (γ) emitters. Diagnostic radionuclides emit radiation that minimally interacts with biological tissues, allowing them to escape and reach external detectors[3], while therapeutic applications require radionuclides that can cause cytotoxicity. Therapeutic methods can include both internal (targeted internal therapy, brachytherapy, etc.) and external therapy (FLASH, proton therapy, etc.). The development and constant improvement of radiopharmaceuticals have significantly expanded clinical applications. Herein, this thesis focuses on internal targeted radionuclide therapy (TRT).

1.2.1. Diagnostics

The two nuclear medicinal imaging techniques are single-photon emission computed tomography (SPECT) and positron emission tomography (PET) (**Figure 1.1**). Unlike structural diagnostic methods (computed tomography (CT), magnetic resonance imaging (MRI), ultrasound (US), and x-ray), nuclear medicine allows for functional imaging to analyze chemical and biological processes within the body[4]. Cutting edge hybrid imaging simultaneously utilizes both PET/SPECT in conjugation with MRI/CT (i.e., PET-CT, SPECT-CT) to get both structural and functional images[4].

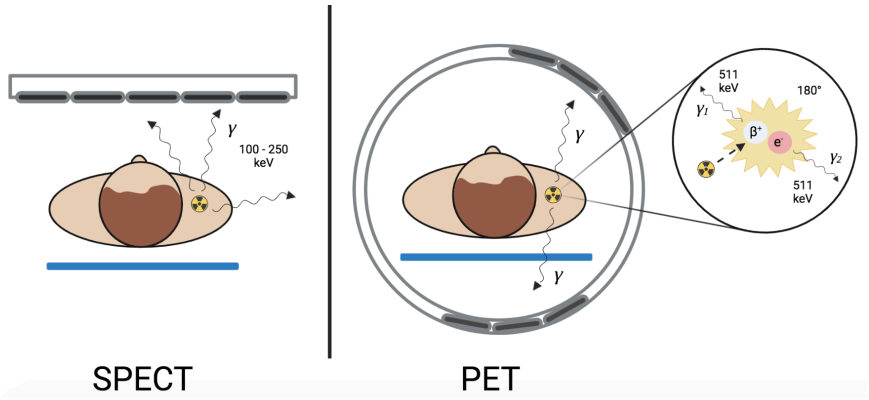

Figure 1.1: Visual representation of SPECT and PET diagnostics

PET utilizes positron emitting radionuclides such as fluorine-18 (^{18}F). As the nuclide decays, it emits a positively charged beta particle (β^+) that travels a short distance (3 - 5 mm) within the body until it collides with an electron (negatively charged beta particle, (β^-))[4]. This collision, also known as an annihilation will release two 511 keV gamma (γ) rays that are emitted 180° from one another[4]. The circular arrangement of PET coincidence detectors allows for the simultaneous detection of the two γ rays[4]. If the two detections are within 12 nanoseconds (ns), it is assumed an annihilation has occurred[4]. With enough annihilation events (10^6), a 3D image with excellent resolution (2 - 3 mm) can be reconstructed[5]. In addition to higher resolution, PET is more sensitive than SPECT with required tracer concentrations of 10^{-8} to 10^{-10} M, compared to ~10^{-6} M[5]. However, the major limitations of PET are high operational costs and a limited number of FDA-approved PET radiotracers.

SPECT, the older modality utilizes gamma cameras that will detect a gamma (γ) emission within 100 – 250 keV[4]. With a powerful computerized calculation system, cross-sectional images allow for a 3D image to be reconstructed[4]. Despite lower resolution pictures (10 – 14 mm), SPECT is the more commonly used methodology[4]. One major reason is the higher availability; as of 2017, there were 330 SPECT machines, 261 SPECT-CT machines, and only 51 PET-CT machines in Canada[6]. The other key reason is the much lower operational costs for SPECT compared to PET. Unlike PET which traditionally employs cyclotron produced "organic" radionuclides (^{11}C, ^{18}F, ^{13}N, and ^{15}O), SPECT can use metallic "inorganic" radionuclides such as technetium-99m (^{99m}Tc) and indium-111 (^{111}In).

1.2.2. Therapeutics

Internal targeted radionuclide therapy (TRT) via the use of radiopharmaceuticals is an emerging therapeutic method due to its highly selective nature, non-surgical approach, and minimal amounts of required radioactivity. There are three types of radioactive particles that can be utilized in TRT – alpha particles (α), beta particles (β^-), and Meitner-Auger electrons (MAE) (**Table 1.1**). Herein, my focus will be on the use of alpha particles for targeted alpha therapy (TAT), a subdivision of targeted radionuclide therapy (TRT).

Table 1.1: Radioactive particles that can be utilized in TRT

Decay	Energy	Range	LET (keV/µm)
α	5 - 9 MeV	40 – 100 µm	50 – 230
β^-	0.05 – 2.3 MeV	0.05 – 12 mm	~ 0.2
Auger Electrons	eV - keV	2 – 500 nm	4 – 26

LET - linear energy transfer (energy deposited per unit distance)

Beta Particles (β^-)

Beta particles are used for medium – large tumors due to their larger penetration depth (0.05 – 12 mm), lower energy deposits (0.05 – 2.3 MeV), and small linear energy transfer (LET; the amount of energy deposited per unit distance) of 0.2 keV/µm. This even distribution of beta particles in heterogenous tumors results in single-strand DNA breakage[4,7], which can be repaired through DNA repair pathways. With sub-lethal damage, very high doses (up to several gigabecquerel (GBq)/cycle) of β^- radiotherapeutics must be

administrated to have therapeutic effects in patients[8]. Common beta emitters such as lutetium-177 (^{177}Lu), yttrium-90 (^{90}Y), and iodine-131 (^{131}I) have been incorporated into FDA approved targeted beta therapeutics including but not limited to: [^{177}Lu]Lu-DOTATATE for neuroendocrine tumors, [^{131}I]NaI for thyroid cancer, and [^{90}Y]Y-ibritumomab tiuxetan (Zevalin®) for non-Hodgkin's lymphoma[9].

Meitner-Auger electrons (MAE)

MAEs have very short penetration depth in tissue (2 – 500 nm) and minor energy deposits (eV – keV) resulting in a moderate LET of 4 – 26 keV/μm[7]. The efficacy of MAEs is dependent on the ability of the targeting vector to internalize such that the radionuclide is localized in the cell nucleus. One benefit of MAEs is their low cellular toxicity in the blood or bone marrow during circulation within the body[4]. This relatively new radiotherapeutic method has a limited number of successful preclinical studies and clinical applications[8,10,11]. Initial studies of MAEs investigated conventionally used imaging & therapeutic radionuclides such as ^{111}In, ^{125}I, ^{99m}Tc, and gallium-67 (^{67}Ga), while new unconventional MAE emitting radionuclides such as antimony-119 (^{119}Sb), lanthanum-135 (^{135}La), and mercury-197m/g ($^{197m/g}$Hg) are being explored[8,10].

Alpha particles (α)

Targeted alpha therapy (TAT) uses alpha emitting radionuclides for small and metastatic tumor applications[7,12]. Alpha particles are highly cytotoxic causing double stranded DNA breakage, due to their small penetration depth of 40 – 100 μm, high energy (5 – 9 MeV) deposit, and large LET of 50 – 230 keV/μm[4,7]. Their cytotoxicity potency is over 100 times greater than beta emitters, such that it requires less than five DNA hits to kill a cell[4]. In 2013, radium-223 [^{223}Ra]Ra-dichloride (Xofigo®) became the first and to date, only FDA-approved targeted alpha therapeutic drug[13]. Over the past decade, five other alpha emitters (actinium-225 (^{225}Ac), bismuth-213 (^{213}Bi), astatine-211 (^{211}At), lead-212 (^{212}Pb), and thorium-227 (^{227}Th)) have gained significant interest for TAT[13].

1.3. Construction of Radiopharmaceuticals

A plethora of radioisotopes can be incorporated into a radiopharmaceutical for either therapy or imaging. Generally, the construction of a radiopharmaceutical will be governed by the chemical nature of the isotope used – either 'organic' (e.g., ^{11}C, ^{18}F) or 'inorganic'/metallic (e.g., ^{68}Ga, ^{111}In). The focus of this thesis is the use of metallic radioisotopes (aka radiometals) – in particular, the emerging alpha-emitter actinium-225 (*vide infra*), as such the construction of a metallic radiopharmaceutical will be discussed. Typically, radiometal-based radiopharmaceuticals consist of four main components;

I) Chelator – provides radionuclide stability through metal-chelator binding
II) Linker – connects the chelator to the targeting vector
III) Targeting vector – a biomolecule with selective binding for over-expressed tumor receptors
IV) "Inorganic" radionuclide – provides the radioactive emission for therapy/imaging

Each component is meticulously chosen as radiopharmaceuticals must be thermodynamically stable, chemically inert, and fairly easy/inexpensive to synthesize. They also must have quick tumor uptake and fast clearance from non-target tissues to achieve high tumor-to-background ratios, which ensures reduced radiation exposure to healthy tissues[4].

1.4. Chelators

Chelators are an essential component of metal-based radiopharmaceuticals. When designing a chelator, radiometal properties such as the ligand donor atom preferences (based on hard-soft-acid-base theory) and coordination number/geometry need to be considered[14]. Chelators can be divided into two types: macrocyclic (closed chain) and acyclic (open chained). Macrocyclic ligands are normally more kinetically inert and thermodynamically stable than acyclic ligands, due to a phenomenon known as the macrocyclic effect[14]. Yet, macrocycles often require heating at extended times for quantitative radiolabeling[14]. The widely adopted bifunctional chelator (BFC) method

utilizes a chelator that I) can bind radionuclides and II) has reactive functional groups that can be covalently coupled to targeting vectors (*vide infra*). With long synthetic alterations of the linker, chelate, and biomolecule performed before radionuclide introduction, unnecessary decay of the precious radiometal can be avoided (**Figure 1.2**). The most attractive quality of the BFC technique is it allows for a countless number of different targeting vectors to be conjugated to limitless numbers of chelators.

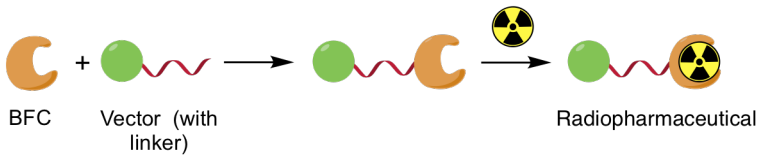

Figure 1.2: Illustration of a radiometal-based radiopharmaceutical containing bifunctional chelator (BFC)

1.4.1. Acyclic Chelators

DTPA (diethylenetriaminepentaacetic acid, N_3O_5), is one of the most widely used acyclic chelators in radiochemistry (**Figure 1.3**). While it can quantitatively radiolabel many radiometals (^{111}In, ^{177}Lu, copper-64 (^{64}Cu), $^{86/90}$Y, ^{68}Ga, ^{213}Bi, and zirconium-89 (^{89}Zr)) at room temperature quickly, it can suffer from low *in vivo* stability. Nevertheless, DTPA has been successful as I) 2 FDA approved SPECT agents - OctreoScan™ and ProstaScint® ([^{111}In]In-DTPA-octreotide (OC) and [^{111}In]In-DTPA-capromab respectively), II) FDA approved β^- therapy Zevalin® ([^{90}Y]Y-ibritumomab tiuxetan), and III) MRI gadolinium (Gd) contrast agents.

CHX-A"-DTPA (2-(p-isothiocyanatobenzyl)-cyclohexyldiethylenetriamine-pentaacetic acid, N_3O_5), a second-generation acyclic chelator has shown improved stability and kinetic inertness, a result of the chiral cyclohexyl motif in the DTPA backbone (**Figure 1.3**). CHX-A"-DTPA has been thoroughly investigated for ^{90}Y, ^{111}In, ^{213}Bi, and ^{177}Lu, and promising clinical trials are underway[15].

1.4.2. Macrocyclic Chelators

TETA (1,4,8,11-Tetraazacyclotetradecane-1,4,8,11-tetraacetic acid, N_4O_4), an octadentate chelator was only heavily investigated for ^{64}Cu radiopharmaceuticals (**Figure**

1.3). In 2001, one clinical trial found [^{64}Cu]Cu-TETA-OC as a potential PET tracer for neuroendocrine tumors[16]. However, newer generation chelators (i.e. NOTA and TETA derivatives) which have improved *in vivo* stability have replaced older generation TETA[14].

NOTA (1,4,7-Triazacyclononane-1,4,7-triacetic acid, N_3O_3), a hexadentate chelator is the current gold standard for complexation of ^{68}Ga and ^{64}Cu, exhibiting favourable radiolabeling conditions and excellent *in vivo* stability[14] (**Figure 1.3**). As ^{68}Ga and ^{64}Cu gain significant interest as PET imaging agents, new promising chelators have arisen. However, due to the commercial availability of NOTA and its bifunctional analogues, NOTA is still considered the "practical" gold standard[14].

DOTA (1,4,7,10-tetraazacyclododecane-1,4,7,10-tetraacetic acid, N_4O_4) a tetraaza macrocyclic chelator, is the current gold standard for complexation of several trivalent radiometal ions (^{111}In, ^{177}Lu, $^{86/90}$Y, ^{225}Ac, and $^{44/47}$Sc)[17] (**Figure 1.3**). DOTA can form kinetically inert complexes but at the expense of slow radiolabeling kinetics and elevated temperatures (60 – 90 °C), which makes conjugation to heat sensitive targeting vectors (i.e. antibodies) quite challenging[18]. Despite conjugation issues, DOTA and DOTA derivatives have been incorporated as chelates into more than 50 clinical trials for PET imaging, β^- therapy, and/or α therapy.

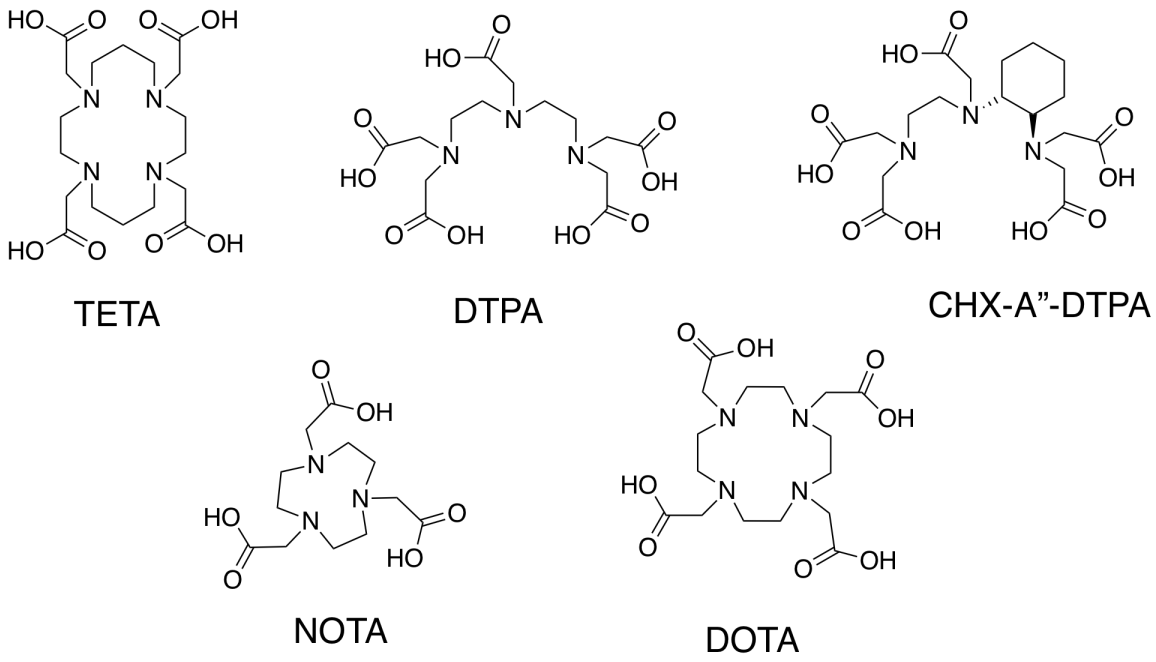

Figure 1.3: Structures of acyclic (CHX-A”-DTPA and DTPA) and macrocyclic (TETA, NOTA, and DOTA) chelators discussed

1.5. Linkers

Linkers, the connector between chelators and the targeting vector are also a critical component as they can affect the pharmacokinetics of the radiopharmaceutical. Linkers can be classified into four categories i) cationic, ii) anionic, iii) neutral, or iv) metabolically cleavable[19]. Common linkers include polyethylene glycol (PEG) to slow excretion through the hepatic system, long hydrocarbon chains increasing lipophilicity, and peptide sequences to improve hydrophilicity[19]. Studies have shown modifying the linker can significantly impact the biodistribution of radiotracers[19–22]. For example, the introduction of a cationic piperidine linker allowed for rapid *in vivo* clearance and increased tumor uptake when compared to neutral 8-aminooctanoic acid (Aoc) peptide linker and neutral PEG linker for preclinical melanoma imaging with ^{68}Ga and ^{18}F[23,21]. By modifying pharmacokinetics of linkers, higher tumor uptake while minimizing undesired organ uptake can be obtained.

1.6. Targeting Vectors/Biomolecules

The choice of targeting vector is crucial, as it will determine the biodistribution and pharmacokinetics of radiopharmaceuticals. Ideally, biomolecules must have a high affinity for receptors that are over-expressed on diseased cells yet minimally expressed (or are absent) on healthy cells. Moreover, the targeting vector's biological half-life should match the physical half-life of the selected radionuclide, exhibit high *in vivo* stability and minimal renal accumulation. Targeting vectors used in radiopharmaceutical design can be categorized into one of 3 classes: antibody, peptide, and other. Each class of targeting vector will have different biological/physiological properties, advantages, and disadvantages.

1.6.1. Antibodies

Antibodies, also known as an immunoglobulin are large Y-shaped proteins crucial to immune systems. With an average weight of 150 kDa and relatively large size, antibodies are slow to circulate and have long biological half-lives. The major benefit of antibodies is their highly specific nature allowing for selective tumor localization. However, antibodies have slow clearance rates which can cause high radiation doses to healthy tissue, resulting in moderate tumor-to-background ratios[24]. One tactic to mitigate this issue is a pre-targeting approach, wherein the targeting vector and cytotoxic radionuclide are administered separately (*vide infra*)[24]. Another method is the use of smaller bioconjugates such as peptides or antibody fragments.

1.6.2. Peptides

Similar to antibodies, peptides offer numerous advantages for radiopharmaceuticals, including high tumor uptake and a vast number of biological targets. Additionally, peptides experience rapid clearance from the blood/non-target tissues due to their significantly smaller size (2-20 amino acids)[25]. Endogenous peptides are known to be metabolically unstable, yet synthetic modifications to improve pharmacokinetics and slow degradation without altering receptor affinity are well developed[3]. Moreover, solid-phase peptide synthesis allows for easy preparation of peptides with diverse modifications. The

major disadvantage of peptides is their excessively rapid clearance can prevent sufficient tumor uptake[3].

1.6.3. Others

Other bioconjugates utilized in radiopharmaceuticals can include nanoparticles (NP) and antibody fragments. The biodistribution of nanocarriers is primarily driven by their large size and shape, although they can be modified with targeting vectors (peptides and antibodies) to increase tumor uptake[26]. For nanocarriers without targeting vectors, they rely on passive targeting, such as the Enhanced Permeability and Retention (EPR) effect[26]; wherein defective vascularization and ineffective lymphatic drainage of tumors allows for large carriers to be trapped and accumulated in tumor tissue[26]. Nanoparticles are predominantly excreted through the hepatic system due to their large size, which can cause unwanted high liver uptake[13]. Antibody fragments have superior tumor penetration depth and rapid blood clearance while maintaining high receptor affinity[24,27,28]. However, similar to peptides, rapid blood clearance of antibody fragments has been associated with reduced tumor uptake[24,27,28].

1.7. Radionuclides

A radionuclide is an unstable atom that undergoes decay, emitting radiation to become stable. Radionuclides used in the nuclear medicine field should have high radionuclidic, radiochemical, and chemical purity[4]. Ideally, the radioisotope should be carrier-free (every atom is radioactive) or have a high specific activity (activity per unit mass)[4]. Additionally, the radionuclide half-life ($t_{1/2}$) should match the biological half-life of the targeting vector. For example, antibodies that can take up to days to circulate are best matched with long lived radioisotopes. For therapeutic isotopes, the emission of gamma rays (in optimal energy ranges) as the radioisotope undergoes decay is valuable as low-dose imaging can be performed to determine the distribution of the radiopharmaceutical for non-invasive dosimetry determination.

1.8. Conjugation

Conjugation between targeting vectors and bifunctional chelators is dependent on the bioconjugation handles on both the linker and the chelator (**Figure 1.4**). Common conjugation techniques include[14]:

I) Carboxylic acid and a primary amine coupling with a coupling reagent

II) Activated esters and a primary amine coupling

III) An isothiocyanate and a primary amine coupling

IV) Inverse Electron-demand Diels-Alder (IEDDA) "click" between a tetrazine and transcyclooctene

V) Copper catalyzed "click" between an azide and an alkyne

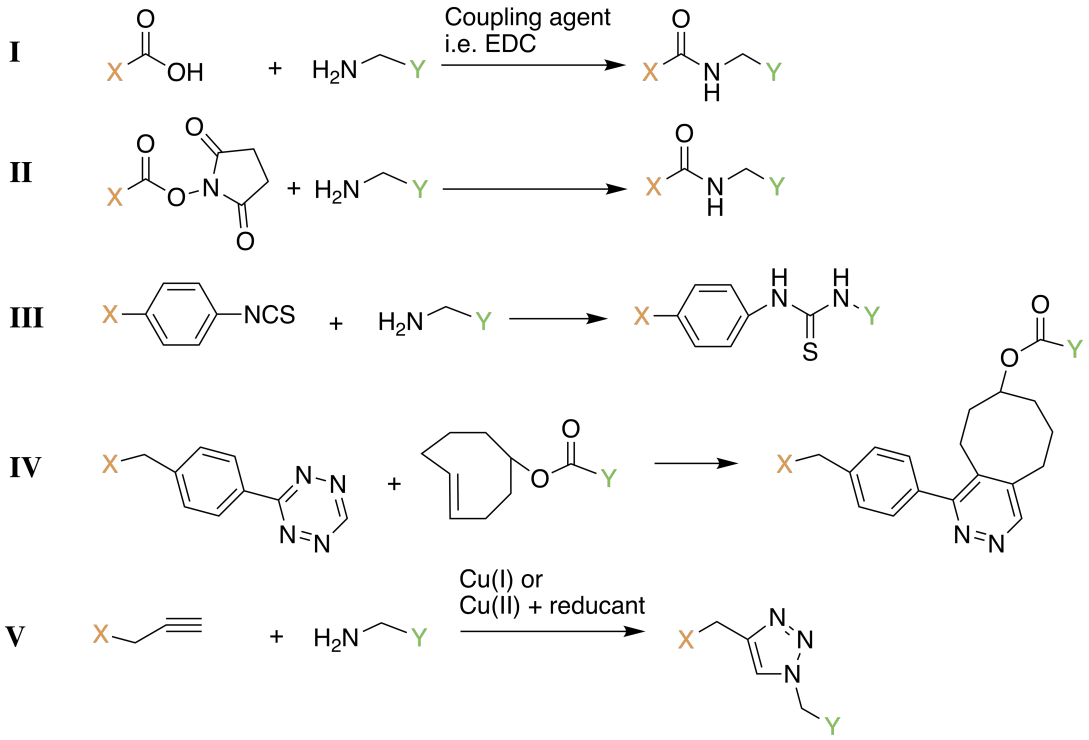

Figure 1.4: Depiction of conjugation methods discussed in this thesis

Bioconjugation must be specific to the available handle, not decrease the binding affinity of the chelate to the radioisotope, and should occur rapidly at mild conditions[14]. The "click" methodology between tetrazine (Tz) and transcyclooctene (TCO) is rapidly gaining interest as the quick metal-free reaction allows for pre-targeting methods[14]. For pre-targeting, the antibody with a TCO handle is introduced into the patient, allowing the

antibody adequate time to circulate and accumulate (**Figure 1.5**). Once accumulated at the tumor, a complimentary chelated radionuclide with a Tz handle is administered. *In vivo*, a rapid "click" reaction between TCO-Tz forms the intact radiopharmaceutical, followed by rapid clearance of excess radioligand.

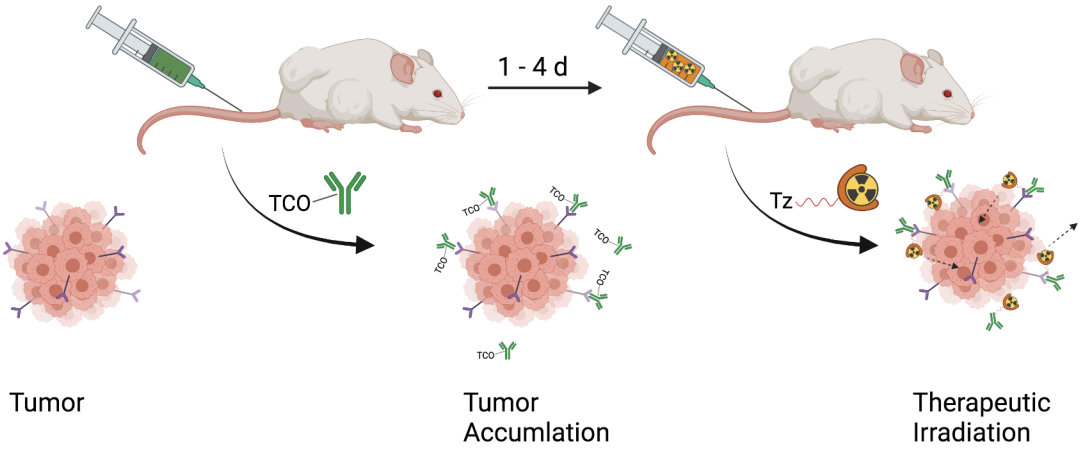

Figure 1.5: Depiction of pretargeted radioiummunotherapy approach (PRIT)

1.9. Special considerations for α-emitting radiopharmaceuticals

1.9.1. Recoiling Daughters

Upon the decay of an α-emitting radioisotope, the daughter nuclide experiences recoil energy. To conserve momentum, the daughter nuclide will recoil 180° from the alpha particle. The heavier daughter nuclide will experience a significantly smaller amount of energy (100 – 200 keV) compared to the lighter, highly energetic (5 – 9 MeV) alpha particle. The recoil energy of a daughter nuclide is calculated using the equation below, where m_α is the mass of the alpha particle, m_{recoil} is the mass of the daughter nuclide and E_α is the energy of the alpha particle[29].

$$E_{recoil} = \frac{m_\alpha}{m_{recoil}} E_\alpha$$

The recoil experienced is 100 - 1000 times stronger than chemicals bonds, resulting in the release of the bound daughter[7]. Consequently, the unchelated daughters, which are often radioactive in themselves, can redistribute through the body providing radiation to undesired organs. Redistribution will be affected by I) distance covered during the recoil,

II) intrinsic affinity of the radionuclide for specific organs, III) active transport, and IV) diffusion processes[7,30].

Redistribution of recoiling daughters

Redistribution of recoiled daughters can be difficult to measure and is therefore mostly studied post-mortem *ex vivo*. Theoretically, recoiled daughters will cover on average 100 nm in water[26], breaking free of its chelate. As the daughter acquires a new position, diffusion processes and active transport will become key[30]. Diffusion of the now free ion will be dependent on the type of medium, as the ion experiences different interactions with blood-like medium or cell-like components (extra/intracellular matrix)[30]. The movement of particles in tissues depends on their size, charge, configuration, and the physicochemical properties of the medium[31]. The majority of the time, the recoiled nuclide is released into the bloodstream, where the intrinsic affinity of the radionuclide will determine its fate.

One effective solution to redistributed recoiled daughters is the use of short-lived α-emitting radionuclides (^{213}Bi or ^{211}At) with simple decay schemes[7]. However, a short half-life can present logistical issues for generator elution, radiolabeling, drug administration, and allowing for sufficient circulation time. In addition, longer lived α-emitting radioisotopes with complex decay schemes offer superior cytotoxicity that is hard to replicate[7].

Retention of recoiled daughters

There are several approaches to deal with recoiling daughters currently under investigation, herein three approaches are described: I) encapsulation in nanocarriers, II) fast tumor accumulation, and III) local administration.

The use of nanocarriers such as metal-based particles, polymersomes, and liposomes has been investigated for recoiled daughter retention[26,30,32–39]. Liposomes (phospholipid vesicle) exhibit insufficient retention (~ 12% of ^{213}Bi) at all sizes between 100 – 800 nm[32]. Polymersomes (polymer vesicle) have been examined for encapsulation of ^{225}Ac and its daughters through simulations and *in vitro* studies. In 2011 Thijssen *et al.,*

examined polymersomes to retain recoiling daughters via a Monte Carlo simulation[26]. A double-layer polymersome was significantly more effective than a single-layer polymersome[26]. Wang *et al.,* compared previous simulations with *in vitro* experiments, wherein 800 nm polymersomes retain ^{221}Fr and ^{213}Bi fairly well (~70% and ~53% respectively)[33]. However, complex alpha decay schemes results in cascading that soft materials such as polymersomes and/or liposomes cannot sufficiently handle. To achieve adequate retention, nanocarriers should have non-organic components. Lanthanide-based phosphate ($LnPO_4$) nanoparticles have shown some promise in reducing toxicity from recoiled ^{225}Ac daughters[34] (*vide infra*).

The second approach hinges on the radiopharmaceutical rapidly taken up by the tumor, minimizing circulation within the body. Internalization promotes the sequestering of the targeted radionuclide in the tumor cell's cytoplasm, leading to a higher accumulation of radioactivity in the tumor, compared to nontarget organs[35]. For example, cyclized α-Melanocyte-Stimulating Hormone (CycMSH/ αMSH), a disease targeting peptide for melanoma skin cancer has shown rapid internalization for various derivatives[20]. Particularly three tracers, [^{68}Ga]Ga-CCZ01048, [^{68}Ga]Ga-CCZ01047, and [^{68}Ga]Ga-CCZ01056 can internalize ~ 36 - 52 % of total bound activity into B16F10 cells after 30 minutes[20].

For large, easily accessible tumors local administration of the radiopharmaceutical offers a simple solution. Notably, a phase I clinical study with locally injected [^{213}Bi]Bi-DOTA-substance P into gliomas showed high target site retention[40]. Moreover, no local/systemic toxicity was observed and radiation induced necrosis of the tumor allowed subsequent resection[40]. This innovative methodology allows for possible treatment for previously non-operable and non-treatable gliomas. Similar promising results were obtained in phase I clinical studies with [^{212}Pb]Pb-labeled trastuzumab[41] and [^{111}At]At-labelled chimeric anti-tenascin C monoclonal antibody (ch81C6)[42]. However, this approach is not feasible for small metastases which cannot be easily localized.

1.10. Actinium

Since the discovery of actinium in 1899, 32 isotopes of actinium have been identified - ranging from ^{205}Ac to ^{236}Ac[43]. Of the 32 isotopes, only two - ^{227}Ac ($t_{1/2}$ = 21.8 y) and ^{228}Ac ($t_{1/2}$ = 6.1 h) - are naturally occurring from the decay of uranium-235 (^{235}U) and ^{232}Th respectively[43]. Despite the spiked interest in actinium-225 for TAT, the fundamental chemistry of this element is still poorly understood; an outcome of limited supply and all actinium isotopes being radioactive[12]. With an ionic radius of 1.12 Å (coordination number (CN) = 6)[12,44] and a +3 oxidation state, actinium is the largest trivalent actinide. Recently Ferrier *et al.,* determined the hydration number of Ac^{3+} to be 10.9 ± 0.5, with an Ac-O_{H20} distance of 2.63 Å[44]. Classified as a "hard" Lewis acid (according to the hard-soft-acid-base theory), actinium prefers nonpolarized electronegative Lewis bases such as oxygen donors[12]. As all isotopes of actinium are radioactive, it is most commonly compared to La^{3+} due to their similar ionic radii (1.03 Å; CN = 6).

1.11. Actinium-225 ($^{225}Ac^{3+}$)

The promising $^{225}Ac^{3+}$ ion has a complex decay scheme, including 4 α decays, two ß$^-$ decays, and two SPECT appropriate γ emissions[13] as seen in **Figure 1.6**. These highly energetic (5.8 MeV, 6.3 MeV, 7.1 MeV, 5.9 MeV, or 8.4 MeV) α decays allow for considerable cytotoxicity per atom of actinium. Moreover, it can generate bismuth-213 (^{213}Bi), a good candidate for TAT currently in clinical trials[13]. As a long-lived radionuclide ($t_{1/2}$ = 9.9 days), it is suitable for antibody conjugation[13]. Within the past decade, there have been several noteworthy clinical successes with $^{225}Ac^{3+}$-radiopharmaceuticals (*vide infra*)[45–54]. However, ^{225}Ac-radiopharmaceuticals remain underdeveloped, an outcome of limited ^{225}Ac radionuclide supply, an inability to form kinetically inert complexes under ideal conditions (quick kinetics and mild temperatures), and recoiling radioactive daughters.

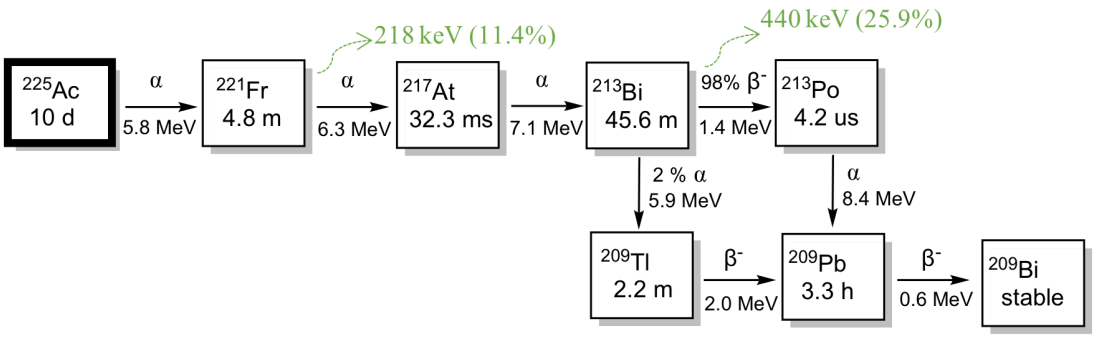

Figure 1.6: The decay scheme of Ac-225 with imaging relevant gamma emissions in green

1.11.1.Ac-225 Production

The current global average production of ^{225}Ac is 63 GBq – the equivalent of only 1000 patient treatments yearly, yet the estimated current demand for ^{225}Ac is 185 GBq per year[13]. The main source of ^{225}Ac originates from thorium-229 (^{229}Th, $t_{1/2}$ = 7340 y) stockpiles extracted from uranium-223 (^{223}U, $t_{1/2}$ = 1.6 x 10^5 y) decay (**Figure 1.7**)[13]. The key advantage of this method is the isolation of high purity radionuclide with no other actinium isotopes present, nevertheless, it fails to meet current demand[13]. One production method under investigation is proton bombardment of radium-226 (^{226}Ra) via the ^{226}Ra(p,2n)^{225}Ac nuclear reaction[13]. The promising ^{226}Ra(p,2n)^{225}Ac reaction can produce 108 Ci (3.9 TBq) monthly with a 1g ^{226}Ra target; however, major safety concerns around the highly radioactive target manufacturing, radiation protection, processing, and recycling has slowed this potential production method from moving forward[13]. The other main production method under investigation is the spallation of thorium-232 (^{232}Th) targets via high energy protons[13]. With the largest potential monthly production at 11.2 TBq, the major disadvantage is the production of dozen of isotopes such as long-lived ^{227}Ac ($t_{1/2}$ = 21.7 y) that requires extensive separation and purification methods[13]. Production method ^{nat}U(p,x)^{225}Ac produces small amounts of pure $^{225}Ac^{3+}$ and mother nuclide ^{225}Ra (which can be eluted every 17 days to produce additional ^{225}Ac)[13]. However, the total produced ^{225}Ac activity for 2016 was only 44.4 MBq, indicating this production method is insignificant compared to the current ^{229}Th generators[13].

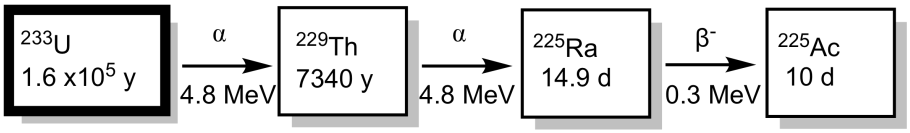

Figure 1.7: The decay scheme of U-233 to Ac-225

1.11.2.Ac-225 Chelation

With a lack of fundamental understanding of $^{225}Ac^{3+}$ coordination chemistry, predicting chemical structures of ligands that complex actinium and exhibit *in vitro* and *in vivo* stability is difficult. The first studies involved commercially available chelates such as EDTA, DTPA, and DOTA that have shown some clinical use[13,55–57]. Out of the 10 chelates initially examined (*vide infra*), only DOTA illustrated quantitative labeling and *in vivo* stability. DOTA quickly became the "gold standard" for the trivalent actinide, leading to DOTA-antibody and DOTA-peptide targeted ^{225}Ac-radiotherapeutics.

Initial studies of [^{225}Ac]Ac-DOTA-antibody conjugates found higher temperatures (>60 °C) were required for adequate ^{225}Ac complexation. As antibodies are unstable at elevated temperatures (>37 °C), a novel two-step procedure was introduced[55]. Bifunctional DOTA-isothiocyanate (DOTA-NCS) was quickly radiolabelled with ^{225}Ac, followed by the conjugation of an antibody yielding an [^{225}Ac]Ac-DOTA-antibody construct[55]. This process was successfully employed for antibodies HuM195, B4, huJ591, mJ591, and 3F8[55]. The radiochemical yield was low at 9.8 ± 4.5 %, however, the radiochemical purity was >90 % for all constructs with moderate specific activities (4.1 ± 2.6 GBq/g)[55]. In hopes of finding a superior option, Maguire *et al.,* investigated a direct 1-step labeling of antibody-DOTA constructs at temperatures suitable for antibodies[58]. Radiolabeling was performed at 37 °C for 2 hours with the addition of radiolytic protectant L-ascorbic acid[58]. Remarkably, the radiochemical yield increased 10 fold (~80%) compared to 2-step methods (6 - 12%) and up to a 30 fold increase in specific activity (~130 GBq/g)[58]. Currently, no other rapid or mild radiolabeling conditions have been discovered for ^{225}Ac radiolabeling with chelate DOTA[58]. Despite that, DOTA is the chelator of choice for all human clinical studies with ^{225}Ac (*vide infra* –**Table 1.3**).

1.11.3. Ac-225 Recoiling Daughters

With 4 α decays per atom of actinium, the bio-distribution of each alpha emission in ^{225}Ac's decay chain (**Figure 1.6**) needs to be evaluated. Nonchelated ^{225}Ac distributes primarily to the liver, spleen, and skeleton with some retention in the kidney[56] (**Table 1.2**). ^{217}At has the shortest half-life (32 ms) of the alpha emitters and is often assumed to have identical biodistribution to ^{221}Fr[13]. The distribution of ^{213}Bi and ^{221}Fr to the renal system (kidneys, renal pelvis, bladder, etc.) is the major limitation of ^{225}Ac TAT.

Table 1.2: Major targeted organs for Ac-225 daughters ($t_{1/2}$ > 3 min)

Daughter	Major targeted organs
Actinium	Liver, spleen, skeleton, and kidneys[56]
Francium	Primarily kidneys[59]
Bismuth	Urine, kidneys, and blood[59]
Lead	Blood, liver, skeleton, and kidneys[30]

Encapsulation in nanoparticles has become one of the leading efforts to capture ^{225}Ac's recoiling daughters. One study examined the effectiveness of gold coated lanthanide phosphate ($LnPO_4$) nanoparticle (NP) to contain the recoiled ^{225}Ac daughters[34]. It hinges on the concept that highly energetic α-particles will only lose <2% of their energy in the layered NP, while the recoiling daughter will only travel 20 nm in bulk $LnPO_4$[34]. The layered NPs consist of $\{La_{0.5}Gd_{0.5}\}PO_4$ core with $GdPO_4$ shells coated in gold[34]. With 4 $GdPO_4$ shells, retention of ^{225}Ac and daughter ^{221}Fr was excellent at >99.99 % and 88% respectively after 3 weeks *in vitro*[34]. Moreover, the authors demonstrated antibody conjugated NPs retained specific binding affinity of the antibody and significant amounts of ^{213}Bi were retained within the NP in various tissues (>70 %)[34].

Jaggi *et al.,* investigated reducing the renal accumulation of unchelated ^{225}Ac daughters through the use of metal chelation and diuretics[59]. Metal chelator 2,3-dimercapto-1-propanesulfonic acid (DMPS) and meso-2,3-dimercaptosuccinic acid (DMSA) were administered orally prior to the injection of [^{225}Ac]Ac-DOTA-lintuzumab into mice and monkeys[59]. DMSA significantly reduced renal ^{213}Bi accumulation (14.8 % ID/g (injected dose per gram) reduction, 6 hrs post injection), but was less potent than DMPS (31.2 % ID/g reduction, 6 hrs post injection (p.i.)) in doing so[59]. In contrast,

diuretics furosemide and chlorothiazide (known to chelate metals and enhance its excretion) minimized the accumulation of both ^{221}Fr and ^{213}Bi[59]. The combination of DMPS with a diuretic caused an excellent reduction of renal ^{213}Bi activity (~75 – 80%)[59]. Preclinically, this study shows metal chelation and diuretics can be used to reduced renal accumulation of ^{225}Ac daughters.

Poty *et al.,* investigated pretargeted α-radioimmunotherapy (PRIT) as an alternative strategy to reduce non-specific toxicities for conventional ^{225}Ac α-radioimmunotherapy (RIT)[60] of pancreatic ductal adenocarcinoma. After 3 days of circulation, tumor uptake for both methods were not significantly different (PRIT: 29.6 ± 6.6 % ID/g, RIT: 31.1 ± 21.4 % ID/g; 3 d p.i.). Conversely, there were significantly higher tumor-to-liver, tumor-to-bone, and tumor-to-spleen ratios for PRIT compared to conventional RIT. The radionuclide daughters' redistribution was followed by performing *ex vivo* Cerenkov imaging immediately after sacrifice and again after secular equilibrium. The radiance in the kidneys dropped ~ 4 fold (from 16,400 p/sec/cm^2/sr to 4,900 p/sec/cm^2/sr) after reaching equilibrium, a result of the free ^{213}Bi, ^{221}Fr, and their β^- daughters accumulating in the kidneys. Poty *et al.,* illustrated PRIT is as effective as RIT while reducing off target toxicities but neither method significantly limited the redistribution of the ^{225}Ac daughters.

1.11.4.Ac-225 Clinical Trials

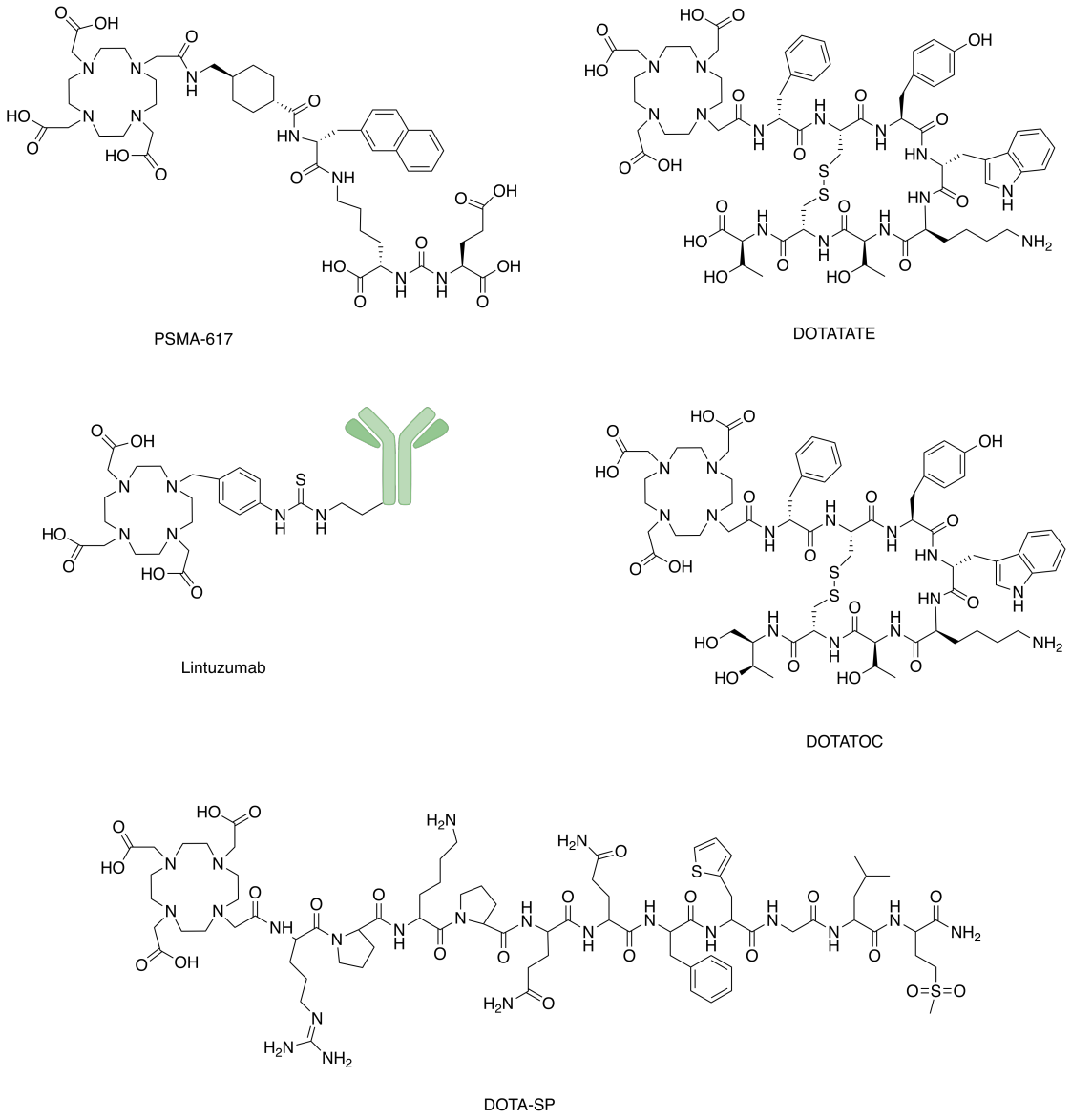

Figure 1.8: Structures of radiopharmaceuticals used in clinical trials with ^{225}Ac (as of September 15, 2021)

With a prolonged half-life ($t_{1/2}$ = 9.9 d), initial ^{225}Ac clinical studies used long-lived antibody conjugates such as lintuzumab as disease targeting vectors (**Figure 1.8** and **Table 1.3**). The first of its kind study was a dose-escalation trial to determine the safety, pharmacology, and biological activity of [^{225}Ac]Ac-lintuzumab in Acute Myeloid Leukemia (AML)[45]. Patients with AML have abnormal immature white blood cells (blasts) populating over 20% of peripheral/bone marrow cells compared to 1 – 5 % for healthy

individuals. [^{225}Ac]Ac-lintuzumab was administrated as 18.5, 37, 74, 111, or 148 kBq per kg of body weight doses to 18 patients[45]. Peripheral blasts were eliminated in 63% of patients and bone marrow blasts reductions were observed in 67% of patients[45] (for those receiving >18.5 kBq/kg doses). However, serious toxicities (grade >3), myelosuppression, and death from sepsis occurred in 2 patients receiving 148 kBq/kg (2/2) and 1 patient receiving 111 kBq/kg (1/2) dosages[45]. A subsequent trial treated 18 patients with 18.5 (n = 3), 37 (n = 6), 55.5 (n = 3) or 74 (n = 6) kBq/kg, diuretic furosemide and low-dose cytarabine (LDAC)[46]. Overall, only 5/18 (28%) patients had complete remission and median progression-free survival was 2.7 months.

Notably, [^{225}Ac]Ac-PSMA-617 (prostate-specific membrane antigen-617) has shown remarkable success in clinical trials targeting metastatic prostate cancer[51,54,52,50] **Figure 1.8** and **Table 1.3**). In 2014/2015, two patients with late-stage metastatic castration-resistant prostate cancer (mCRPC) were offered [^{225}Ac]Ac-PSMA-617 as salvation therapy after exhausting conventional therapy options[54]. Patient A received 3 cycles of 9 - 10 MBq of [^{225}Ac]Ac-PSMA-617 (100 kBq/kg of body weight) at bi-monthly intervals, with one additional 6 MBq consolidation therapy session[54]. Patient B received 3 cycles of 6.4 MBq of [^{225}Ac]Ac-PSMA-617 (100 kBq/kg of body weight) at bi-monthly intervals[54]. Two months after the last cycle, both patients' PET/CT scans and laboratory tests (prostate specific antigen (PSA) <0.1 ng/mL) indicated they were in complete remission[54]. A subsequent trial in 2015/2016, treated 40 patients with 100 kBq/kg of body weight at bi-monthly intervals, where 87% of surviving patients had a PSA decline of any degree and 63% of patients had a PSA decline >50%[51]. It should be noted, both patients in the first study and 10% of the patients in the second clinical trial experienced intolerable xerostomia[51,54]. In another recent clinical trial, 17 chemotherapy-naïve patients with advanced metastatic prostate cancer were treated[52]. The first cycle was 100 kBq/kg of body weight with subsequent cycles either increasing, remaining constant, or decreasing activity based on patient response[52]. Remarkably, seventy-one percent (12/17) of patients reported a PSA decline of >80% after only the first cycle[52]. A tolerable grade ½ xerostomia was found in all patients, indicating the de-escalation of the administrated dose is a possible way to minimize side effects while maintaining therapeutic efficacy[52]. Another approach to mitigate severe xerostomia was evaluated during a tandem study of [^{177}Lu]Lu-PSMA-

617 with low activity [^{225}Ac]Ac-PSMA-617[50]. Herein, 20 patients received 1.5 – 7.9 MBq of [^{225}Ac]Ac-PSMA-617, followed directly by 5.0 – 11.6 GBq of [^{177}Lu]Lu-PSMA-617[50]. Sixty-five percent (13/20) of patients had a PSA decline of >50%, and xerostomia was mild (grade 2) in only 25% (5/20) of patients[50]. This study suggests tandem therapy with [^{225}Ac]Ac-PSMA-617/[^{177}Lu]Lu-PSMA-617 can minimize xerostomia while also providing alternative therapeutic options for those who are resistant to [^{177}Lu]Lu-PSMA-617.

Table 1.3: Summary of clinical trials with Ac-225 unless otherwise specified (as of September 15, 2021)

Paper reference	Phase	Targeting Vector		# of patients	Administered ^{225}Ac
		mAb	Small molecule		
Juric 2011[45]	I	Lintuzumab		20	18.5 to 148 kBq/kg
Juric 2016[46]	I	Lintuzumab with low-dose Cytarabine		18	18.5 to 74 kBq/kg
Kratochwil 2016[54]	I		PSMA-617	2	100 kBq/kg
Kratochwil 2018[51]	I		PSMA-617	40	100 kBq/kg
Sathekge 2019[52]	I		PSMA-617	17	100 kBq/kg†
Sathekge 2020[53]	I/II		PSMA-617	73	100 kBq/kg†
Khreish 2020[50]	I		^{225}Ac-PSMA-617 with ^{177}Lu-PSMA-617	20	60 kBq/kg
Ballal 2020[47]	I		DOTATATE	32	100 kBq/kg
Zhang 2020[48]	I		DOTATOC	1	9.8 MBq
Królicki 2021[49]	I		DOTA-SP	21	10, 20, or 30 MBq

† patients originally received 100 kBq/kg and subsequent doses were determined based on patient response.

Currently, there are 4 [^{225}Ac]Ac-lintuzumab clinical studies in progress or actively recruiting; other ^{225}Ac clinical trials actively recruiting include: [^{225}Ac]Ac-JNJ-69086420

for advanced prostate cancer, [^{225}Ac]Ac-FP1-1434 for advance solid tumors[15]. With promising phase I/II ^{225}Ac clinical results and several ^{225}Ac clinical trials currently underway, the development of chelators that can form kinetically inert ^{225}Ac complexes under ideal conditions (quick kinetics and mild temperatures) with favourable biodistribution is essential.

1.12. Thesis Overview

This thesis presents the design, synthesis, and optimization of radiopharmaceuticals for targeted alpha therapy applications with actinium-225. Chapter 2 reports three novel radiopharmaceuticals: **2.1** (DOTA-CCZ-N-Me-α-CycMSH), **2.2** (Macropa-CCZ-N-Me-α-CycMSH), and **2.6** (Macropa-α-CycMSH) for targeted alpha therapy of malignant melanoma. Specifically, chapter 2 investigates the effect of choice of chelate and targeting vector/linker modifications on ^{225}Ac complexation, *in vitro* stability, and biodistribution of ^{225}Ac-radiopharmaceuticals. Chapter 3 reports the synthesis and characterization of two novel macrocyclic chelators (**3.6** and **3.12**) and their subsequent ability to complex ^{225}Ac. By directly comparing these novel chelators with previously reported chelators, the impact of donor arms on diaza-18-crown-6 ligands as chelators for ^{225}Ac is investigated.

Chapter 2.

Evaluating αMSH radiopharmaceuticals for ^{225}Ac targeted alpha therapy

2.1. Introduction

With over 80,000 cases a year in Canada, skin cancer is the most diagnosed cancer with more cases than breast, prostate, lung, and colon cases combined[61]. Skin cancer is categorized into two main types: melanoma skin cancer and non-melanoma skin cancer. Non-melanoma skin cancer includes basal cell carcinoma (BCC) and squamous cell carcinoma (SCC), which account for ~95 - 99% of all skin cancers[62]. While melanoma skin cancer only accounts for 1 - 5% of diagnosed skin cancers, it causes the majority of skin cancer related deaths[63]. For cancers that tend to metastasize such as malignant melanoma, early diagnosis and treatments are crucial for long-term survival[63]. Early-stage melanoma skin cancer has a 5-year survival of 88%, while late-stage melanoma has a 5-year survival rate of only 34%[1]. Diagnostic options include biopsy, ultrasound, CT, MRI, PET, and PET-CT[63]. Dependent on the stage of melanoma, treatment possibilities include surgically removing the melanoma (best for local, early-stage melanoma), radiation therapy used as adjuvant treatment, or oral medications/IVs for late-stage developments including immunotherapy, chemotherapy, and/or targeted therapy[63].

As malignant melanoma is one of the most resistant cancers to conventional chemotherapy, the development of immunotherapy and targeted therapy is of great interest[64]. Several specific markers for malignant melanoma cells have been studied[64]. With expression in nearly all melanomas (>80%) and low expression levels in normal tissues, melanocortin 1 receptor (MC1R) has been the focus antigen for melanoma targeted imaging and therapy[64]. The melanocortin (MC) family consists of five melanocortin receptors (MC1R to MC5R) that belong to G protein-coupled receptors[64]. Alpha-melanocyte stimulating hormone (α-MSH), a tridecapeptide is a non-selective naturally occurring ligand to the MC family of receptors (except MC2R)[64]. Impressively, α-MSH binds to MC1R with subnanomolar binding affinity (K_i = 0.23 nM)[65]. However, as an

endogenous peptide, α-MSH is subject to degradation *in vivo*. Over the past decade, α-MSH derivatives with improved *in vivo* stability and binding affinity to MC1R have been investigated[20,35,64]. The most promising α-MSH analogues contain lactam cyclization and unnatural amino acid substitution[23] (Nle^4-cyclo[Asp^5-His^6-D-Phe^7-Arg^8-Trp^9-Lys^{10}]; Nle-CycMSH) as illustrated in **Figure 2.1**.

Development and optimization of Nle-CycMSH based conjugates with chelator DOTA and series of linkers have been investigated for imaging[20–23]. The introduction of cationic piperidine linker allowed for high tumor uptake and rapid *in vivo* clearance for two derivatives ([^{68}Ga]Ga-CCZ01048[23] and [^{18}F]CCZ01064[20]). To date, only two studies investigated emerging radionuclide ^{225}Ac for possible melanoma targeting therapy with a Nle-CycMSH derivative[66,67]. Both studies used the same Nle-CycMSH based peptide with piperidine linker, but the chelate of choice differed, Ramogida *et al.,* evaluated gold standard DOTA[66] while Yang *et al.,* evaluated novel crown[67] chelate (**Figure 2.1**). *In vivo* biodistribution of [^{225}Ac]Ac-DOTA-α-CycMSH revealed moderate tumor uptake (5.2 ± 1.8% ID/g) 2 hours post injection. *In vivo* biodistribution of [^{225}Ac]Ac-crown-α-CycMSH revealed higher tumor uptake (12.7 ± 2.3% ID/g) 2 hours post injection.

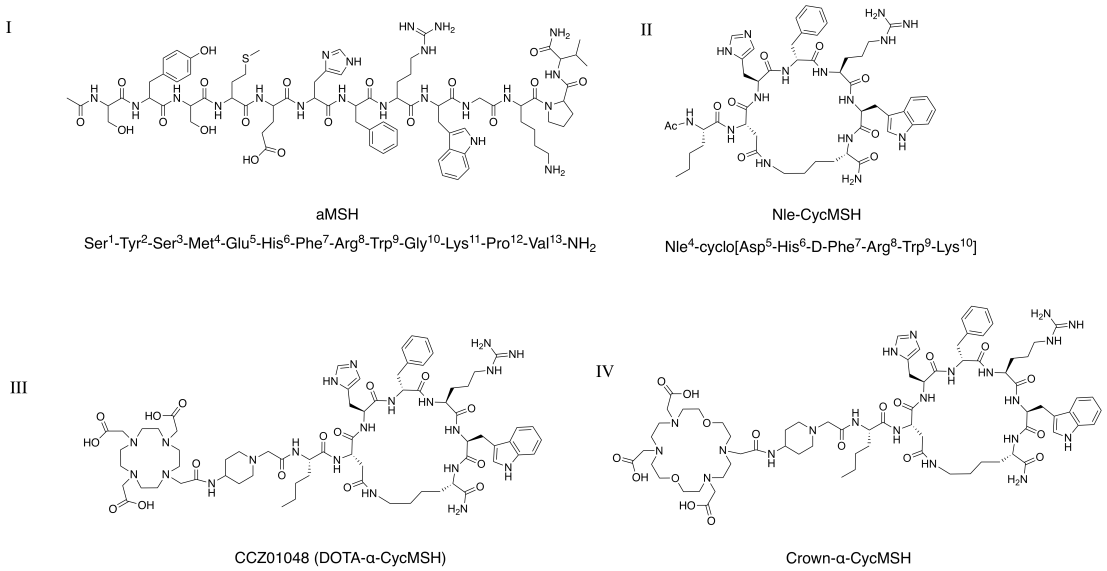

Figure 2.1: Structures of I) endogenous alpha-melanocyte stimulating hormone (α-MSH), II) Nle-CycMSH (an α-MSH analogue), III) DOTA-α-CycMSH, and IV) crown-α-CycMSH

2.2. Aim of the Project

Many tactics have been investigated for increasing tumor uptake and *in vivo* stability, reducing off-target uptake, and exhibiting rapid *in vivo* clearance[20–22,67–69]. Herein, I investigate the effect of some of those tactics with three novel radiotracers: **2.1** (DOTA-CCZ-N-Me-α-CycMSH), **2.2** (macropa-CCZ-N-Me-α-CycMSH), and **2.6** (VB-02-32/ macropa-α-CycMSH). The intrinsic characteristics of a chelator such as lipophilicity, charge, and coordination number can significantly impact the biodistribution of radiopharmaceuticals[67]. As such, I evaluate **2.6**, a macropa-α-CycMSH derivative - a direct comparison to DOTA[66] and crown[67]. Two novel tracers: **2.1** (DOTA) and **2.2** (macropa) contain slight linker and targeting vector modifications when compared to **2.5** to allow for longer blood circulation, theoretically increasing radiation dose delivery to tumor sites[68] (**Figure 2.2**). Due to patent protection, the structures of **2.1** and **2.2** cannot be disclosed. In this chapter, the ideal radiolabeling conditions, *in vitro* stability, and/or *in vivo* biodistribution of **2.1**, **2.2**, and **2.6** are determined.

2.3. Results/Discussion

2.3.1. Synthesis Methodology

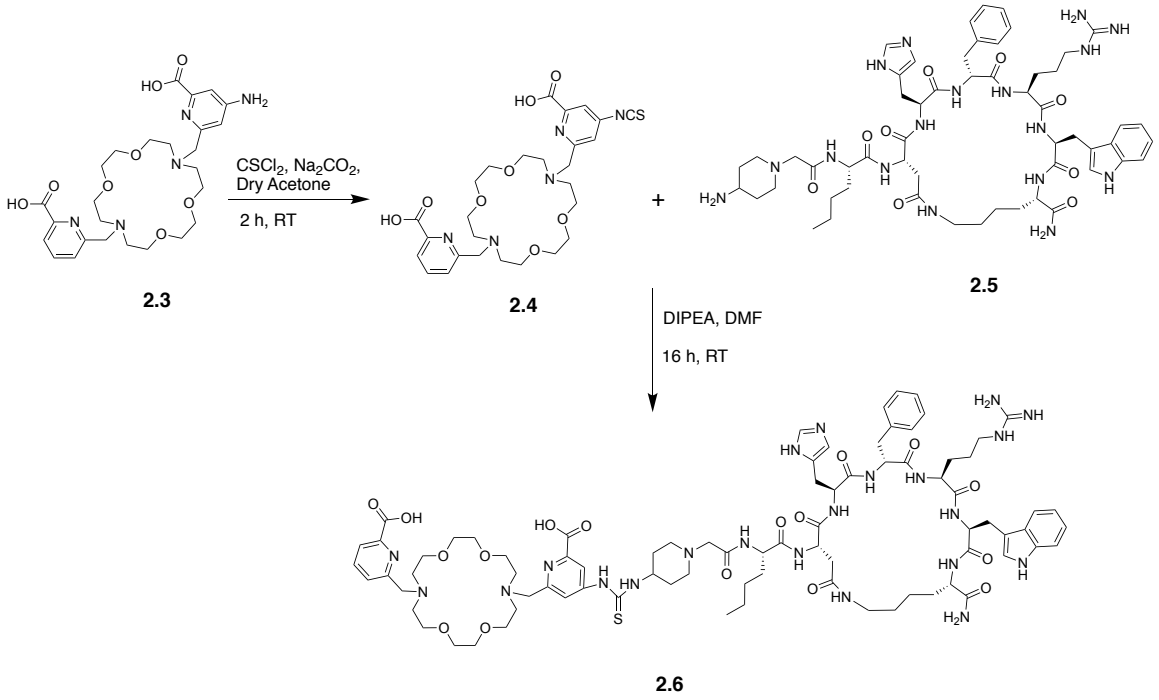

Scheme 2.1: Synthetic route of novel macropa-α-CycMSH bioconjugate 2.6

Both **2.1** (DOTA-CCZ-N-Me-α-CycMSH) and **2.2** (Macropa-CCZ-N-Me-α-CycMSH), were synthesized and characterized by Dr. Chengcheng Zhang at British Columbia Cancer Agency (BCCA). Peptide **2.5** was synthesized and characterized by Dr. Chengcheng Zhang at British Columbia Cancer Agency (BCCA). **2.6** (macropa-α-CycMSH) was synthesized following a modified procedure as per Thiele *et al.*[17] as shown in **Scheme 2.1**. Precursor macropa-NH_2 (**2.3**) was provided as a trifluoroacetic acid (TFA) salt by the Wilson group at Cornell University. Functionalization of **2.3** with thiophosgene and sodium carbonate in dry acetone formed the isothiocyanate **2.4**. Due to substantial light, moisture, and temperature sensitivity of **2.4**, the crude product was immediately carried forward to the next reaction after a quick workup. Conjugation of crude **2.4** and purified **2.5** (CCZ01048 peptide) yielded novel macropa-α-CycMSH bioconjugate **2.6**, which was purified via semi-preparative high performance liquid chromatography (HPLC) using method 2A, resulting in a low yield of 2.5%.

2.3.2. Actinium-225 radiolabeling and *in vitro* stability

Ideal radiolabeling conditions yield high specific activity products under mild temperatures (ambient – 40°C), quickly (<15 min is ideal) and with high (>90%) radiochemical yield. By adjusting the pH and temperature of the reaction, ideal radiolabeling conditions for **2.1**, **2.2**, and **2.6** (molar activity, M.A. = 20 kBq/nmol of ligand) were developed for low amounts of ^{225}Ac (<100 kBq). **2.1**, a DOTA construct requires elevated temperatures (85ºC) for 1 hr and a pH of ~ 6 to obtain quantitative radiochemical yield (RCY). When reaction temperatures were lowered to 75ºC and 65ºC insufficient complexation was achieved (between 18 – 42% RCY). Conversely, the macropa-CCZ-N-Me-α-CycMSH (**2.2**) derivative proved to be robust, with >99% RCY at ambient temperatures (25ºC) within 1 hr for a wide range of pHs (5 – 7). Macropa-α-CycMSH (**2.6**) was able to quantitatively label using the same conditions as macropa-CCZ-N-Me-α-CycMSH (pH ~ 6, 1 hr at ambient temperature).

Radiopharmaceuticals must be kinetically inert, such that when injected into patients the radionuclide is not transchelated with endogenous proteins within the blood. To determine the *in vitro* stability of **2.1**, **2.2**, and **2.6**, the radiometal-complexes were challenged with human serum (3:1 serum to:radiometal-complex) over 10 days. The results for the stability of [^{225}Ac]Ac-DOTA-CCZ-N-Me-α-CycMSH), [^{225}Ac]Ac-macropa-CCZ-N-Me-α-CycMSH, and [^{225}Ac]Ac-macropa-α-CycMSH are compiled in **Table 2.1**. All three tracers show excellent stability *in vitro*, remaining >90% intact after 7 days. While complex stability *in vitro* can indicate the kinetic inertness, caution must be taken as *in vitro* studies rarely accurately predict *in vivo* stability of the radiopharmaceutical[70]. As such, further studies to determine *in vivo* stability and biodistribution are warranted.

Table 2.1: Summary of 10-day *in vitro* human serum stability assay for novel radiotracers, with all reported data as % RCY (intact) at that specific time point (n = 3 for each data point)

	1 H	1D	3D	4D	5D	7D	8D	10D
2.1	>99	98.4 ± 0.2	96 ± 1.1	>99	N.D*	N.D*	91.1 ± 8.0	91.2 ± 5.9
2.2	>99	>99	>99	>99	N.D*	>99	N.D*	>99
2.6	>99	>99	>99	N.D*	97.5 ± 2.6	94.4 ± 4.1	N.D*	N.D*

* N.D – no data

2.3.3. Biodistribution Results

Biodistribution studies require high purity, carrier-free ^{225}Ac extracted from uranium-233 (^{223}U, $t_{1/2}$ = 1.6 x 10^5 y) decay (source A, *vide infra).* With limited pure radionuclide supply, the biodistribution of only **2.1** and **2.2** were investigated herein.

2.1 was precluded from *in vivo* studies due to low % RCY (<10%) during radiolabeling with high amounts of ^{225}Ac (8.71 MBq). As such, the biodistribution of [^{225}Ac]Ac-macropa-CCZ-N-Me-α-CycMSH (M.A = 1.38 MBq/nmol) was evaluated for two different injected radioactivities. A total of 8 (n = 4) B16F10 tumor bearing mice were injected with either dose 1 (103.6 kBq/75 pmol of ligand) or dose 2 (51.8 kBq/37.5 pmol of ligand). After two hours post injection (2 hr p.i.), all mice were sacrificed, and the harvested organs of interest were measured immediately after sacrifice and after secular equilibrium was met (>6 hr). As there was no statistical difference between time points, results are reported after equilibrium was met. [^{225}Ac]Ac-macropa-CCZ-N-Me-α-CycMSH demonstrated quick excretion through the renal system, with moderate-to-high uptake in the bladder, kidneys, and urine. Moderate off-target uptake was observed for the spleen (1.85 ± 0.64% ID/g), blood (2.13 ± 0.33 % ID/g), and gall bladder (3.35 ± 0.66 % ID/g), while more significant uptake was seen in the liver (5.93 ± 0.4 % ID/g). Tumor uptake was low at 2.50 ± 0.49 and 0.67 ± 0.11 % ID/g for dose 1 and dose 2 respectively (see **Figure 2.2**). With low tumor and moderate off-target uptake, [^{225}Ac]Ac-macropa-CCZ-N-Me-α-CycMSH demonstrates poor tumor-to-normal tissue ratios (**Table 2.2**).

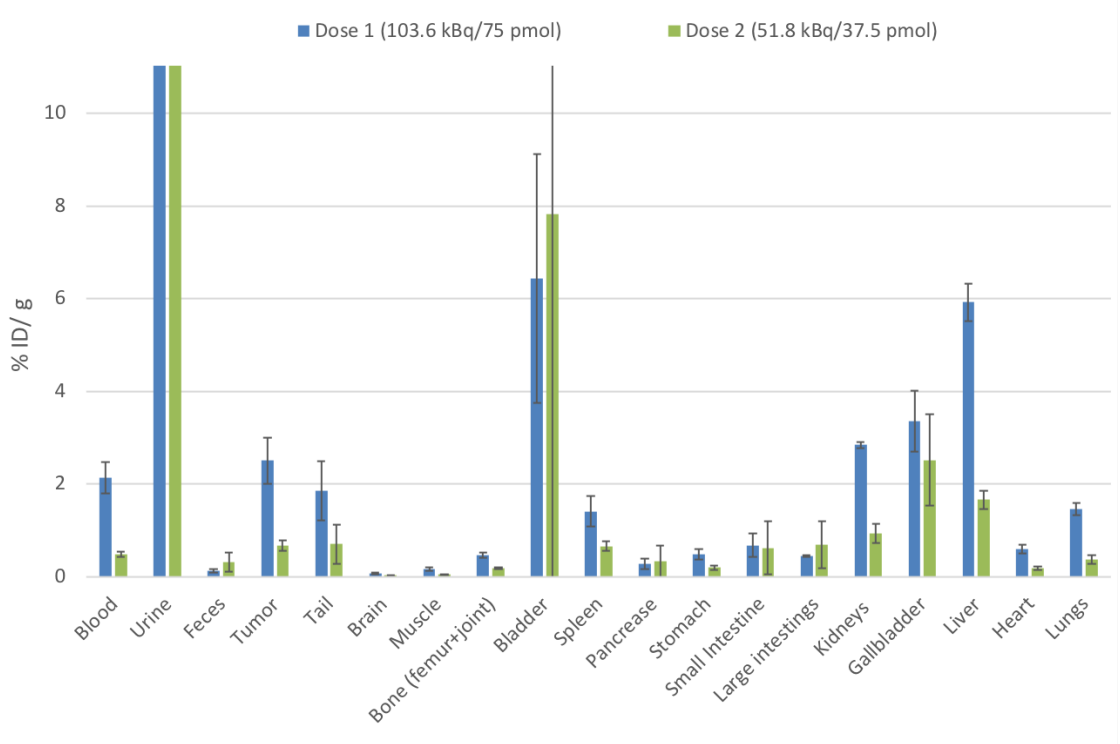

Figure 2.2: **Biodistribution of [^{225}Ac]Ac-macropa-CCZ-N-Me-α-CycMSH at 2 hr post-injection for dose 1 (103.6 KBq/75 pmol of ligand) and dose 2 (51.8 kBq/37.5 pmol of ligand) in B16F10 tumor bearing mice**

Table 2.2: **Summary of tumor-to-normal tissue ratios for [^{225}Ac]Ac-macropa-CCZ-N-Me-α-CycMSH at 2 hr post-injection for dose 1 (103.6 KBq/75 pmol of ligand) and dose 2 (51.8 kBq/37.5 pmol of ligand)**

	Tumor	Tumor: kidney	Tumor: blood	Tumor: liver	Tumor: spleen	Tumor: gallbladder
Dose 1	2.50 ± 0.49	0.88 ± 0.16	1.17 ± 0.18	0.42 ± 0.07	1.80 ± 0.46	0.78 ± 0.24
Dose 2	0.67 ± 0.11	0.71 ± 0.21	0.73 ± 0.12	0.40 ± 0.05	1.03 ± 0.21	0.33 ± 0.24

*all results are reported as %ID/g, measured in window A (80 – 120 keV)

One explanation for the low tumor uptake is the sub-optimal radiopharmaceutical preparation and formulation conditions: I) [^{225}Ac]Ac-macropa-CCZ-N-Me-α-CycMSH was prepared the day before injection, allowing for significant radiolysis and 2) purification of the tracer was performed via Sep-Pak (compared to HPLC purification). In a recent study, the optimal preparation and formulation of [^{225}Ac]Ac-crown-α-CycMSH was evaluated by varying the time of preparation, purification of tracer, and addition of radiolytic protectant L-ascorbate[67]. The construct prepared the day before injection, even

with the addition of L-ascorbate was low (4.84 ± 3.2 % ID/g). Constructs prepared the same day as injection with L-ascorbate saw a dramatic increase in tumor uptake (12.7 ± 2.3 % ID/g). Moreover, the tracers prepared the same day as injection had minimal uptake in non-target tissues, leading to superior tumor-to-blood, bone, and kidney ratios. Radiolysis of [^{225}Ac]Ac-macropa-CCZ-N-Me-α-CycMSH could lead to peptide degradation resulting in low tumor uptake or destroy the chelator encapsulating ^{225}Ac. Consequently, the intrinsic affinity of unbound ^{225}Ac can cause high off-target uptake in the liver, spleen, skeleton, and kidneys[56]. Another possible explanation for off-target uptake in the urine, kidneys, and blood is the intrinsic affinity of the ejected radioactive daughters ^{221}Fr and ^{213}Bi for these organs (*vide supra* - **Table 1.2**). The purification of the tracer via HPLC, the addition of a radiolytic protectant, and/or immediate injection could minimize degraded [^{225}Ac]Ac-macropa-CCZ-N-Me-α-CycMSH being injected into the mouse, ultimately increasing tumor uptake and decreasing off-target uptake.

2.4. Conclusion & Future Work

In chapter 2, three novel radiopharmaceuticals for malignant melanoma therapy, **2.1** (DOTA-CCZ-N-Me-α-CycMSH), **2.2** (macropa-CCZ-N-Me-α-CycMSH), and **2.6** (macropa-α-CycMSH) were examined. Macropa constructs (**2.2** and **2.6**) were robust with >99% RCY at ambient temperatures for a wide range of pHs (5 – 7), whereas DOTA construct **2.1** required elevated temperatures (85 ºC) for 1 hr to obtain a quantitative radiochemical yield. The kinetic inertness was studied *in vitro* via a human serum stability assay, wherein all three radiopharmaceuticals exhibited favourable stability with >90% RCY after 7 days. The biodistribution of [^{225}Ac]Ac-macropa-CCZ-N-Me-α-CycMSH was investigated for two doses (103.6 KBq/75 pmol of ligand or 51.8 kBq/37.5 pmol of ligand). Tumor uptake was low at 2.50 ± 0.49 and 0.67 ± 0.11 % ID/g for dose 1 and dose 2 respectively, while off-target uptake was moderate leading to low tumor-to-normal tissue ratios. A possible explanation for low tumor & moderate normal tissue uptake is the preparation and formulation of [^{225}Ac]Ac-macropa-CCZ-N-Me-α-CycMSH, but further studies need to be performed to confirm. Many tactics have been investigated for increasing tumor uptake and *in vivo* stability, reducing off-target uptake, and exhibiting rapid *in vivo* clearance[20–22,67–69]. As intrinsic characteristics of a chelator and linker can significantly

impact the biodistribution of radiopharmaceuticals[67], this chapter aimed to study those effects *in vivo*.

Future work for this project is dependent on the purity of supplied ^{225}Ac. If high purity, carrier-free ^{225}Ac extracted from uranium-233 is available, further animal studies can be performed. Specifically, an *in vivo* biodistribution study of **2.2** and **2.6**, wherein [^{225}Ac]Ac-macropa-CCZ-N-Me-α-CycMSH and [^{225}Ac]Ac-macropa-α-CycMSH are prepared the day of injection, with L-ascorbate, and purified via HPLC, should be conducted in the future. The biodistribution evaluation of **2.6** is a direct comparison to [^{225}Ac]Ac-crown-α-CycMSH and [^{225}Ac]Ac-DOTA-α-CycMSH investigating the effect of chelator choice on *in vivo* biodistribution. The biodistribution of [^{225}Ac]Ac-**2.2** prepared with optimized radiopharmaceutical preparation and formulation conditions will provide experimental reasoning for the low tumor uptake and high non-target tissue of [^{225}Ac]Ac-macropa-CCZ-N-Me-α-CycMSH.

2.5. Experimental

2.5.1. Materials and Methods

All solvents and reagents were purchased from commercial suppliers (TCI America, Fisher Scientific, Macrocyclic, and Sigma Aldrich). Solvents noted as "dry" were obtained following storage over 3 Å molecular sieves. ^{1}H and ^{13}C NMR spectra were referenced to the residual solvent peak and recorded at 25 ^{o}C (unless noted otherwise) on Bruker AV400, AV500, or AV600 instruments. Deionized water (>18 MΩ cm) was used via Millipore-Direct (Milli-Q IQ 7000) purification. High-resolution electrospray-ionization mass spectrometry (HR-ESI-MS) was performed on an Agilent 6210 time-of-flight instrument (TOF). The semi-preparative HPLC used for the purification of non-radioactive compounds was an Agilent 1100 series consisting of a G1311A Quaternary Pump, G2260A autosampler, and G1315B variable wavelength absorbance detector. Purification was performed with a Kinetex semi-preparative C18 column, 5 μm, 100 Å, 150 x 10.0 mm at a flow rate of 3.0 mL/min unless otherwise noted. Gradient HPLC methods utilized a binary mobile phase that contained H_2O with 0.1 % TFA (A) and

Acetonitrile (CH_3CN) with 0.1 % TFA (B). HPLC Method 2A: 10% B (0 – 5 minutes), 10 – 100% B (5 – 40 minutes).

$^{225}Ac/^{225/227}Ac^{\dagger}$ radiolabelling reactions were monitored via aluminum backed silica thin layer chromatography (TLC) plates (TLC-SG, silica gel 60, F_{254}, MERCK, Germany). Developed TLC plates were counted using an AR-2000 imaging scanner equipped with PD-10 gas and analysis of RCYs was carried out using WinScan V3_14 software at least 8 h later to allow for daughter isotopes to decay completely. Radioactivity and radionuclidic purity were determined using a High Purity Germanium (HPGe) detector (Mirion Technologies (Canberra) Inc.) with Genie 2000 software by measurement of gamma emission lines for ^{213}Bi ($t_{1/2}$ = 45.6 min, 440 KeV, 25.9% abundance) and ^{221}Fr ($t_{1/2}$ = 4.9 min, 218 KeV, 11.4% abundance).

2.5.2. Synthesis Methodology

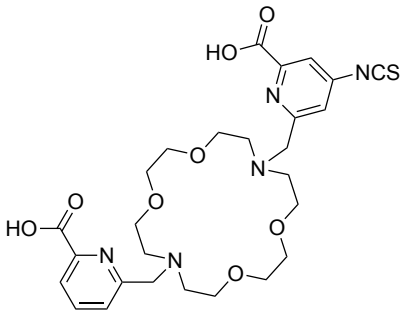

6-((16-((6-carboxypyridin-2-yl)methyl)-1,4,10,13-tetraoxa-7,16-diazacycloocta decan -7-yl)methyl)-4-isothiocyanatopicolinic acid (macropa-NCS, 2.4). Macropa-NCS was prepared with slight modifications from previously published procedures[17]. $CSCl_2$ (50 µL, 0.7 mmol, 20 Eq) was slowly added to a suspension of Macropa-NH_2·4 TFA (**2.3**; 4-Amino-6-((16-((6-carboxypyridin-2-yl)methyl)-1,4,10,13-tetraoxa-7,16- diaza-cyclooctadecan-7-yl)methyl)picolinic acid) reported in Thiele *et al.*, (30 mg, 29.9 µmol, 1 Eq) and Na_2CO_3 (47.5 g, 0.5 mol, 15 Eq) in dry acetone (3 mL). After stirring the reaction for 3 hours under argon at room temperature, the solvent was removed under reduced pressure. ESI-MS calcd. for $[C_{27}H_{35}N_5O_8S + 2H]^{+2}$: 295.61787; found 295.6 $[(M+2H)]^{+2}$. No NMR was obtained for this product.

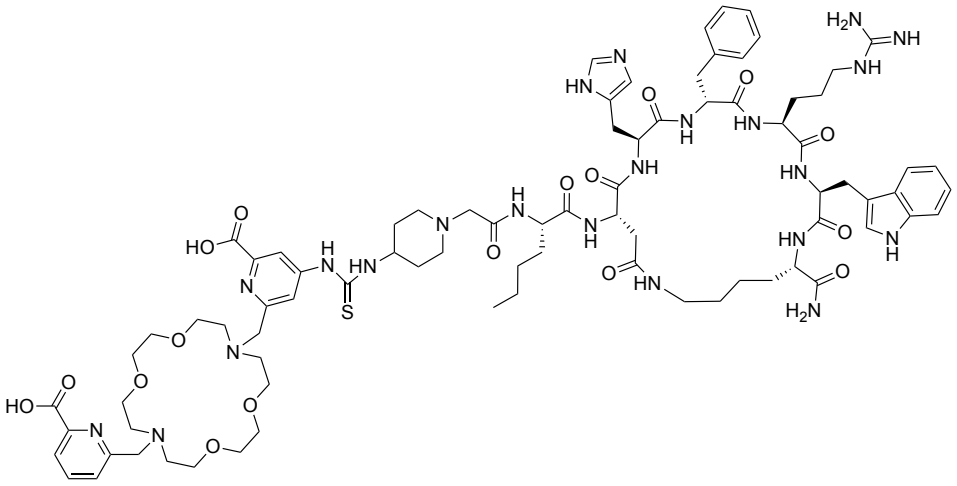

4-(3-(1-(2-(((S)-1-(((3S,6S,9R,12S,15S,23S)-12-((1H-imidazol-5-yl)methyl)-3-((1H-indol-3-yl)methyl)-9-benzyl-23-carbamoyl-6-(3-guanidinopropyl)-2,5,8,11,14,17-hexaoxo-1,4,7,10,13,18-hexaazacyclotricosan-15-yl)amino)-1-oxohexan-2-yl) amino)-2-oxoethyl)piperidin-4-yl)thioureido)-6-((16-((6-carboxypyridin-2-yl)methyl)-1,4,10,13-tetraoxa-7,16-diazacyclooctadecan-7-yl)methyl)picolinic acid (VB-02-32, 2.6). N-N-Diisopropylethylamine (DIPEA; 25 µL, 0.14 mmol, 20 Eq) was added to a solution of macropa-NCS (9.8 mg, 16.6 µmol, 2 Eq) and purified CCZ01048 peptide **2.5** (8 mg, 7.1 µmol, 1 Eq) in dry dimethylformamide (DMF; 0.75 mL) After stirring the reaction overnight (12 h) under argon at room temperature, the solvent was removed under reduced pressure. The solid was re-dissolved in 23% CH_3CN (with 0.1 % TFA) and purified via HPLC, using method 2A to yield a colourless oil (300 µg, yield = 2.5%). ESI-MS calcd. for $[C_{82}H_{113}N_{22}O_{17}S + H]^+$: 1711.852578; found 1711.8 [M+H]. No NMR was obtained for this product.

2.5.3. ^{225}Ac Sources

Two sources of Actinium-225 were used within this chapter: A) ^{225}Ac extracted from uranium-233 (^{223}U) decay and B) ^{225}Ac produced from irradiated thorium (^{232}Th(p,x) $^{225/227}$Ac†). Actinium-225 acquired from uranium-233 decay (Source A) was obtained from Canadian Nuclear Laboratories (CNL) and purified via a DGA resin as described in Ramogida *et al*[66]*.,* to ensure radionuclide purity. $^{225/227}$Ac† acquired from irradiated thorium (Source B) was obtained from TRIUMF and the separation of $^{225/227}$Ac† from irradiated thorium was performed as described in Robertson *et al*. 2020[71]. The ^{225}Ac was received as

a 0.01 M HNO_3 solution in final concentrations of either 93.5 or 29.2 kBq/μL. The $^{225/227}Ac^{\dagger}$ was received as a 0.01 M HNO_3 solution in final concentrations of 50.9 kBq/μL.

2.5.4. ^{225}Ac Radiolabeling Studies

Stock solutions (1x 10^{-3} M) of **2.1**, **2.2**, and **2.6** were made with ultra-pure deionized water. Temperature-dependent and pH-dependent radiolabeling studies were performed by the addition of $^{225/227}Ac^{\dagger}$ or ^{225}Ac (~100 kBq) to a solution containing ligand sock (5 μL; or deionized water for negative controls) in either 0.2 M sodium acetate (NaOAc) pH 6.0 or 0.2 M NaOAc pH 7. The actinium reaction mixtures were gently agitated using a vortex mixer and the pH was confirmed to be between 5 - 7 by spotting a portion (1 - 2 μL) of the reaction mixture on pH paper. The radiochemical yield (RCY) was analyzed after 30 and/or 60 minutes at room temperature/elevated temperatures. The iTLC plate system used was: Method A - aluminum backed silica with citrate buffer (0.4 M, pH 4.0). Free ^{225}Ac migrates with the solvent front ($R_f = 1$) while ^{225}Ac-ligand complexes will remain at the baseline ($R_f = 0$).

TLC radio-chromatograms of the radiolabeling (with ligand and control) can be found in the Appendix. Measurements were performed in triplicate.

2.5.5. Human Serum Stability

The ^{225}Ac-complexes (**2.1**, **2.2**, and **2.6**) were prepared using the pre-determined ideal radiolabeling conditions as described above. After confirming a radiochemical yield >95% by TLC, 180 μL of human serum (3:1 volume, stored at −5°C and thawed at ambient temperature) was added to each radiolabeling solution (60 μL). A control was also prepared using water instead of ligand. At various times (1 hr to 7 d), small aliquots (3 – 7 μL) were spotted on iTLC plates and developed using Method A (*vide supra*) described above.

TLC radio-chromatograms of the serum competition assay (with ligand and control) can be found in the Appendix. Measurements were performed in triplicates.

2.5.6. *In Vivo* Biodistribution

Animal experiments were conducted according to the guidelines established by the Canadian Council on Animal Care and approved by Animal Ethics Committee of the University of British Columbia. B16F10 tumors were inoculated by injection of 1 x 10^6 B16F10 cells on the right shoulder of each mouse. A total of eight female C57BL/6J mice were used in biodistribution studies for two doses of macropa-CCZ-N-Me-α-CycMSH (*n* = 4 for each dose) once the tumor grew to ~ 8 – 10 mm in diameter.

Radiotracers were prepared with a high specific activity (>200 kBq/nmol) with the predetermined ideal radiolabeling conditions. Purification of the radiotracers was performed by loading the radiolabeling reactions onto a pre-conditioned C18 Light SepPack to remove free $^{225}Ac^{3+}$, collecting the purified peptide in 100% ethanol. The radiotracers were further diluted with 0.9% NaCl saline, ensuring the % ethanol concentration was <10% by volume in the final formulation to minimize undesired ethanol effects seen in mice. Quality control reactions were conducted in parallel and analyzed via iTLC to ensure >98% chemical purity by preparing an unlabeled reaction of ^{225}Ac in buffer solution. Through an intravenous tail injection, 100 µL of the purified radiolabeling reactions was injected into each mouse, recording the time of injection. After 2 hours, the mice are sacrificed by CO_2 asphyxiation under isoflurane anesthesia. Cardiac puncture was promptly performed to recover blood and the organs of interest are harvested, rinsed with 1 x phosphate buffered saline (PBS), and blotted dry. Organs of interest were weighed and measured via a calibrated gamma counter (Packard Cobra II Auto-gamma counter, Perkin Elmer, Waltham, MA, USA) using energy windows A) 60 – 120 keV and B) 180 – 260 keV. Counting was performed immediately after sacrifice and after secular equilibrium was met. Radioactivity was decay corrected and normalized to injected dose and expressed as the percentage of the injected dose per gram of tissue. No differences were noted between the data measured immediately and at equilibrium, or between different energy windows; therefore, the biodistributions are reported using the data acquired after equilibrium using window A.

Chapter 3.

Optimizing pendant donor arms of diaza-18-crown-6 ligands as chelators for ^{225}Ac

3.1. Introduction

A chelator with ideal radiolabeling conditions (*vide supra*) can be achieved by tuning the chelator to the radiometal properties such as coordination number/geometry, ligand donor atom preference, ionic radius, and charge[72]. As mentioned, the highly cytotoxic actinium-225 ($^{225}Ac^{3+}$) is a promising radionuclide for targeted alpha therapy with several remarkable clinical trials. With a lack of fundamental knowledge for actinium, chelators for actinium-225 are tuned on the basis that it is the largest trivalent actinide with a preference for oxygen donors and a coordination number of 8 or 10.

Initially polyaminocarboxylate and polyaminophosphonate chelates were screened for their ability to coordinate ^{225}Ac and form stable complexes *in vitro* and/or *in vivo*[13,55–57] (see **Figure 3.1**). McDevitt *et al.,* compared ^{225}Ac complexation with DTPA, DOTA, TETA, DOTPA, TETPA, and DOTMP at 37ºC after 2 hours[55]. Only DOTA and DOTMP were successful in chelation, with 100% and 78% radiochemical yields respectively[55]. When challenged with 25% serum, the ^{225}Ac-DOTMP complex rapidly dissociated while the DOTA complex retained >90% intact after 10 days[55].

HEHA was one of the first novel macrocyclic chelators specifically designed for ^{225}Ac complexation[73]. With pendent carboxylate arms and polyaza core, HEHA (N_6O_6) is structurally similar to DOTA (N_4O_4) with a larger macrocyclic core[73]. Deal *et al*., compared the in vivo stability of HEHA to EDTA, CHX-A"-DTPA, PEPA, and DOTA (alongside acetate as a control)[73]. Quantitative complexation (>95%) was obtained within 30 minutes at 40ºC for all ligands except PEPA (80%)[73]. The [^{225}Ac]Ac-DOTA complex had significantly decreased uptake in the liver (3.3 % ID/g) and exhibited quicker excretion than EDTA, CHX-A"-DTPA, and PEPA. [^{225}Ac]Ac-HEHA had the lowest organ uptake, with <0.3% ID/g of radioactivity after 5 days in any organ[73]. However, the authors speculate the overall -3 charge of the complex caused extremely fast excretion, giving the

illusion of *in vivo* stability[73]. When the *in vitro* stability of [^{225}Ac]Ac-HEHA-antibody conjugates were evaluated, >50% decomposed after 24 h[73]. While a larger 18-membered macrocyclic cavity of HEHA may be better matched to large $^{225}Ac^{3+}$ ion, the overall charge may not be suitable for *in vitro* and *in vivo* stability. DOTA, the only initial chelate that provided complexation, *in vitro* and *in vivo* stability is considered the current gold standard in ^{225}Ac chelation chemistry.

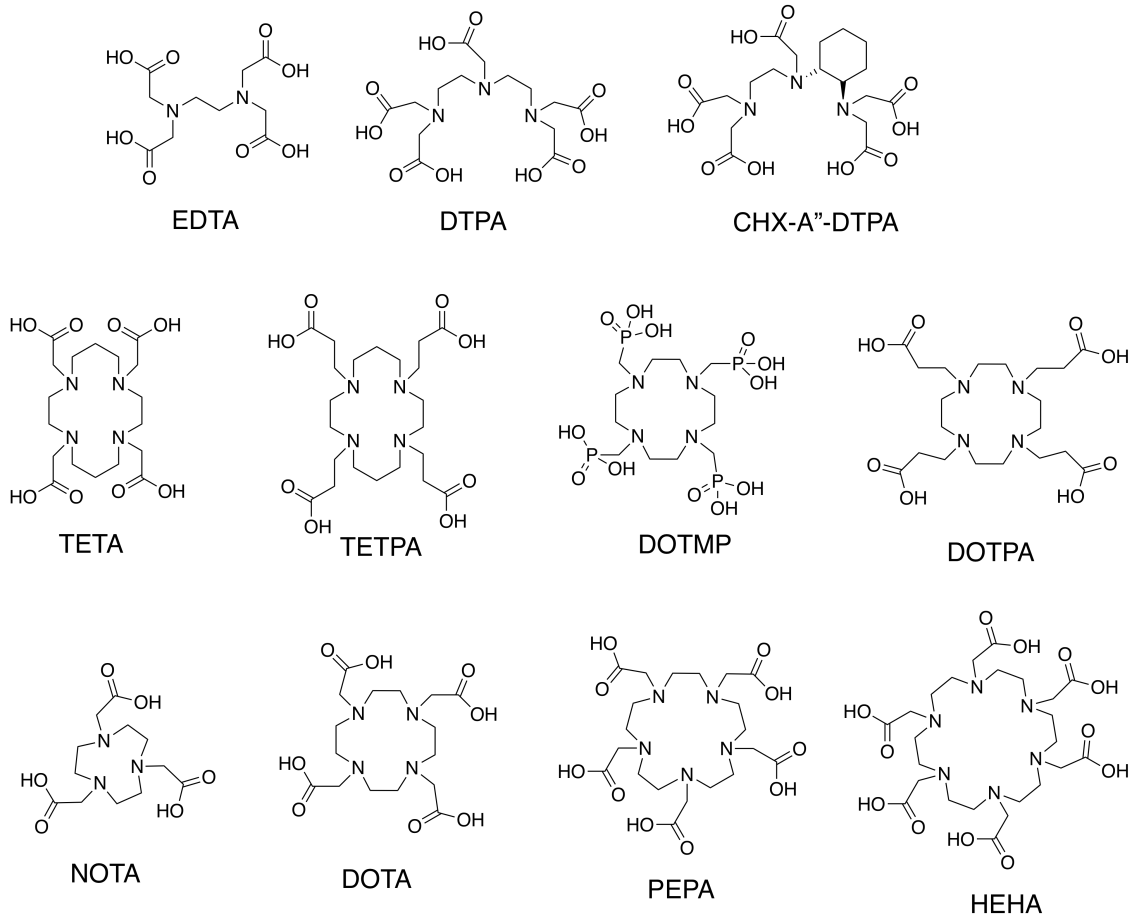

Figure 3.1: Structures of acyclic and macrocyclic chelators initially investigated for actinium-225

With an intrinsic preference for smaller metal ions and slow complexation, DOTA is a mediocre "gold standard" for ^{225}Ac. In the past decade, there have been significant efforts in developing ^{225}Ac chelates that form kinetically inert complexes quickly under mild temperatures[17,18,66,67,72,74]. Various macrocyclic and acyclic chelates have been proposed for $^{225}Ac^{3+}$ chelation; the majority of which outperformed DOTA at ambient temperatures[17,66,67,72,74]. Notably, 5 chelates (CHX-octapa[66], py4pa[74], noneunpa[72],

macropa[17] and crown[67], **Figure 3.2**) can successfully complex $^{225}Ac^{3+}$ (RCY >90%) at ambient temperatures with chelator concentrations as low as 10^{-6} M within one hour. Moreover, they have shown favourable *in vitro* stabilities via a human serum and/or a lanthanum competition assay (**Table 3.1**). However, only crown, macropa, py4pa were further investigated via biodistribution studies when conjugated to CycMSH[67] (for malignant melanoma), RPS-070[75] (a PSMA derivative for prostate cancer), and Trastuzumab[74] (for ovarian cancer) respectively. Perhaps the most interesting fact is that these five promising ligands weren't reported for ^{225}Ac complexation until 2017 – 2021, demonstrating much of ^{225}Ac fundamental chelation including predicting chemical structures of ligands that complex actinium and exhibit *in vitro* and *in vivo* stability is unknown.

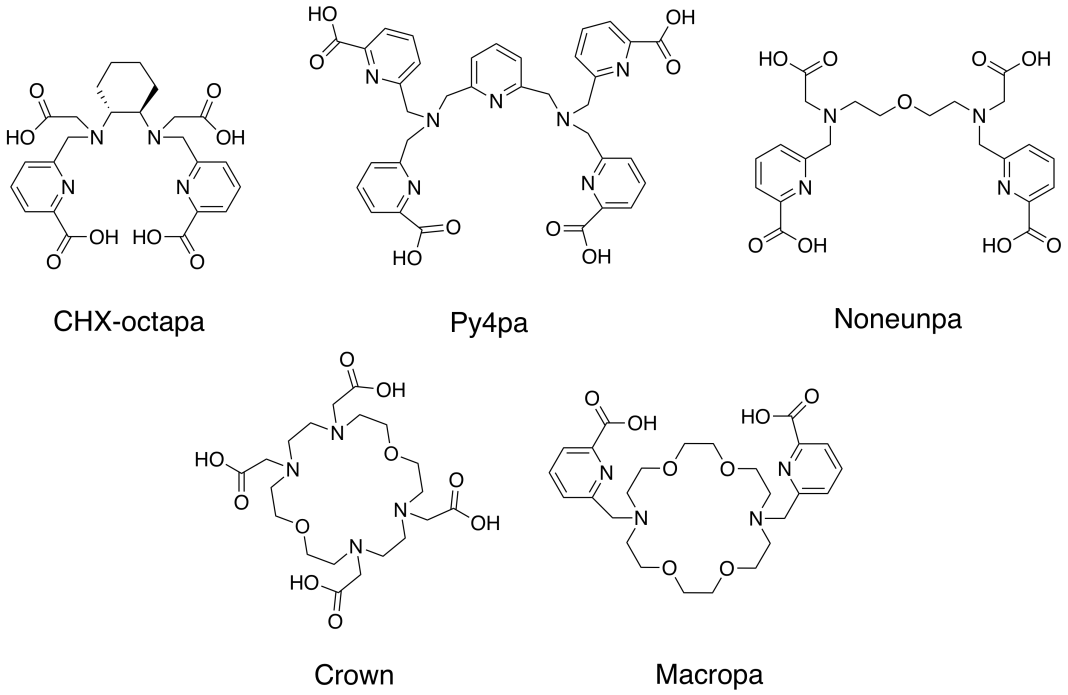

Figure 3.2: Structures of CHX-octapa, py4pa, noneunpa, crown, and macropa chelators discussed

Table 3.1: Labeling, *in vitro* and *in vivo* data for CHX-octapa, py4pa, noneunpa, crown, and macropa chelators discussed

Chelator	Labeling (at 10^{-6} M)	*In Vitro* Stability (% intact)		*In vivo*
		La^{3+}	Serum	
CHX-octapa[66]	~ 94% RCY at ambient temp within 30 min	4% over 7 d	96% over 7 d	N.D*
py4pa[74]	~ 97% RCY at ambient temp within 30 min	N.D*	99% over 7 d	Yes - high tumor uptake & moderate normal tissue uptake
noneunpa[72]	>95% RCY at ambient temp within 10 min	N.D*	90% over 7 d	N.D*
macropa[17]	>99% RCY at ambient temp within 5 min	91% over 7 d	90% over 7 d	Yes – high tumor uptake & moderate/low normal tissue uptake[17,75]
crown[67]	>96% RCY at ambient temp within 10 min	18.8% over 5d	90% over 5 d	Yes - high tumor uptake & low normal tissue uptake

3.2. Aim of Project

With the reported success of macropa (N_4O_6), two novel ligands (**3.6** and **3.12**) with similar characteristics were designed; a diaza-18-crown-6 macrocyclic ligand with hydroxypyridinone (HOPO) groups. The HOPO groups offer hard oxygen donors, and HOPO derivatives have proven complexation with $^{89}Zr^{4+}$, Fe^{3+}, Ga^{3+}, and several actinides. Recently, Fiszbein *et al.,* investigated the impact of donor arms on diaza-18-crown-6 ligands as chelators for ^{213}Bi[76]; macropa, macroquin-SO_3, and macropaquin exhibited impressive ^{213}B complexation. Herein, I investigate, **3.6** (macrohopo), **3.12** (macrohopo′), **3.13** (macroquin-SO_3), **3.14** (macropaquin), **3.15** (macropa), and standard DOTA for ^{225}Ac complexation. The focus of this chapter is to study the effect of varied rigidity, coordinating atoms (N_4O_6 vs N_2O_6), and pendant donor arm basicity of diaza-18-crown-6 macrocyclic chelators on the ability to complex ^{225}Ac.

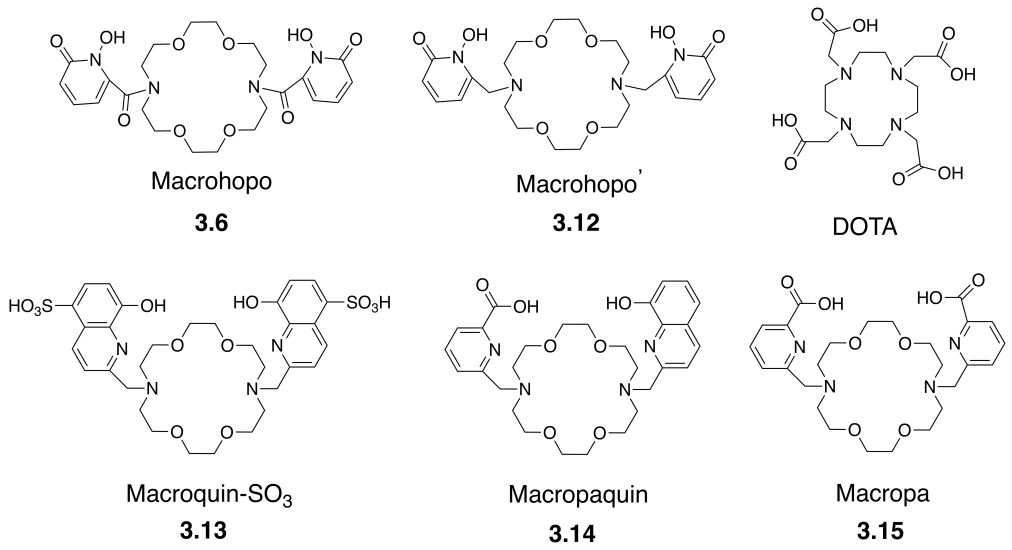

Figure 3.3: Structures of chelators DOTA, macropa, macropaquin, macroquin-SO_3, novel macrohopo and macrohopo′ investigated in this chapter

3.3. Results/ Discussion

The ligands investigated, **3.6** (macrohopo), **3.12** (macrohopo′), **3.13** (macroquin-SO_3), **3.14** (macropaquin), **3.15** (macropa), and standard DOTA feature varied intrinsic characteristics (as seen in **Figure 3.3**) which can affect the ligands ability to complex ^{225}Ac and therefore ^{225}Ac radiolabeling efficiency and complex stability with each ligand should be studied.

3.3.1. Synthesis and characterization

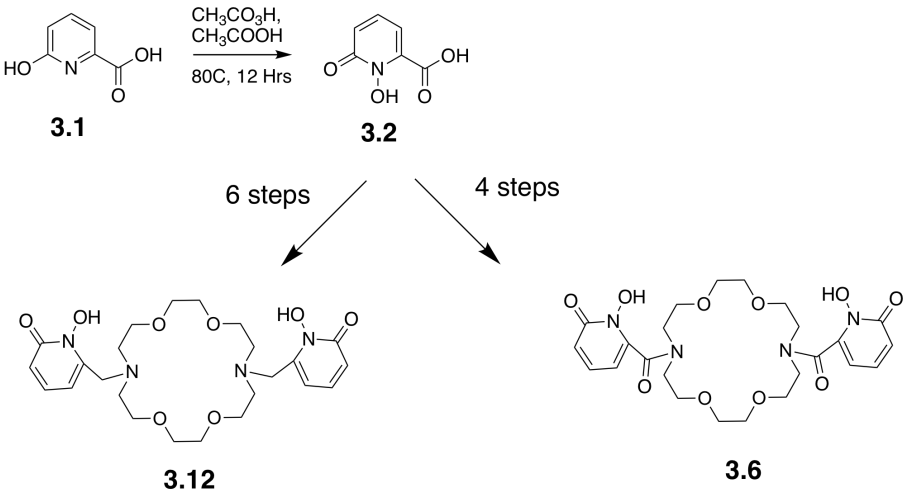

Scheme 3.1: Outlined synthesis of macrohopo (3.6) and macrohopo′ (3.12) from same starting material; 6-hydroxypicolinic acid (3.1)

As illustrated in **Scheme 3.1**, macrohopo (**3.6**) and macrohopo′ (**3.12**) were synthesized from the same commercially available starting reagent; 6-hydroxypicolinic acid (**3.1**). Oxidation of **3.1** with peracetic acid and glacial acetic acid formed **3.2** as a pale pink solid in good yield (81%). After the first step, **3.6** and **3.12** were synthesized through two separate routes as demonstrated in **Scheme 3.2** and **Scheme 3.3**.

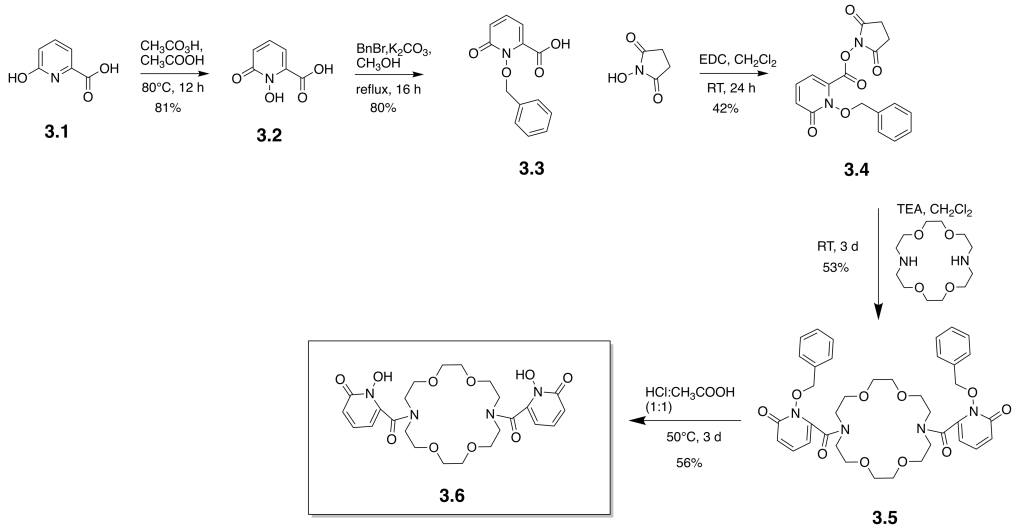

Scheme 3.2: Synthesis of precursors 3.2 – 3.5 and macrohopo (3.6)

Protection of **3.2** via benzyl bromide and potassium carbonate in methanol formed benzyl protected acid **3.3** as a peach solid in good yield (80%). Subsequent reaction of **3.3** with *N*-hydroxysuccinimide and 1-ethyl-3-(3-dimethylaminopropyl) carbodiimide (EDC) formed succinimide **3.4**, which was purified by silica column chromatography obtaining a white crystalline solid in moderate yield (42%). Coupling of **3.4** with commercially available 4,13-diaza-18-crown-6-ether produced **3.5.** After two silica column purifications, **3.5** was achieved as a white solid in moderate yields (53%). Deprotection of **3.5** with 1:1 v:v of concentrated hydrochloric acid and acetic acid formed the final ligand **3.6** which was purified via preparative high performance liquid chromatography (HPLC) using method 3A, resulting in a good yield of 56%.

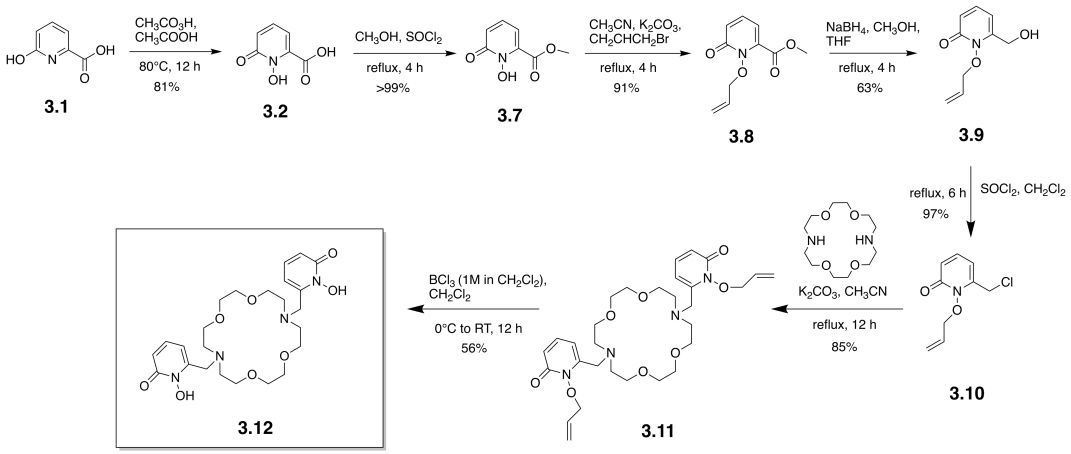

Scheme 3.3: Synthesis of precursors 3.7 – 3.11 and macrohopo′ (3.12)

Products **3.2** – **3.10** have been previously reported and were synthesized following established procedures[77]. The addition of thionyl chloride ($SOCl_2$) in methanol produced methyl ester **3.7** in quantitative yields (>99%). Subsequent protection with allyl bromide and potassium carbonate in acetonitrile (CH_3CN) yielded **3.8** as a pale brown/orange solid in good yield (91%). Reduction of the protected methyl ester **3.8** with sodium borohydride in methanol formed the protected alcohol **3.9** in moderate yields (63%). Halogenation of **3.9** with thionyl chloride in dry dichloromethane (DCM) produced **3.10** in excellent yields (97%). Conjugation of **3.10** with commercially available 4,13-diaza-18-crown-6-ether produced **3.11**. Products **3.7** to **3.10** were easily worked up with minimal purification. While **3.11** required two separate silica column purifications to produce a brown solid (yield = 85%). Subsequent deprotection of **3.11** with boron trichloride (1M in dry DCM)

formed **3.12** as a brown solid. **3.12** was purified via preparative high performance liquid chromatography (HPLC) using method 3A, resulting in a moderate yield of 56%.

Intermediates **3.2** – **3.5** and **3.7** – **3.11** were fully characterized using high resolution electrospray ionization mass spectrometry (HR-ESI-MS) and NMR (^{1}H, ^{13}C, COSY, HSQC, and HMBC). Previously reported compounds (**3.2**, **3.7** – **3.10**) were in good agreement with reported NMR spectra & mass spectrometry values. Final compounds **3.6** and **3.12** were successfully complexed with lanthanum perchlorate ($La(ClO_4)_3 \bullet 6H_2O$), and their metal complexes were fully characterized using HR-ESI-MS and NMR (^{1}H, ^{13}C, COSY, HSQC, and HMBC).

The ^{1}H NMR spectra at 25 °C in dimethylsulfoxide-d_6 (DMSO-d_6) of **3.6** shows three distinct peaks at 7.41, 6.54, and 6.22 ppm corresponding to the HOPO pendant arms and an unresolvable multiplet at 3.55 ppm corresponding to the macrocyclic core (**Figure 3.4**). Variable temperature (VT) NMR experiments from 10 to 40°C in D_2O were performed, but there were no spectral changes. Upon complexation with La^{3+}, studying the ^{1}H NMR spectra for the pendant donors arm region shows one major isomer with one (or more) isomers present in solution (**Figure 3.4**). VT NMR (30 to 50°C) of [La(macrohopo)][ClO_4] showed no spectral changes (see Appendix **Figure A30**).

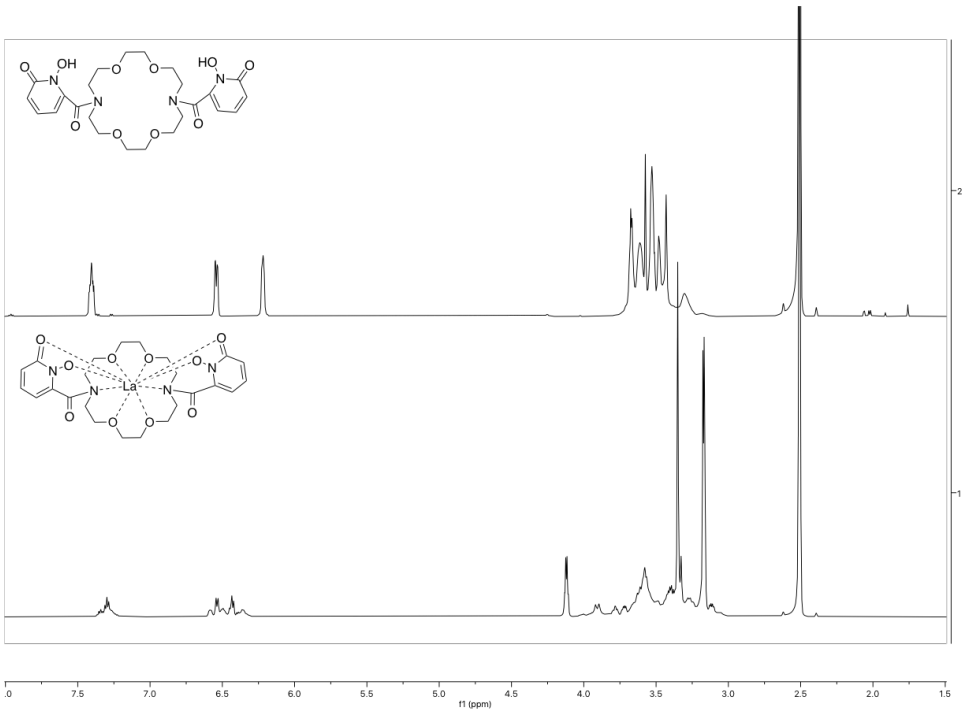

Figure 3.4: ^{1}H NMR spectra at 25 °C in DMSO-d_6 of 3.6 (top) and [La(macrohopo)][ClO_4] (bottom)

The ^{1}H NMR spectra at 25 °C in DMSO-d_6 of **3.12** indicates a C_2 symmetry, as reflected by chemical equivalents of the pendant donor arms (see **Figure 3.5**). Upon complexation with La^{3+}, the ^{1}H NMR spectrum (**Figure 3.5** and **Figure 3.6**) shows distinct coupling patterns in the pendant donor arm region, which in conjunction with ^{13}C-, COSY-, HMBC-, and HSQC- NMR spectra was utilized to determine that two isomers are present in solution. Correlation between I) a_1, b_1, and c_1 and II) a_2, b_2, and c_2 were evident on the COSY with no correlation between a_1 and a_2, b_1 and b_2, and c_1 and c_3 indicating two separate isomers (see Appendix **Figure A28**). The relative chemical equivalence between the asymmetric (a_2, b_2, and c_2) and the symmetric (a_1, b_1, and c_1) pendant donor arms indicate a 1:1 ratio is present (**Figure 3.6**). Variable temperature (VT) NMR was performed, increasing the ratio of the asymmetric isomer (60:40) as temperature increased (see Appendix **Figure A31**).

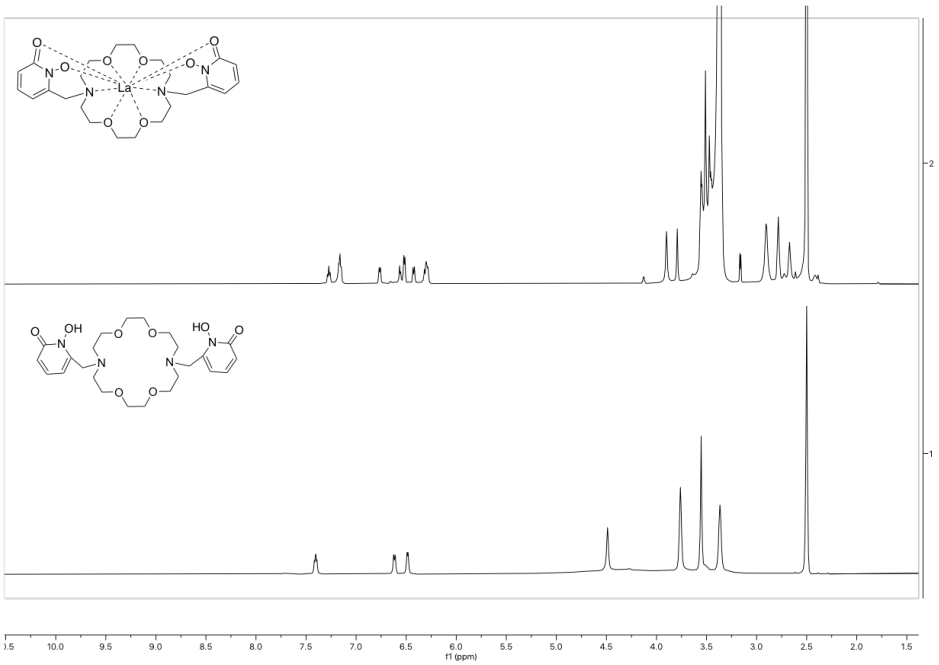

Figure 3.5: **^{1}H NMR spectra at 25 °C in DMSO-d$_6$ of [La(macrohopo′)][ClO4] (top) and 3.12 (bottom)**

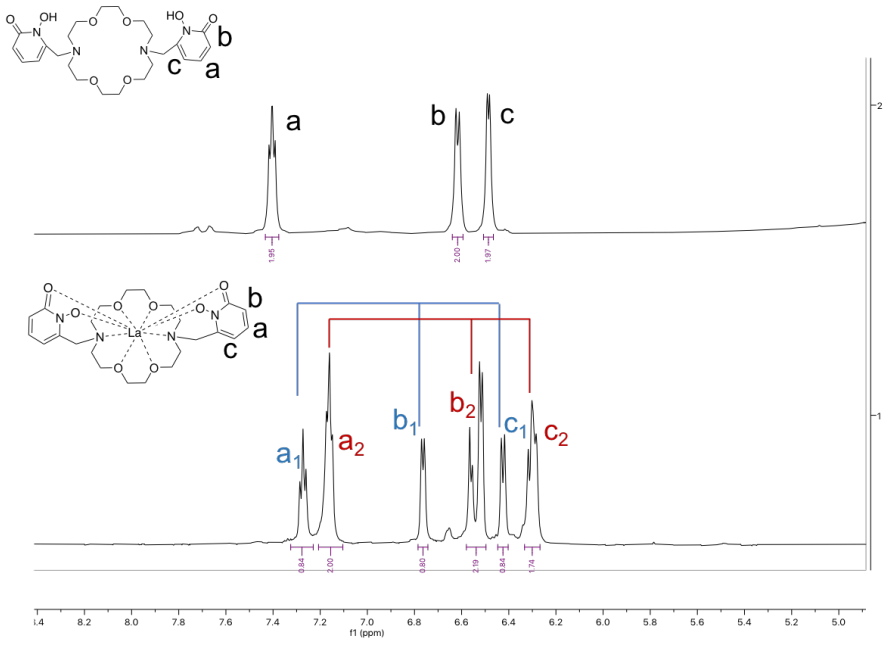

Figure 3.6: **^{1}H NMR spectra at 25 °C in DMSO-d$_6$ of [La(macrohopo′)][ClO4] (bottom) and 3.12 (top) illustrating a 1:1 asymmetric:symmetric ratio in solution; red – asymmetric, blue – symmetric**

Chelates macropa (**3.15**), macropaquin (**3.14**), and macroquin-SO_3 (**3.13**) were synthesized and characterized by Fiszbein, D at Cornell University (Wilson Group) based on established procedures[17,78,79]. Lanthanum complexation of macropa has been previously reported by Thiele *et al.,* wherein full characterization (including NMR, IR, HPLC, x-ray crystallography, and UV-vis spectroscopy) was performed[17]. Lanthanum complexation of macropaquin (**3.14**) and macroquin-SO_3 (**3.13**) was not performed.

3.3.2. UV-Vis

In situ complexation of **3.6** and **3.12** with lanthanum ($La(ClO_4)_3 \bullet 6H_2O$) was observed using UV-Vis. A solution of lanthanum perchlorate was added to either **3.6** or **3.12** in 0.1 M KCl/0.1 M HEPES (4-(2-hydroxyethyl)-1-piperazineethanesulfonic acid) buffer solution (pH = 7.4) at 0.5 equivalents increments until excess metal (≥2 Eq) was present. Formation of [La(macrohopo)][ClO_4] occurred when 1.0 equivalents of lanthanum was added to the ligand solution, indicated by the λ_{max} shift from 323 nm to 314 nm (**Figure 3.7**). As excess metal was added, the λ_{max} at 314 nm did not significantly shift in absorbance or wavelength, indicating a 1:1 metal to chelate (La:macrohopo) ratio. Complexation of **3.12** occurred when 0.5 equivalents of lanthanum was added to the ligand solution, indicated by the λ_{max} shift from 318 nm to 309 nm (**Figure 3.7**). Similarly to **3.6**, a 1:1 metal to chelate ratio is demonstrated.

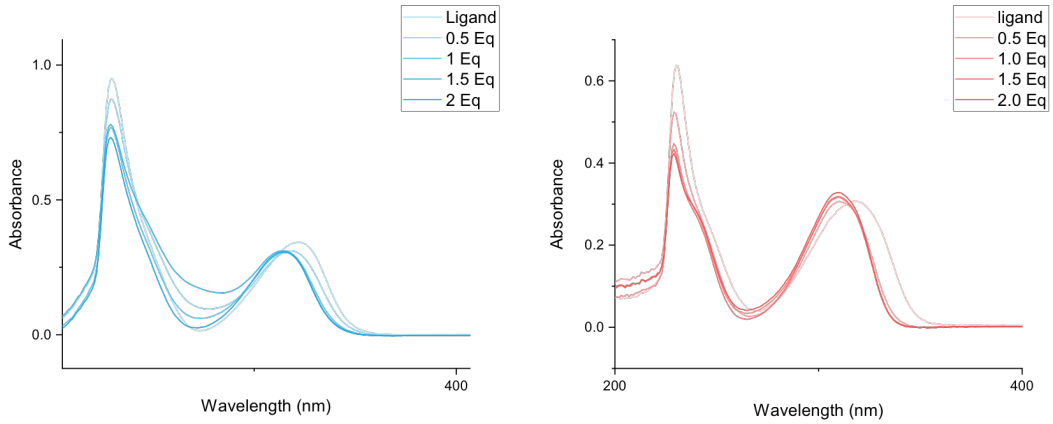

Figure 3.7: UV-Vis spectra of in situ lanthanum complexation with novel chelators 3.6 (left) and 3.12 (right)

A possible explanation for [La(macrohopo′)][ClO_4] formation occurring at 0.5 metal Eq instead of 1 equivalent is the inability to get elemental analysis (EA) of macrohopo′. Precise molecular weights of these ligands are crucial when dealing with 10^{-5} M final ligand concentrations. Unaccounted TFA, acetonitrile, and/or water molecules present in the final compound, can significantly vary the Eq of ligand present ultimately impacting the amount of metal required for complexation.

3.3.3. Initial Radiolabeling

Determination of ideal $^{225}Ac^{3+}$ radiolabeling conditions at final ligand concentrations of 10^{-3} or 10^{-4} M (buffer, pH, and reaction time) were performed during initial radiolabeling experiments. Subsequent concentration dependence studies were executed using the ideal radiolabeling conditions and the results are compiled in **Figure 3.8**. Not surprisingly, gold standard DOTA required heating at 80 °C for 1 hr to obtain quantitative labelling at 10^{-3} M. DOTA was able to maintain quantitative labeling at 10^{-4} M; however, as ligand concentrations decreased to 10^{-5}, 10^{-6}, and 10^{-7} M, the radiochemical yield decreased to 37.5 ± 7.9, 4.5 ± 0.8 and <1% respectively. Macropa results were comparable to previous impressive findings, with quantitative labeling achieved for 10^{-6} M final ligand concentrations at ambient temperatures[17]. Impressively, within 5 minutes macropaquin can achieve >95% RCY for 10^{-5} M at ambient temperatures (pH 5.5). For 10^{-6} M, macropaquin exhibits slower kinetics with 26.0% RCY at 5 minutes and 92.6% RCY after 1 hour. With a RCY >90%, macropaquin becomes the 6th reported ligand that can obtain quantitative ^{225}Ac labeling at ambient temperatures within 1 hour for 10^{-6} M. Conversely, macroquin-SO_3 was able to achieve quantitative labeling at 10^{-4} and 10^{-5} M, but dropped to 47.6 ± 47.1% RCY for 10^{-6} M at ambient temperatures (pH 7.0). At even 10^{-3} M final ligand concentration, macrohopo was unable to complex ^{225}Ac at ambient temperatures in a variety of buffers (0.1 M HEPES, NaOAc, NH_4OAc, MeOH, and EtOH) and pHs (between 5.5 – 10.0) after 1 hr. Heating the reaction to 80 °C and/or allowing it to proceed for longer (2 hr) did not facilitate ^{225}Ac complexation. Due to limited radionuclide

supply, macrohopo′ was not investigated for ^{225}Ac complexation at this time, but will be performed in future.

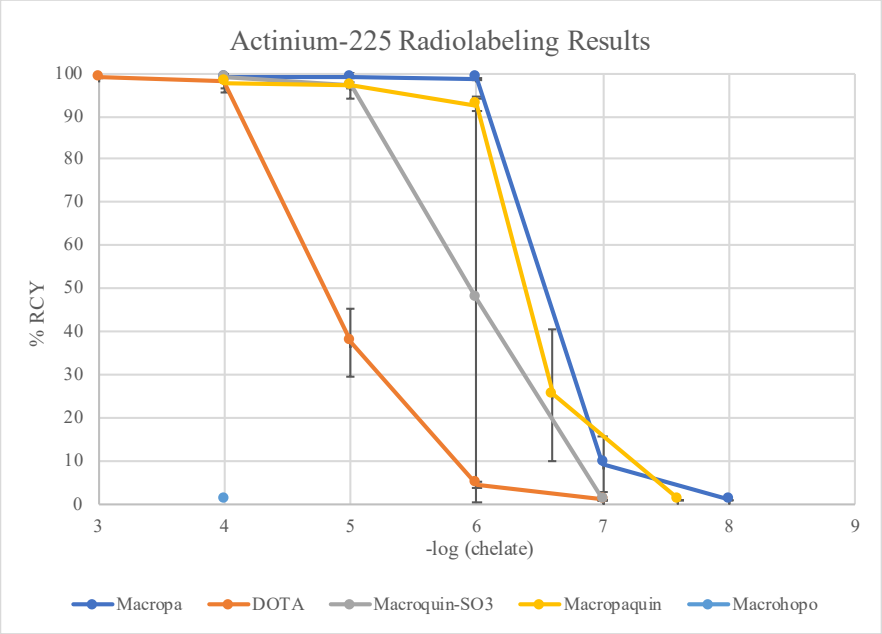

Figure 3.8: Radiochemical yields (RCY, %) for $^{225}Ac^{3+}$ radiolabeling reactions of DOTA (pH 5.5, 85 °C, 1h), macropa (pH 6, RT, 1h), macropaquin (pH 5.5, RT, 1h), macroquin-SO_3 (pH 6, RT, 1h) and macrohopo (pH 5 – 11, 85 °C, 1h)

The ligands investigated, **3.6** (macrohopo), **3.13** (macroquin-SO_3), **3.14** (macropaquin), and **3.15** (macropa), feature varied intrinsic characteristics which can affect the ligands ability to complex ^{225}Ac. As protons compete with metal ions for binding sites on ligands, ligand basicity is an important factor for a ligand's metal affinity[80]. Thiele *et al.,* determined the protonation constants (K_a) for macropa, macropaquin, and macroquin-SO_3[80] (Appendix Table A1). The replacement of picolinate arms on macropa by 8-hydroxyquinoline groups decreases the basicity of the nitrogen atoms of the macrocyclic core[80], a trend seen with various other chelators[80–84]. While the SO_3 electron withdrawing groups of macroquin-SO_3 produce more acidic phenols (log K_{a1} = 9.34 and log K_{a2} = 9.43) when compared to macropaquin (log K_{a1} = 10.33), macropaquin and macroquin-SO_3 do not exist fully deprotonated in solution below pH of 8.0[80]. At physiological pH (7.4), 43% of macropa is fully deprotonated whereas, the monoprotonated species of macropaquin predominates (56%) and macroquin-SO_3 presents (78%) as a diprotonated species. The

increased overall basicity of macropaquin may explain the slower kinetics at 10^{-6}M chelator concentrations when compared to macropa. The 1,2-hydroxypyridinone groups in **3.6** and **3.12** have a reported log k_a value of 5.87[85], and the secondary amines of diaza-18-crown-6 macrocycles typically range from 6 – 9[76,79,80,86]. Theoretically, **3.6** and **3.12** should exhibit slightly lower/comparable overall basicity to macropaquin and macroquin-SO_3. However, experimental determination of the protonation constants for **3.6** and **3.12**, were not performed at this time.

The hydroxypyridinone groups on **3.6** and **3.12** offer hard oxygen donors, appropriate for ^{225}Ac complexation. With four oxygens and two nitrogens on the macrocyclic backbone, the hydroxypyridinone pendent arms facilitate a 10 coordination species (N_2O_8). The inability of **3.6** to complex actinium may be associated with pendant donor arms rigidity, a result of the carbonyl group on the pendant donor arms. If the HOPO pendant donor arms on **3.12** don't participate in the coordination, poor ^{225}Ac complexation of the diaza-18-crown-6 macrocycle can be expected.

Interestingly, all chelators with superior ^{225}Ac complexation (CHX-octapa[66], py4pa[74], noneunpa[72], macropa[17] and crown[67] and macropaquin) contain ≥1 aminocarboxylate group with a large core that can accommodate the large ^{225}Ac actinide and overall +1 or -1 charge. Yet, they vary in flexibility (macrocyclic vs acyclic), coordination number (CN = 8, 10, and/or 11), coordinating atoms (N_4O_4, N_7O_4, and N_4O_6), and pendant donor arm basicity.

3.4. Conclusion & Future Work

In chapter 3, two novel HOPO ligands (**3.6** and **3.12**) were synthesized and characterized via NMR, HPLC, MS, and UV-Vis. The ability to complex lanthanum ($^{225}Ac^{3+}$ closest non-radioactive surrogate) was examined, wherein both ligands illustrated complexation with multiple isomers present. A 1:1 metal:chelate ratio for the lanthanum complexes was studied via UV-Vis as a shift in λ_{max} from 323 nm to 314 nm for **3.6** and 318 nm to 309 nm for **3.12**. Initial radiolabeling of macropa and DOTA were consistent with reported data, while macropaquin shows great promise. Conversely, **3.6** was unable

to complex ^{225}Ac under any conditions and due to limited radionuclide supply, **3.12** was not investigated.

Future work for this project is intensive, including both non-radioactive and radioactive work. Specifically, fundamental characterization of **3.6** and **3.12** such as pKa determination, thermodynamic affinity for La^{3+}, and DFT calculations are essential. When ^{225}Ac becomes available, **3.12** should be investigated for ^{225}Ac complexation, utilizing the same condition as **3.6** radiolabeling. By directly comparing **3.6** and **3.12**, the effect of pendant donor arm flexibility can be investigated. Furthermore, with promising initial radiolabeling for macropaquin, its kinetic inertness should be evaluated *in vitro* via a human serum assay. As two novel ligands, **3.6** and **3.12** should be screened for radionuclides with similar intrinsic properties as $^{225}Ac^{3+}$. Particularly with $^{89}Zr^{4+}$, a hard, oxophilic cation with proven complexation and excellent *in vitro* stability for an octadentate acyclic HOPO chelator[87].

3.5. Experimental

3.5.1. Materials and Methods

All solvents and reagents were purchased from commercial suppliers (TCI America, Fisher Scientific, Macrocyclic, and Sigma Aldrich). Solvents noted as "dry" were obtained following storage over 3 Å molecular sieves. ^{1}H and ^{13}C NMR spectra were referenced to the residual solvent peak and recorded at 25°C (unless noted otherwise) on Bruker AV400, AV500, or AV600 instruments. Deionized water (>18 MΩ cm) was used via Millipore-Direct (Milli-Q IQ 7000) purification systems. High-resolution electrospray-ionization mass spectrometry (HR-ESI-MS) was performed on an Agilent 6210 time-of-flight instrument (TOF). Semi-preparative and preparative HPLC were used for the purification of non-radioactive compounds. Semi-preparative purification was performed on an Agilent 1100 series consisting of a G1311A Quaternary Pump, G2260A autosampler, and G1315B variable wavelength absorbance detector. Semi-preparative purification was performed with a Kinetex semi-preparative C18 column, 5 μm, 100 Å, 150 x 10.0 mm at a flow rate of 3.0 mL/min unless otherwise noted. Preparative purification was performed on an Agilent 1100 series consisting of a G1361A Quaternary Pump, G2260A autosampler,

and G1365D variable wavelength absorbance detector. Preparative purification was performed with a Gemini-NX preparative C18 column, 5 µm, 110 Å, 100 x 30.0 mm at a flow rate of 15.0 mL/min unless otherwise noted. Gradient HPLC methods utilized a binary mobile phase that contained H_2O with 0.1 % TFA (A) and CH_3CN with 0.1 % TFA (B). HPLC methods:

- 3A: 2 – 50% B (0 – 20 min), 50 – 100% B (20 – 22 min), 100% B (22 – 24 min), 100 – 2% B (24 – 26 min), 2% B (26 – 30 min).
- 3B: 2 – 50% B (0 – 10 min), 50 – 100% B (10 – 12 min), 100 – 10% B (12 – 14 min), 10% B (14 – 15 min).
- 3C: 5 – 15% B (0 – 20 min), 15 – 100% B (20 – 24 min), 100% B (24 – 26 min), 100 – 2% B (26 – 28 min), 2% B (28 – 30 min).

3.5.2. Synthesis Methodology

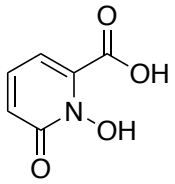

1-hydroxy-6-oxo-1,6-dihydropyridine-2-carboxylic acid* (*1,2-HOPO-Acid, 3.2). Compound **3.2** was prepared as previously reported[77]. Peracetic acid (15 mL) was carefully added dropwise to a white suspension of 6-hydroxypicolinic acid (5.0 g, 36 mmol, 1 Eq) in glacial acetic acid (30 mL) while stirring. The flask was heated to 80°C for 12 hrs before the solid was filtered and washed with diethyl ether to yield **3.2** as a cream solid (4.50 g, yield = 80.6%). The ^{1}H NMR data for the product was in good agreement with those previously reported in the literature; ^{1}H NMR (400 MHz, DMSO-d_6) δ 7.44 (dd, J = 9.0, 7.0, Ar-H, 1H), 6.71 (dd, J = 9.0, 1.7, Ar-H, 1H), 6.66 (dd, J = 7.0, 1.7, Ar-H, 1H). ^{13}C NMR (101 MHz, DMSO-d_6), δ 161.9 (*C*OOH), 157.1 (*C*=O), 138.8 (*C*COOH), 136.5 (Ar-C), 120.3 (Ar-C), 106.3 (Ar-C). HR-ESI-HRMS calcd. for $[C_6H_5NO_4 + H]^+$: 156.02913; found 156.0289 $[M+H]^+$.

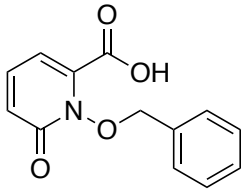

1-(benzyloxy)-6-oxo-1,6-dihydropyridine-2-carboxylic acid (1,2-HOPO-OBn-Acid, 3.3). Benzyl bromide (1.10 ml, 9.3 mmol, 1.2 Eq) and potassium carbonate (2.1 g, 15.5 mmol, 2 Eq) were added to a white suspension of 1,2-HOPO Acid **3.2** (1.2 g, 7.7 mmol, 1 Eq) in methanol (30 mL). The white suspension was refluxed at 75°C overnight (16 h), producing a dark green transparent solution after ~10 minutes followed by a brown solution with a grey precipitate after 16 h. The solution was filtered via a Büchner funnel, the solvent was removed under reduced pressure, and the resulting brown residue was dissolved in water. The addition of concentrated HCl dropwise formed a white precipitate which was filtered, washed with water, and dried under vacuum to yield **3.3** as a peach solid (1.52 g, yield = 80.1%). ^{1}H NMR (400 MHz, DMSO-d_6) δ 7.49 (m, Ar-H, 3H), 7.44 (m, Ar-H, 3H), 6.74 (dd, *J* = 9.3, 1.7, Ar-H, 1H), 6.56 (dd, *J* = 6.8. 1.7, Ar-H, 1H), 5.28 (s, OC*H*$_2$C$_6$H$_5$, 2H). ^{13}C NMR (101 MHz, DMSO-d_6), δ 161.6 (*C*OOH), 157.6 (*C*=O), 140.5 (*C*COOH), 138.6 (Ar-C), 133.8 (OCH$_2$*C*C$_5$H$_5$), 129.6 (Ar-C), 129.0 (Ar-C), 128.5 (Ar-C), 124.0 (Ar-C), 105.9 (Ar-C), 77.9 (O*C*H$_2$C$_6$H$_5$). HR-ESI-MS calcd. for [$C_{13}H_{11}NO_4$ + H]$^+$: 246.07608; found 246.0755 [M+H]$^+$.

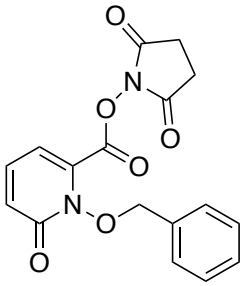

2,5-dioxopyrrolidin-1-yl 1-(benzyloxy)-6-oxo-1,6-dihydropyridine-2-carboxylate (1,2-HOPO-OBn-Succ, 3.4). *N*-hydroxysuccinimide (420 mg, 3.7 mmol, 1.2 Eq) and 1-ethyl-3-(3-dimethylaminopropyl)carbodiimide (704 mg, 3.7 mmol, 1.2 Eq) were added to a solution of **3.3** (750 mg, 3.1 mmol, 1 Eq) in dry CH_2Cl_2 (70 mL). After stirring the reaction mixture for 12 h under argon, the peach suspension was washed with water (50 mL) and

brine (50 mL), the organic layer was dried over Na_2SO_4, filtered, and the solvent was removed under reduced pressure. The crude product was purified by silica column chromatography (using CH_2Cl_2:CH_3CN 5:1 as eluent) to obtain a white crystalline solid (439 mg, yield = 41.9 %). ^{1}H NMR (400 MHz, $CDCl_3$), δ 7.56 (m, Ar-H, 2H), 7.36 (m, Ar-H, 4H), 6.95 (m, Ar-H, 2H), 5.38 (s, OC*H*$_2$C$_6$H$_5$, 2H), 2.92 (s, O=CC*H*$_2$C*H*$_2$C=O, 4H). ^{13}C NMR (101 MHz, $CDCl_3$), δ 168.5 (O=*C*CH$_2$CH$_2$*C*=O), 158.5 (*C*=OON), 155.2 (C=O), 136.8 (Ar-C), 133.3 (Ar-C), 130.4 (Ar-C), 129.4 (Ar-C), 129.1 (Ar-C), 128.7 (Ar-C), 111.7 (Ar-C), 79.0 (O*C*H$_2$C$_6$H$_5$), 25.8 (O=C*C*H$_2$*C*H$_2$C=O). HR-ESI-MS calcd. for [$C_{17}H_{14}N_2O_6$ + H]$^+$: 343.09246; found 343.0909 [M+H]$^+$.

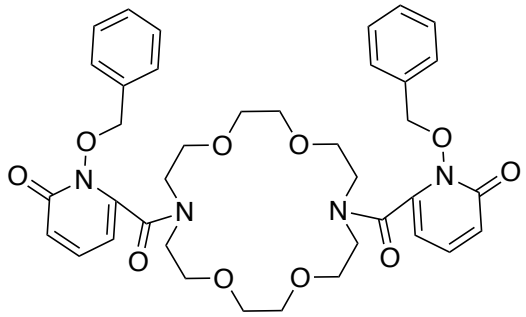

6,6'-(1,4,10,13-tetraoxa-7,16-diazacyclooctadecane-7,16-dicarbonyl)bis(1-(benzyloxy)pyridin-2(1H)-one)(1,2-HOPO-OBn-crown, 3.5). 4,13-Diaza-18-crown-6-ether (150 mg, 0.6 mmol, 1 Eq) was added to a solution of **3.4** (489 mg, 1.4 mmol, 2.5 Eq) in dry CH_2Cl_2 (8 mL). Triethylamine (TEA) was added at RT and the reaction was left stirring under argon for 24 hrs. The solvent was removed under reduced pressure yielding a brown oil. The residual was dissolved in CH_2Cl_2 (50 mL), washed with water and brine (2 x 50 mL), and the organic layer was dried over sodium sulfate. The solvent was removed under reduced pressure to yield a brown transparent solution. The crude product was purified via silica column chromatography (using CH_2Cl_2:MeOH 9:1 as the eluent) followed by another silica column (using $CHCl_3$:MeOH 9:1 as the eluent) to yield a white solid (217 mg, yield = 52.9%). ^{1}H NMR (600 MHz, $CDCl_3$), δ 7.53 (m, Ar-H, 4H), 7.35 (m, Ar-H, 8H), 6.71 (m, Ar-H, 2H), 6.07 (m, Ar-H, 2H), 5.65 (m, OC*H*$_2$C$_6$H$_5$, 2H), 5.02 (m, OC*H*$_2$C$_6$H$_5$, 2H), 3.47 (m, $C_{12}N_2O_4$*H*$_{24}$, 24H). ^{13}C NMR (151 MHz, $CDCl_3$), δ 162.3 ($C_{12}NO_4H_{24}$N*C*=O), 158.5 (C=O), 143.2 (Ar-C), 138.5 (Ar-C), 138.4 (Ar-C), 133.7 (Ar-

C), 130.5 (Ar-C), 130.5 (Ar-C), 129.4 (Ar-C), 129.4 (Ar-C), 128.6 (Ar-C), 123.1 (Ar-C), 102.9 (Ar-C), 102.8 (Ar-C), 79.4 ($OCH_2C_6H_5$), 70.6 ($C_{12}N_2O_4H_{24}$), 70.5 ($C_{12}N_2O_4H_{24}$), 70.4 ($C_{12}N_2O_4H_{24}$), 70.4 ($C_{12}N_2O_4H_{24}$), 70.2 ($C_{12}N_2O_4H_{24}$), 69.8 ($C_{12}N_2O_4H_{24}$), 69.7 ($C_{12}N_2O_4H_{24}$), 69.5 ($C_{12}N_2O_4H_{24}$), 69.4 ($C_{12}N_2O_4H_{24}$), 69.3 ($C_{12}N_2O_4H_{24}$), 69.2 ($C_{12}N_2O_4H_{24}$), 69.0 ($C_{12}N_2O_4H_{24}$), 69.0 ($C_{12}N_2O_4H_{24}$), 49.5 ($C_{12}N_2O_4H_{24}$), 49.5 ($C_{12}N_2O_4H_{24}$), 49.4 ($C_{12}N_2O_4H_{24}$), 46.3 ($C_{12}N_2O_4H_{24}$), 46.2 ($C_{12}N_2O_4H_{24}$), 46.2 ($C_{12}N_2O_4H_{24}$), 46.1 ($C_{12}N_2O_4H_{24}$). HR-ESI-MS calcd. for $[C_{38}H_{44}N_4O + H]^+$: 717.3130; found 717.3108 $[M+H]^+$.

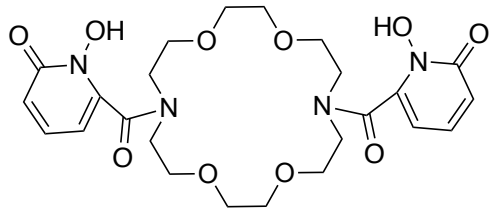

6,6'-(1,4,10,13-tetraoxa-7,16-diazacyclooctadecane-7,16-dicarbonyl)bis(1-hydroxypyridin-2(1H)-one) (macrohopo, 3.6). Concentrated hydrochloric acid (3.2 mL) and glacial acetic acid (3.2 mL) (1:1v/v) was added to 1,2-HOPO-OBn-Crown **3.5** (100 mg, 0.14 mmol). After heating the reaction at 50°C for 3d, the solvent was removed under reduced pressure. The brown crude residue was dissolved in H_2O and purified via HPLC, using method 3A (preparative) or 3B (semipreparative) to yield a colourless oil (34.5 mg, yield = 56.1%). ^{1}H NMR (600 MHz, D_2O) δ 7.48 (td, J = 9.2, 7.0 Hz, Ar-H, 2H), 6.66 (m, Ar-H, 2H), 6.45 (ddd, J = 6.6, 4.6, 1.7 Hz, Ar-H, 2H), 3.76 – 3.38 (m, $C_{12}N_2O_4\mathit{H_{24}}$, 24H). ^{13}C NMR (151 MHz, D_2O) δ 163.5, 163.5, 160.2, 140.6, 140.5, 139.8, 139.8, 120.2, 117.1, 115.2, 106.4, 69.9, 69.9, 69.7, 69.7, 68.6, 68.5, 67.9, 67.8, 49.6, 49.6, 46.4, 46.4. HR-ESI-MS calcd. for $[C_{24}H_{32}N_4O_{10} + H]^+$: 537.2191; found 537.2186 $[M+H]^+$. Elemental Analysis: calcd. (found) for $C_{24}H_{32}N_4O_{10}\cdot 1\ TFA\cdot 2H_2O$: C, 45.48 (45.57); H 5.43 (5.11); N 8.16 (7.95)%.

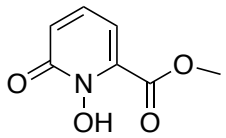

Methyl 1-hydroxy-6-oxo-1,6-dihydropyridine-2-carboxylate, (1,2-HOPO-methylester, 3.7). Compound **3.7** was prepared as previously reported[77]. Thionyl chloride (5.8 mL, 78.0 mmol, 4 Eq) was added dropwise to a white suspension of **3.2** (3.0 g, 19.3 mmol, 1 Eq) in dry methanol (38.5 mL) at 0°C. After the mixture was refluxed for 4 hours at 85°C, the orange solution was cooled to room temperature. The solvent was removed under reduced pressure yielding **3.7** as an orange solid (3.25 g, yield >99 %). The ^{1}H NMR data for the product was in good agreement with those previously reported in the literature. ^{1}H NMR (400 MHz, DMSO-d_6), 7.44 (dd, J = 9.2, 6.8 Hz, Ar-H, 1H), 6.69 (dd, J = 9.1, 1.6 Hz, Ar-H, 1H), 6.52 (dd, J = 6.9, 1.6 Hz, Ar-H, 1H), 3.87 (s, CO_2CH_3, 3H). ^{13}C NMR (101 MHz, DMSO-d_6) δ 161.3 (CO_2CH_3), 158.0 (C=O), 138.7 (Ar-C), 137.8 (Ar-C), 122.5 (Ar-C), 105.7 (Ar-C), 53.7 (CO_2CH_3). HR-ESI-MS calcd. for $[C_7H_7NO_4 + H]^+$: 170.04478; found 170.04448 $[M+H]^+$.

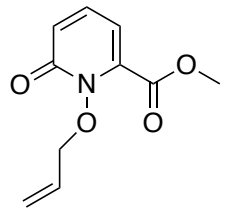

Methyl-1-(allyloxy)-6-oxo-1,6-dihydropyridine-2-carboxylate (1,2-HOPO-allyl-methylester, 3.8). Compound **3.8** was prepared as previously reported[77]. Allyl bromide (4.1 mL, 47.80, 2.5 Eq) and potassium carbonate (6.60 g, 47.80 mmol, 2.5 Eq) were added to an orange suspension of **3.7** (3.24 g, 19.17 mmol, 1 Eq) in acetonitrile (42 mL). The flask was refluxed at 90°C, for 4 hrs before the mixture was filtered and the solvent was removed under reduced pressure. The residue was dissolved in toluene and the solvent was removed under reduced pressure to yield **3.8** as a pale orange solid (3.65 g, yield = 91.1%). The ^{1}H NMR data for the product was in good agreement with those previously reported in the literature. ^{1}H NMR (500 MHz, $CDCl_3$) δ 7.30 (m, Ar-H, 1H), 6.80 (dd, J = 9.2, 1.6 Hz, Ar-H, 1H), 6.52 (dd, J = 6.8, 1.6 Hz, Ar-H, 1H), 6.08 (m, OCH_2CHCH_2, 1H), 5.43 (m,

OCH_2CHCH_2, 2H), 4.90 (m, OCH_2CHCH_2, 2H), 3.93 (s, CH_3, 3H). ^{13}C NMR (126 MHz, $CDCl_3$) δ 160.6 (CO_2CH_3), 158.9 (C=O), 138.7 (quart. C) 137.2 (Ar-C), 130.6 (OCH_2CHCH_2), 126.0 (Ar-C), 122.0 (OCH_2CHCH_2), 108.0 (Ar-C), 78.1 (OCH_2CHCH_2), 53.4 (CO_2CH_3). HR-ESI-MS calcd. for $[C_{10}H_{11}NO_4 + H]^+$: 210.0761; found 210.0766 $[M+H]^+$.

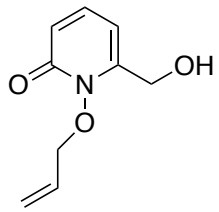

1-(allyloxy)-6-(hydroxymethyl)pyridin-2(1H)-one (1,2-HOPO-allyl-hydroxide, 3.9). Compound **3.9** was prepared as previously reported[77]. Sodium borohydride (4.09 g, 108.3 mmol, 7 Eq) was added to a solution of **3.8** (3.24 g, 15.5 mmol, 1 Eq) in tetrahydrofuran (42 mL) at room temperature. The flask was refluxed at 80°C for 15 minutes before the dropwise addition of methanol (2.4 mL) over 2 hours. The solution was then cooled to 0°C and quenched by the addition of ammonium chloride (4.2 mL). After stirring for an additional 15 minutes, the solvents were removed under reduced pressure. The residue was extracted with CH_2Cl_2 until the aqueous layer was a colourless transparent solution. The combined organic layers were dried with sodium sulfate and the solvent was removed under reduced pressure to yield **3.9** as an off white solid (1.49 g, yield = 62.5 %). The ^1H NMR data for the product was in good agreement with those previously reported in the literature. ^1H NMR (500 MHz, $CDCl_3$) δ 7.29 (dd, J = 9.2, 6.9 Hz, Ar-H, 1H), 6.57 (dd, J = 9.1, 1.7 Hz, Ar-H, 1H), 6.27 (dd, J = 6.9, 1.9, Ar-H, 1H), 6.04 (m, OCH_2CHCH_2, 1H), 5.41 (m, OCH_2CHCH_2, 2H), 4.81 (d, J = 6.7, OCH_2CHCH_2, 2H), 4.68 (s, CH_2OH, 2H), 2.95 (s, CH_2OH, 1H). ^{13}C NMR (126 MHz, $CDCl_3$) δ 159.5 (C=O), 148.4 (Ar-C), 138.5 (Ar-C), 130.2 (OCH_2CHCH_2), 122.6 (OCH_2CHCH_2), 120.7 (Ar-C), 103.6 (Ar-C), 77.2 (OCH_2CHCH_2), 59.6 (CH_2OH). HR-ESI-MS calcd. for $[C_9H_{11}NO_3 + H]^+$: 182.0812; found 182.0806 $[M+H]^+$.

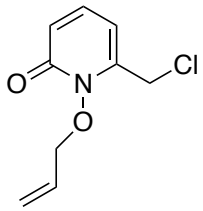

1-(allyloxy)-6-(chloromethyl)pyridin-2(1H)-one (1,2-HOPO-allyl-chloride, 3.10). Compound **3.10** was prepared as previously reported[77]. Thionyl chloride (3.6 mL, 49.6 mmol, 6 Eq) was added dropwise to a yellow solution of **3.9** (1.5 g, 8.2 mmol, 1 Eq) in dry CH_2Cl_2 (36 mL) at room temperature. After refluxing at 50°C for 6 hours, the solution was then cooled to 0°C and quenched with the addition of ice water (30 mL). After stirring the biphasic reaction mixture for an additional 30 minutes, the phases were separated, and the aqueous phase was further extracted with CH_2Cl_2 (3 x 40 mL). The combined organic phases were dried with sodium sulfate and the solvent was removed under reduced pressure to yield **3.10** as a brown crystalline solid (1.59 g, yield = 97.0%). The ^{1}H NMR data for the product was in good agreement with those previously reported in the literature. ^{1}H NMR (500 MHz, $CDCl_3$) δ 7.27 (d, *J* = 7.0 Hz, Ar-H, 1H), 6.66 (dd, *J* = 9.3, 1.7 Hz, Ar-H, 1H), 6.25 (dd, *J* = 6.8, 1.7 Hz, Ar-H, 1H), 6.11 (m, $OCH_2C\mathit{H}CH_2$, 1H), 5.45 (m, $OCH_2CHC\mathit{H_2}$, 2H), 4.93 (d, *J* = 6.6 Hz, $OC\mathit{H_2}CHCH_2$, 2H), 4.57 (s, $C\mathit{H_2}Cl$, 2H). ^{13}C NMR (126 MHz, $CDCl_3$) δ 159.2 (C=O), 144.3 (Ar-C), 137.8 (Ar-C), 130.3 ($OCH_2\mathit{C}HCH_2$), 123.0 (Ar-C), 122.4 ($OCH_2CH\mathit{C}H_2$), 106.3 (Ar-C), 77.4 ($O\mathit{C}H_2CHCH_2$), 39.4 ($\mathit{C}H_2Cl$). HR-ESI-MS calcd. for $[C_9H_{10}NO_2Cl + H]^+$: 200.0463; found 200.0472 $[M+H]^+$.

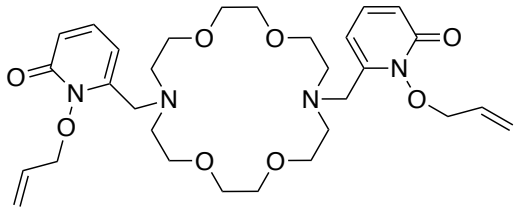

6,6'-((1,4,10,13-tetraoxa-7,16-diazacyclooctadecane-7,16-diyl)bis(methylene))bis(1-(allyloxy)pyridin-2(1H)-one) (1,2-HOPO-allyl-crown, 3.11). 4,13-Diaza-18-crown-6-ether (287 mg, 1.1 mmol, 1 Eq) and potassium carbonate (605 mg, 4.4 mmol, 4 Eq) were added to a solution of **3.10** (547 mg, 2.7 mmol, 2.5 Eq) in dry acetonitrile (7.5 mL). The suspension was refluxed at 80 °C overnight. After the addition of water (10 mL), the

suspension was extract with CH_2Cl_2 (10 mL) and the combined organic fractions water dried with sodium sulfate. The solvent was removed under reduced pressure to yield a brown oil. The crude product was purified via silica column chromatography (using a gradient of CH_2Cl_2:MeOH 99:1 to CH_2Cl_2:MeOH 90:10 as the eluent). The solvent was removed under reduced pressure to yield **3.11** as a brown solid (550 mg, yield = 85.3%). ^{1}H NMR (MeOD, 600 MHz), δ7.47 (dd, J = 9.1, 7.0 Hz, Ar-H, 2H), 6.67 (dd, J = 7.01, 1.7 Hz, Ar-H, 2H), 6.55 (dd, J = 9.1, 1.8 Hz, Ar-H, 2H), 6.14 (m, OCH_2CHCH_2, 2H) 5.47 (m, OCH_2CHCH_2, 2H), 5.38 (m, OCH_2CHCH_2, 2H), 4.82 (m, OCH_2CHCH_2, 4H), 3.89 (s, NCH_2, 4H), 3.63 (t, *J* = 5.5 Hz, NCH_2CH_2O, 8H), 3.57 (s, OCH_2CH_2O, 8H), 2.89 (t, *J* = 5.5 Hz, NCH_2CH_2O, 8H). ^{13}C NMR (MeOD, 151 MHz), δ 162.1 (C=O), 150.4 (Ar-C), 140.8 (Ar-C), 132.2 (OCH_2CHCH_2), 122.4 (OCH_2CHCH_2), 120.0 (Ar-C), 108.2(Ar-C), 78.2 (OCH_2CHCH_2), 71.8 (OCH_2CH_2O), 71.0 (NCH_2CH_2O), 55.7 (NCH_2 or NCH_2CH_2O), 55.6 (NCH_2 or NCH_2CH_2O). HR-ESI-MS calcd. for $[C_{30}H_{44}N_4O_8 + H]^+$: 589.3232; found 589.3243 $[M+H]^+$.

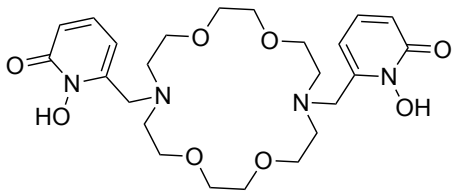

6,6'-((1,4,10,13-tetraoxa-7,16-diazacyclooctadecane-7,16-diyl)bis(methylene))bis(1-hydroxypyridin-2(1H)-one) **(macrohopo′*, 3.12).** Boron trichloride (1M in CH_2Cl_2, 1.8 mL, 1.8 mmol, 7 Eq) was added dropwise to a brown solution of **3.11** (142.4 mg, 0.3 mmol, 1 Eq) in dry CH_2Cl_2 (2 mL) at 0°C under argon. The solution was warmed to room temperature and allowed to stir overnight under argon. The solid precipitate was filtered and washed with CH_2Cl_2 and air dried to yield a yellow/white solid. The yellow solid was dissolved in H_2O and purified via HPLC, using method 3A (preparative) or 3C (semipreparative) to yield a colourless oil (74.2 mg, yield = 56.2%). The ^{1}H NMR data for the product is as followed: ^{1}H NMR (600 MHz, DMSO) δ 7.40 (m, Ar-C, 2H), 6.62 (d, *J* = 9.1, Ar-C, 2H), 6.49 (d, *J* = 7.0, Ar-C, 2H), 4.49 (s, NCH_2, 4H), 3.76 (t, J = 5.0 Hz, NCH_2CH_2O, 8H), 3.55 (s, OCH_2CH_2O, 8H), 3.37 (t, NCH_2CH_2O, 8H).^{13}C NMR (151 MHz, DMSO) δ 158.0 (C=O), 140.1 (Ar-C), 136.6 (Ar-C), 119.7 (Ar-C), 108.6 (Ar-C),

69.6 (O*C*H_2*C*H_2O), 65.0 (NCH$_2$*C*H_2O), 53.7 (NC*H*$_2$CH$_2$O), 53.2 (N*C*H_2). HR-ESI-MS calcd. for [$C_{24}H_{36}N_4O_8$ + H]$^+$: 509.2606; found 509.2591 [M+H]$^+$.

3.5.3. Non-radioactive metal complexation

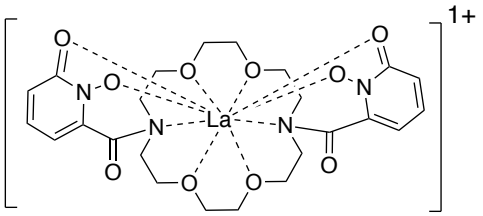

[La(macrohopo)][ClO$_4$]. A solution of La(ClO$_4$)$_3$• 6H$_2$O (17 mg, 31.3 µmol, 1.1 Eq) in CH$_3$OH (0.5 mL) was added to a solution of macrohopo (15 mg, 28 µmol, 1 Eq) in in CH$_3$OH (0.5 mL) at room temperature upon which time a precipitate formed immediately. The white suspension was centrifuged (2 min, 14,800 rpm), removing the supernatant and washing the pelleted with CH$_3$OH (2 x 0.5 mL) followed by (C$_2$H$_5$)$_2$O (2 x 0.5 mL). The pellet was then air-dried on filter paper to give the complex as a white solid (17.4 mg, yield = 77.9%). The ^{1}H NMR data (600 MHz, DMSO) δ 7.31 (m, Ar-H, 2H), 6.48 (m, Ar-H, 4H), 3.50 (m, C$_{12}$N$_2$O$_4$*H*$_{24}$, 33H). ^{13}C NMR (151 MHz, DMSO) δ 163.8, 162.4, 162.2, 142.8, 133.1 113.7, 106.7, 70.9, 70.4, 69.2, 68.5, 49.1, 47.5, 44.5, 40.5. ESI-MS calcd. for [$C_{24}H_{30}N_4O_{10}La$]$^+$: 673.1025; found 673.1 [M]$^+$

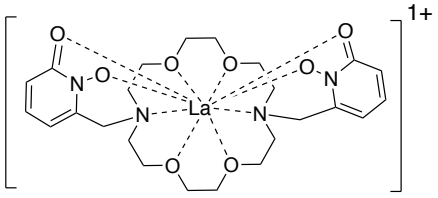

[La(macrohopo′)][ClO4]. A solution of La(ClO$_4$)$_3$• 6H$_2$O (24 mg, 43.3 µmol, 1.1 Eq) in CH$_3$OH (0.5 mL) was added to a solution of macrohopo′ (20 mg, 39.3 µmol, 1Eq) and triethylamine (22 µL, 0.2 mmol, 4 Eq) in CH$_3$OH (0.5 mL) at room temperature. A precipitate formed immediately. The white suspension was centrifuged (2 min, 14,800 rpm), removing the supernatant and washing the pelleted with CH$_3$OH (2 x 0.5 mL) followed by (C$_2$H$_5$)$_2$O (2 x 0.5 mL). The pellet was then air-dried on filter paper to give the complex as a white solid (20.3 mg, yield = 80.2%). The ^{1}H NMR data (600 MHz,

DMSO) δ 7.27 (m, Ar-H, 1H), 7.16 (m, Ar-H, 2H), 6.76 (m, Ar-H, 1H), 6.54 (m, Ar-H, 2H), 6.43 (m, Ar-H, 1H), 6.30 (m, Ar-H, 1H), 3.90 (s, 2H), 1.83 (s, 2H), 3.56 (m), 3.51 (s), 3.47 (m), 3.16 (d, 1H), 2.90 (s, 5H), 2.78 (t, 4H), 2.67 (s, 3H). ^{13}C NMR (151 MHz, DMSO) δ 162.4, 162.7, 147.9, 147.5, 147.2, 131.1, 132.1, 110.3, 110.1, 107.2, 107.1, 106.8, 105.6, 99.5, 70.6, 69.9, 65.4, 54.9, 54.4, 53.8, 46.1 (extrapolated from ^{13}C, HSQC, and HMBC). HR-ESI-MS calcd. for $[C_{24}H_{34}N_4O_8La]^+$: 645.1440; found 645.1414 $[M]^+$.

3.5.4. UV-Vis

Stock solutions of $La(ClO_4)_3 \bullet 6H_2O$ (1 x 10^{-3} M), **3.6** (1 x 10^{-3} M), and **3.12** (1 x 10^{-3} M) were prepared in MQ H_2O. Increasing amounts of $La(ClO_4)_3$ were added to a cuvette containing 50 μL of either i) **3.6** stock solution or i) **3.12** stock solution and a buffering solution (0.1 M KCl/0.1 M HEPES). The final concentration of **3.6** and **3.12** was 2.5 x 10^{-5} M and 5.0 x 10^{-5} M respectively. The complexation of the metal ion was monitored by the shift in λ_{max} from 323 nm to 314 nm for **3.6** and 318 nm to 309 nm for **3.12**.

3.5.5. ^{225}Ac Sources

All ^{225}Ac used for Chapter 3 was produced from irradiated thorium (^{232}Th(p,x) $^{225/227}$Ac†), herein referred to as $^{225/227}$Ac†. Separation of $^{225/227}$Ac† from irradiated thorium (^{232}Th(p,x) $^{225/227}$Ac†) was performed as described in Chapter 2.

3.5.6. ^{225}Ac Radiolabeling Studies

Stock solutions (1x 10^{-2} & 1x 10^{-3} M) of macropa (**3.15**), DOTA, macrohopo (**3.6**), macropaquin (**3.15**), and macropaquin-SO3 (**3.13**) were made with ultra-pure deionised water. Serial dilutions were used to prepare initial ligand solutions of 10^{-4} M, 10^{-5} M, 10^{-6} M, and 10^{-7} M with ultra-pure water. Concentration-dependent radiolabeling studies were performed by the addition of $^{225/227}$Ac† (20 – 40 kBq) to a solution containing ligand sock (10 μL; or deionized water for negative controls) in a variety of buffers. The actinium reaction mixtures were gently agitated using a vortex mixer and the pH was confirmed to

be between 5 - 11 by spotting a portion (1 - 2 μL) of the reaction mixture on pH paper. The radiochemical yield (RCY) was analyzed after 5, 60, and/or 120 minutes at room temperature/elevated temperatures. TLC imaging was performed using an AR-2000 imaging scanner equipped with PD-10 gas, and analysis of RCYs was carried out using WinScan V3_14 software. iTLC plate systems are as followed:

- Method A - aluminum backed silica with citrate buffer (0.4 M, pH 4.0). Free ^{225}Ac migrates with the solvent front ($R_f = 1$) while ^{225}Ac-ligand complexes will remain at the baseline ($R_f = 0$).
- Method B – paper backed iTLC-silicic acid with EDTA (50 mM, pH 7) as mobile phase. Free ^{225}Ac migrates with the solvent front ($R_f = 1$) while ^{225}Ac-ligand complexes will remain at the baseline ($R_f = 0$)

TLC radio-chromatograms of the initial radiolabeling (positive control, labeling, and a negative control) can be found in the Appendix. Measurements were done in triplicates.

References

(1) Canadian Cancer Society. https://cancer.ca/en/cancer-information/resources/publications/ 2019-canadian-cancer-statistics. (Accessed August 2021)

(2) Mayo Clinic. https://www.mayoclinic.org/diseases-conditions/cancer/diagnosis-treatment/drc-20370594. (Accessed August 2021)

(3) Kostelnik, T. I., and Orvig, C. (2019) Radioactive Main Group and Rare Earth Metals for Imaging and Therapy. *Chem. Rev. 119*, 902–956.

(4) Knapp, R., and Dash, A. (2017) Radiopharmaceuticals for therapy. *Springer*.

(5) Zeglis, B. M., and Lewis, J. S. (2011) A practical guide to the construction of radiometallated bioconjugates for positron emission tomography. *Dalt. Trans. 40*, 6168–6195.

(6) Canadian Medical Imaging Inventory. https://www.cadth.ca/imaginginventory. (Accessed August 2021)

(7) Poty, S., Francesconi, L. C., McDevitt, M. R., Morris, M. J., and Lewis, J. S. (2018) α-emitters for radiotherapy: From basic radiochemistry to clinical studies—part 1. *J. Nucl. Med. 59*, 878–884.

(8) Carbo-Bague, I., and Ramogida, C. F. (2021) Emerging Therapeutic Radiopharmaceuticals and Their Theranostic Pairs. *Encycl. Inorg. Bioinorg. Chem.*

(9) Cardinal Health. FDA-approved radiopharmaceuticals. https://www.cardinalhealth.com/en/product-solutions/pharmaceutical-products/nuclear-medicine/safety-and-compliance/fda-approved.html (Accessed August 2021)

(10) Ku, A., Facca, V. J., Cai, Z., and Reilly, R. M. (2019) Auger electrons for cancer therapy – a review. *EJNMMI Radiopharm. Chem. 4*.

(11) Vallis, K. A., Reilly, R. M., Scollard, D., Merante, P., Brade, A., Velauthapillai, S., Caldwell, C., Chan, I., Freeman, M., Lockwood, G., Miller, N. A., Cornelissen, B., Petronis, J., and Sabate, K. (2014) Phase I trial to evaluate the tumor and normal tissue uptake, radiation dosimetry and safety of (111)In-DTPA-human epidermal growth factor in patients with metastatic EGFR-positive breast cancer. *Am. J. Nucl. Med. Mol. Imaging 4*, 181–92.

(12) Thiele, N. A., and Wilson, J. J. (2018) Actinium-225 for targeted α therapy: Coordination chemistry and current chelation approaches. *Cancer Biother. Radiopharm. 33*, 336–348.

(13) Robertson, A. K. H., Ramogida, C. F., Schaffer, P., and Radchenko, V. (2018) Development of 225 Ac Radiopharmaceuticals: TRIUMF Perspectives and Experiences. *Curr. Radiopharm. 11*, 156–172.

(14) Price, E. W., and Orvig, C. (2014) Matching chelators to radiometals for radiopharmaceuticals. *Chem. Soc. Rev. 43*, 260–290.

(15) Clinical Trials. https://www.clinicaltrials.gov/ct2/home. (Accessed August 2021)

(16) Anderson, C. J., Dehdashti, F., Cutler, P. D., Schwarz, S. W., Laforest, R., Bass, L. A., Lewis, J. S., and Mccarthy, D. W. (2001) 64Cu-TETA-Octreotide as a PET Imaging Agent for Patients with Neuroendocrine Tumors. *J. Nucl. Med. 42*, 213–221.

(17) Thiele, N. A., Brown, V., Kelly, J. M., Amor-Coarasa, A., Jermilova, U., MacMillan, S. N., Nikolopoulou, A., Ponnala, S., Ramogida, C. F., Robertson, A. K. H., Rodríguez-Rodríguez, C., Schaffer, P., Williams, C., Babich, J. W., Radchenko, V., and Wilson, J. J. (2017) An Eighteen-Membered Macrocyclic Ligand for Actinium-225 Targeted Alpha Therapy. *Angew. Chemie - Int. Ed. 56*, 14712–14717.

(18) Dai, L., Jones, C. M., Chan, W. T. K., Pham, T. A., Ling, X., Gale, E. M., Rotile, N. J., Tai, W. C. S., Anderson, C. J., Caravan, P., and Law, G. L. (2018) Chiral DOTA chelators as an improved platform for biomedical imaging and therapy applications. *Nat. Commun. 9*, 1–10.

(19) Liu, S. (2008) Bifunctional coupling agents for radiolabeling of biomolecules and target-specific delivery of metallic radionuclides. *Adv. Drug Deliv. Rev. 60*, 1347–1370.

(20) Zhang, C., Lin, K. S., and Bénard, F. (2017) Molecular Imaging and Radionuclide Therapy of Melanoma Targeting the Melanocortin 1 Receptor. *Mol. Imaging 16*, 1–15.

(21) Zhang, C., Zhang, Z., Lin, K. S., Lau, J., Zeisler, J., Colpo, N., Perrin, D. M., and Bénard, F. (2018) Melanoma Imaging Using 18 F-Labeled α-Melanocyte-Stimulating Hormone Derivatives with Positron Emission Tomography. *Mol. Pharm. 15*, 2116–2122.

(22) Zhang, C., Zhang, Z., Zeisler, J., Colpo, N., Lin, K. S., and Bénard, F. (2020) Selective Cyclized α-Melanocyte-Stimulating Hormone Derivative with Multiple N-Methylations for Melanoma Imaging with Positron Emission Tomography. *ACS Omega 5*, 10767–10773.

(23) Zhang, C., Zhang, Z., Lin, K. S., Pan, J., Dude, I., Hundal-Jabal, N., Colpo, N., and Bénard, F. (2017) Preclinical melanoma imaging with 68Ga-labeled α-melanocyte-stimulating hormone Derivatives using PET. *Theranostics 7*, 805–813.

(24) Verhoeven, M., Seimbille, Y., and Dalm, S. U. (2019) Therapeutic applications of pretargeting. *Pharmaceutics 11*.

(25) Sgouros, G., Bodei, L., McDevitt, M. R., and Nedrow, J. R. (2020) Radiopharmaceutical therapy in cancer: clinical advances and challenges. *Nat. Rev. Drug Discov. 19*, 589–608.

(26) Thijssen, L., Schaart, D. R., De Vries, D., Morgenstern, A., Bruchertseifer, F., and Denkova, A. G. (2012) Polymersomes as nano-carriers to retain harmful recoil nuclides in alpha radionuclide therapy: A feasibility study. *Radiochim. Acta 100*, 473–481.

(27) Wong, J. Y. C. (2006) Basic immunology of antibody targeted radiotherapy. *Int. J. Radiat. Oncol. Biol. Phys. 66*, S8.

(28) Holliger, P., and Hudson, P. J. (2005) Engineered antibody fragments and the rise of single domains. *Nat. Biotechnol. 23*, 1126–1136.

(29) Ehmann, and Vance. (1991) Radiochemistry and nuclear methods of analysis. John Wiley and Sons Inc.

(30) de Kruijff, R. M., Wolterbeek, H. T., and Denkova, A. G. (2015) A critical review of alpha radionuclide therapy-how to deal with recoiling daughters? *Pharmaceuticals 8*, 321–336.

(31) Stylianopoulos, T., Poh, M. Z., Insin, N., Bawendi, M. G., Fukumura, D., Munn, L. L., and Jain, R. K. (2010) Diffusion of particles in the extracellular matrix: The effect of repulsive electrostatic interactions. *Biophys. J. 99*, 1342–1349.

(32) Sofou, S., Thomas, J. L., Lin, H. Y., McDevitt, M. R., Scheinberg, D. A., and Sgouros, G. (2004) Engineered liposomes for potential α-particle therapy of metastatic cancer. *J. Nucl. Med. 45*, 253–260.

(33) Wang, G., de Kruijff, R. M., Rol, A., Thijssen, L., Mendes, E., Morgenstern, A., Bruchertseifer, F., Stuart, M. C. A., Wolterbeek, H. T., and Denkova, A. G. (2014) Retention studies of recoiling daughter nuclides of 225Ac in polymer vesicles. *Appl. Radiat. Isot. 85*, 45–53.

(34) McLaughlin, M. F., Woodward, J., Boll, R. A., Wall, J. S., Rondinone, A. J., Kennel, S. J., Mirzadeh, S., and Robertson, J. D. (2013) Gold Coated Lanthanide Phosphate Nanoparticles for Targeted Alpha Generator Radiotherapy. *PLoS One 8*, 2–9.

(35) Raposinho, P. D., Correia, J. D. G., Oliveira, M. C., and Santos, I. (2010) Melanocortin-1 receptor-targeting with radiolabeled cyclic α-melanocyte-stimulating hormone analogs for melanoma imaging. *Biopolymers 94*, 820–829.

(36) Zhu, C., Bandekar, A., Sempkowski, M., Banerjee, S. R., Pomper, M. G., Bruchertseifer, F., Morgenstern, A., and Sofou, S. (2016) Nanoconjugation of PSMA-Targeting Ligands Enhances Perinuclear Localization and Improves Efficacy of Delivered Alpha-Particle Emitters against Tumor Endothelial Analogues. *Mol. Cancer Ther. 15*, 106–113.

(37) Bandekar, A., Zhu, C., Jindal, R., Bruchertseifer, F., Morgenstern, A., and Sofou, S. (2014) Anti–Prostate-Specific Membrane Antigen Liposomes Loaded with 225 Ac for Potential Targeted Antivascular α-Particle Therapy of Cancer. *J. Nucl. Med. 55*, 107–114.

(38) de Kruijff, R. M., Drost, K., Thijssen, L., Morgenstern, A., Bruchertseifer, F., Lathouwers, D., Wolterbeek, H. T., and Denkova, A. G. (2017) Improved 225 Ac daughter retention in InPO4 containing polymersomes. *Appl. Radiat. Isot. 128*, 183–189.

(39) Zhu, C., Sempkowski, M., Holleran, T., Linz, T., Bertalan, T., Josefsson, A., Bruchertseifer, F., Morgenstern, A., and Sofou, S. (2017) Alpha-particle radiotherapy: For large solid tumors diffusion trumps targeting. *Biomaterials 130*, 67–75.

(40) Cordier, D., Forrer, F., Bruchertseifer, F., Morgenstern, A., Apostolidis, C., Good, S., Müller-Brand, J., Mäcke, H., Reubi, J. C., and Merlo, A. (2010) Targeted alpha-radionuclide therapy of functionally critically located gliomas with 213Bi-DOTA-[Thi8,Met(O2)11]- substance P: A pilot trial. *Eur. J. Nucl. Med. Mol. Imaging 37*, 1335–1344.

(41) Meredith, R. F., Torgue, J., Azure, M. T., Shen, S., Saddekni, S., Banaga, E., Carlise, R., Bunch, P., Yoder, D., and Alvarez, R. (2014) Pharmacokinetics and imaging of 212Pb-TCMC-trastuzumab after intraperitoneal administration in ovarian cancer patients. *Cancer Biother. Radiopharm. 29*, 12–17.

(42) Zalutsky, M. R., Reardon, D. A., Akabani, G., Coleman, R. E., Friedman, A. H., Friedman, H. S., McLendon, R. E., Wong, T. Z., and Bigner, D. D. (2008) Clinical experience with α-particle-emitting 211 At: Treatment of recurrent brain tumor patients with 211 At-labeled chimeric antitenascin monoclonal antibody 81C6. *J. Nucl. Med. 49*, 30–38.

(43) Deblonde, G. J. P., and Abergel, R. J. (2016) Active actinium. *Nat. Chem. 8*, 1084.

(44) Ferrier, M. G., Stein, B. W., Batista, E. R., Berg, J. M., Birnbaum, E. R., Engle, J. W., John, K. D., Kozimor, S. A., Lezama Pacheco, J. S., and Redman, L. N. (2017) Synthesis and Characterization of the Actinium Aquo Ion. *ACS Cent. Sci. 3*, 176–185.

(45) Jurcic, J. G., and Rosenblat, T. L. (2014) Targeted Alpha-Particle immunotherapy for acute myeloid leukemia. *Am. Soc. Clin. Oncol. Educ. B.* 126–131.

(46) Jurcic, J. G., Levy, M. Y., Park, J. H., Ravandi, F., Perl, A. E., Pagel, J. M., Smith, B. D., Estey, E. H., Kantarjian, H., Cicic, D., and Scheinberg, D. A. (2016) Phase I Trial of Targeted Alpha-Particle Therapy with Actinium-225 (225Ac)-Lintuzumab and Low-Dose Cytarabine (LDAC) in Patients Age 60 or Older with Untreated Acute Myeloid Leukemia (AML). *Blood 128*, 4050–4050.

(47) Ballal, S., Yadav, M. P., Bal, C., Sahoo, R. K., and Tripathi, M. (2020) Broadening horizons with 225Ac-DOTATATE targeted alpha therapy for gastroenteropancreatic neuroendocrine tumour patients stable or refractory to 177Lu-DOTATATE PRRT: first clinical experience on the efficacy and safety. *Eur. J. Nucl. Med. Mol. Imaging 47*, 934–946.

(48) Zhang, J., Kulkarni, H. R., and Baum, R. P. (2020) Peptide Receptor Radionuclide Therapy Using 225Ac-DOTATOC Achieves Partial Remission in a Patient with Progressive Neuroendocrine Liver Metastases after Repeated β-Emitter Peptide Receptor Radionuclide Therapy. *Clin. Nucl. Med. 45*, 241–243.

(49) Królicki, L., Bruchertseifer, F., Kunikowska, J., Koziara, H., Pawlak, D., Kuliński, R., Rola, R., Merlo, A., and Morgenstern, A. (2021) Dose escalation study of targeted alpha therapy with [225Ac]Ac-DOTA-substance P in recurrence glioblastoma – safety and efficacy. *Eur. J. Nucl. Med. Mol. Imaging*.

(50) Khreish, F., Ebert, N., Ries, M., Maus, S., Rosar, F., Bohnenberger, H., Stemler, T., Saar, M., Bartholomä, M., and Ezziddin, S. (2020) 225Ac-PSMA-617/177Lu-PSMA-617 tandem therapy of metastatic castration-resistant prostate cancer: pilot experience. *Eur. J. Nucl. Med. Mol. Imaging 47*, 721–728.

(51) Kratochwil, C., Bruchertseifer, F., Rathke, H., Hohenfellner, M., Giesel, F. L., Haberkorn, U., and Morgenstern, A. (2018) Targeted a-therapy of metastatic castration-resistant prostate cancer with 225 Ac-PSMA-617: Swimmer-Plot Analysis Suggests efficacy regarding duration of tumor control. *J. Nucl. Med. 59*, 795–802.

(52) Sathekge, M., Bruchertseifer, F., Knoesen, O., Reyneke, F., Lawal, I., Lengana, T., Davis, C., Mahapane, J., Corbett, C., Vorster, M., and Morgenstern, A. (2019) 225Ac-PSMA-617 in chemotherapy-naive patients with advanced prostate cancer: a pilot study. *Eur. J. Nucl. Med. Mol. Imaging 46*, 129–138.

(53) Sathekge, M., Bruchertseifer, F., Vorster, M., Lawal, I. O., Knoesen, O., Mahapane, J., Davis, C., Reyneke, F., Maes, A., Kratochwil, C., Lengana, T., Giesel, F. L., van de Wiele, C., and Morgenstern, A. (2020) Predictors of overall and disease-free survival in metastatic castration-resistant prostate cancer patients receiving 225Ac-PSMA-617 radioligand therapy. *J. Nucl. Med. 61*, 62–69.

(54) Kratochwil, C., Bruchertseifer, F., Giesel, F. L., Weis, M., Verburg, F. A., Mottaghy, F., Kopka, K., Apostolidis, C., Haberkorn, U., and Morgenstern, A. (2016) 225Ac-PSMA-617 for PSMA-Targeted a -Radiation Therapy of Metastatic Castration-Resistant Prostate Cancer 1941–1945.

(55) Mcdevitt, M. R., Ma, D., Simon, J., Keith Frank, R., and Scheinberg, D. A. (2002) Design and synthesis of ^{225}Ac radioimmunopharmaceuticals. *Appl. Radiat. Isot. 57*, 841–847.

(56) Davis, I. A., Glowienka, K. A., Boll, R. A., Deal, K. A., Brechbiel, M. W., Stabin, M., Bochlser, P. N., Mirzadeh, S., and Kennel, S. J. (1999) Comparison of 225 Actinium Chelates : Tissue distribution and radiotoxicity. *Nucl. Med. Biol. 26*, 581–589.

(57) Beyer, G. J., Offord, R., Künzi, G., Aleksandrova, Y., Ravn, U., Jahn, S., Barker, J., Tengblad, O., and Lindroos, M. (1997) The influence of EDTMP-concentration on the biodistribution of radio-lanthanides and 225-Ac in tumor-bearing mice. The ISOLDE Collaboration. *Nucl. Med. Biol. 24*, 367–372.

(58) Maguire, W. F., McDevitt, M. R., Smith-Jones, P. M., and Scheinberg, D. A. (2014) Efficient 1-step radiolabeling of monoclonal antibodies to high specific activity with 225Ac for a-particle radioimmunotherapy of cancer. *J. Nucl. Med. 55*, 1492–1498.

(59) Jaggi, J. S., Kappel, B. J., McDevitt, M. R., Sgouros, G., Flombaum, C. D., Cabassa, C., and Scheinberg, D. A. (2005) Efforts to control the errant products of a targeted in vivo generator. *Cancer Res. 65*, 4888–4895.

(60) Poty, S., Carter, L. M., Mandleywala, K., Membreno, R., Abdel-Atti, D., Ragupathi, A., Scholz, W. W., Zeglis, B. M., and Lewis, J. S. (2019) Leveraging bioorthogonal click chemistry to improve 225 AC-radioimmunotherapy of pancreatic ductal adenocarcinoma. *Clin. Cancer Res. 25*, 868–880.

(61) Melanoma network of Canada. https://www.melanomanetwork.ca/stats-and-facts/. (Accessed August 2021)

(62) Canadian Cancer Society.https://cancer.ca/en/cancer-information/cancer-types/skin-non-melanoma. (Accessed August 2021)

(63) Canadian Cancer Society. https://cancer.ca/en/cancer-information/cancer-types/skin-melanoma. (Accessed August 2021).

(64) Rosenkranz, A. A., Slastnikova, T. A., Durymanov, M. O., and Sobolev, A. S. (2013) Malignant melanoma and melanocortin 1 receptor. *Biochem. 78*, 1228–1237.

(65) Schiöth, H. B., Muceniece, R., Mutulis, F., Prusis, P., Lindeberg, G., Sharma, S. D., Hruby, V. J., and Wikberg, J. E. . (1997) Selectivity of Cyclic [d-Nal7] and [d-Phe7] Substituted MSH Analogues for the Melanocortin Receptor Subtypes. *Peptides 18*, 1009–1013.

(66) Ramogida, C. F., Robertson, A. K. H., Jermilova, U., Zhang, C., Yang, H., Kunz, P., Lassen, J., Bratanovic, I., Brown, V., Southcott, L., Rodríguez-Rodríguez, C., Radchenko, V., Bénard, F., Orvig, C., and Schaffer, P. (2019) Evaluation of polydentate picolinic acid chelating ligands and an α-melanocyte-stimulating hormone derivative for targeted alpha therapy using ISOL-produced 225Ac. *EJNMMI Radiopharm. Chem. 4*, 1–20.

(67) Yang, H., Zhang, C., Yuan, Z., Rodriguez-Rodriguez, C., Robertson, A., Radchenko, V., Perron, R., Gendron, D., Causey, P., Gao, F., Bénard, F., and Schaffer, P. (2020) Synthesis and Evaluation of a Macrocyclic Actinium-225 Chelator, Quality Control and In Vivo Evaluation of 225Ac-crown-αMSH Peptide. *Chem. - A Eur. J. 26*, 11435–11440.

(68) Kuo, H. T., Merkens, H., Zhang, Z., Uribe, C. F., Lau, J., Zhang, C., Colpo, N., Lin, K. S., and Bénard, F. (2018) Enhancing Treatment Efficacy of 177Lu-PSMA-617 with the Conjugation of an Albumin-Binding Motif: Preclinical Dosimetry and Endoradiotherapy Studies. *Mol. Pharm. 15*, 5183–5191.

(69) Doedens, L., Opperer, F., Cai, M., Beck, J. G., Dedek, M., Palmer, E., Hruby, V. J., and Kessler, H. (2010) Multiple N -Methylation of MT-II Backbone Amide Bonds Leads to Melanocortin Receptor Subtype hMC1R Selectivity: Pharmacological and Conformational Studies. *J. Am. Chem. Soc. 132*, 8115–8128.

(70) Ramogida, C. F., and Orvig, C. (2013) Tumor targeting with radiometals for diagnosis and therapy. *Chem. Commun. 29*, 4720–4739.

(71) Robertson, A. K. H., McNeil, B. L., Yang, H., Gendron, D., Perron, R., Radchenko, V., Zeisler, S., Causey, P., and Schaffer, P. (2020) 232Th-Spallation-Produced 225Ac with Reduced 227Ac Content. *Inorg. Chem. 59*, 12156–12165.

(72) Wharton, L., Kurakina, E., Radchenko, V., Schaffer, P., and Orvig, C. (2021) Chemical Promiscuity of Non-Macrocyclic Multidentate Chelating Ligands for Radiometal Ions: H4neunpa-NH2vs H4noneunpa. *Inorg. Chem. 60*, 4076–4092.

(73) Deal, K. A., Davis, I. A., Mirzadeh, S., Kennel, S. J., and Brechbiel, M. W. (1999) Improved in vivo stability of actinium-225 macrocyclic complexes. *J. Med. Chem. 42*, 2988–2992.

(74) Li, L., Rousseau, J., Jaraquemada-Peláez, M. D. G., Wang, X., Robertson, A., Radchenko, V., Schaffer, P., Lin, K. S., Bénard, F., and Orvig, C. (2021) 225Ac-H4py4pa for Targeted Alpha Therapy. *Bioconjug. Chem. 32*, 1348–1363.

(75) Kelly, J. M., Amor-Coarasa, A., Ponnala, S., Nikolopoulou, A., Williams, C., Thiele, N. A., Schlyer, D., Wilson, J. J., DiMagno, S. G., and Babich, J. W. (2019) A Single Dose of 225 Ac-RPS-074 Induces a Complete Tumor Response in an LNCaP Xenograft Model. *J. Nucl. Med. 60*, 649–655.

(76) Fiszbein, D. J., Brown, V., Thiele, N. A., Woods, J. J., Wharton, L., Macmillan, S. N., Radchenko, V., Ramogida, C. F., and Wilson, J. J. (2021) Tuning the Kinetic Inertness of Bi3+Complexes: The Impact of Donor Atoms on Diaza-18-Crown-6 Ligands as Chelators for 213Bi Targeted Alpha Therapy. *Inorg. Chem. 60*, 9199–9211.

(77) Workman, D. G., Hunter, M., Dover, L. G., and Tétard, D. (2016) Synthesis of novel Iron(III) chelators based on triaza macrocycle backbone and 1-hydroxy-2(H)-pyridin-2-one coordinating groups and their evaluation as antimicrobial agents. *J. Inorg. Biochem. 160*, 49–58.

(78) Roca-Sabio, A., Mato-Iglesias, M., Esteban-Gómez, D., Tóth, É., Blas, A. de, Platas-Iglesias, C., and Rodríguez-Blas, T. (2009) Macrocyclic Receptor Exhibiting Unprecedented Selectivity for Light Lanthanides. *J. Am. Chem. Soc. 131*, 3331–3341.

(79) Thiele, N. A., Fiszbein, D. J., Woods, J. J., and Wilson, J. J. (2020) Tuning the Separation of Light Lanthanides Using a Reverse-Size Selective Aqueous Complexant. *Inorg. Chem. 59*, 16522–16530.

(80) Thiele, N. A., Macmillan, S. N., and Wilson, J. J. (2018) Rapid Dissolution of BaSO 4 by Macropa, an 18-Membered Macrocycle with High Affinity for Ba 2+. *J. Am. Chem. Soc. 140*, 17071–17078.

(81) Wang, X., Jaraquemada-Peláez, M. D. G., Rodríguez-Rodríguez, C., Cao, Y., Buchwalder, C., Choudhary, N., Jermilova, U., Ramogida, C. F., Saatchi, K., Häfeli, U. O., Patrick, B. O., and Orvig, C. (2018) H4octox: Versatile Bimodal Octadentate Acyclic Chelating Ligand for Medicinal Inorganic Chemistry. *J. Am. Chem. Soc. 140*, 15487–15500.

(82) Wang, X., Jaraquemada-Peláez, M. D. G., Cao, Y., Pan, J., Lin, K. S., Patrick, B. O., and Orvig, C. (2019) H2hox: Dual-Channel Oxine-Derived Acyclic Chelating Ligand for 68 Ga Radiopharmaceuticals. *Inorg. Chem. 58*, 2275–2285.

(83) Boros, E., Ferreira, C. L., Cawthray, J. F., Price, E. W., Patrick, B. O., Wester, D. W., Adam, M. J., and Orvig, C. (2010) Acyclic chelate with ideal properties for 68Ga PET imaging agent elaboration. *J. Am. Chem. Soc. 132*, 15726–15733.

(84) Price, E. W., Cawthray, J. F., Bailey, G. A., Ferreira, C. L., Boros, E., Adam, M. J., and Orvig, C. (2012) H4octapa: An Acyclic Chelator for 111 In Radiopharmaceuticals. *J. Am. Chem. Soc. 134*, 8670–8683.

(85) Cilibrizzi, A., Abbate, V., Chen, Y. L., Ma, Y., Zhou, T., and Hider, R. C. (2018) Hydroxypyridinone Journey into Metal Chelation. *Chem. Rev. 118*, 7657–7701.

(86) Thiele, N. A., Woods, J. J., and Wilson, J. J. (2019) Implementing f-block metal ions in medicine: tuning the size selectivity of expanded macrocycles. *Inorg. Chem. 58*, 10483–10500.

(87) Deri, M. A., Ponnala, S., Zeglis, B. M., Pohl, G., Dannenberg, J. J., Lewis, J. S., and Francesconi, L. C. (2014) Alternative Chelator for 89 Zr Radiopharmaceuticals: Radiolabeling and Evaluation of 3,4,3-(LI-1,2-HOPO). *J. Med. Chem. 57*, 4849–4860.

Appendix

^{1}H & ^{13}C NMR Spectra

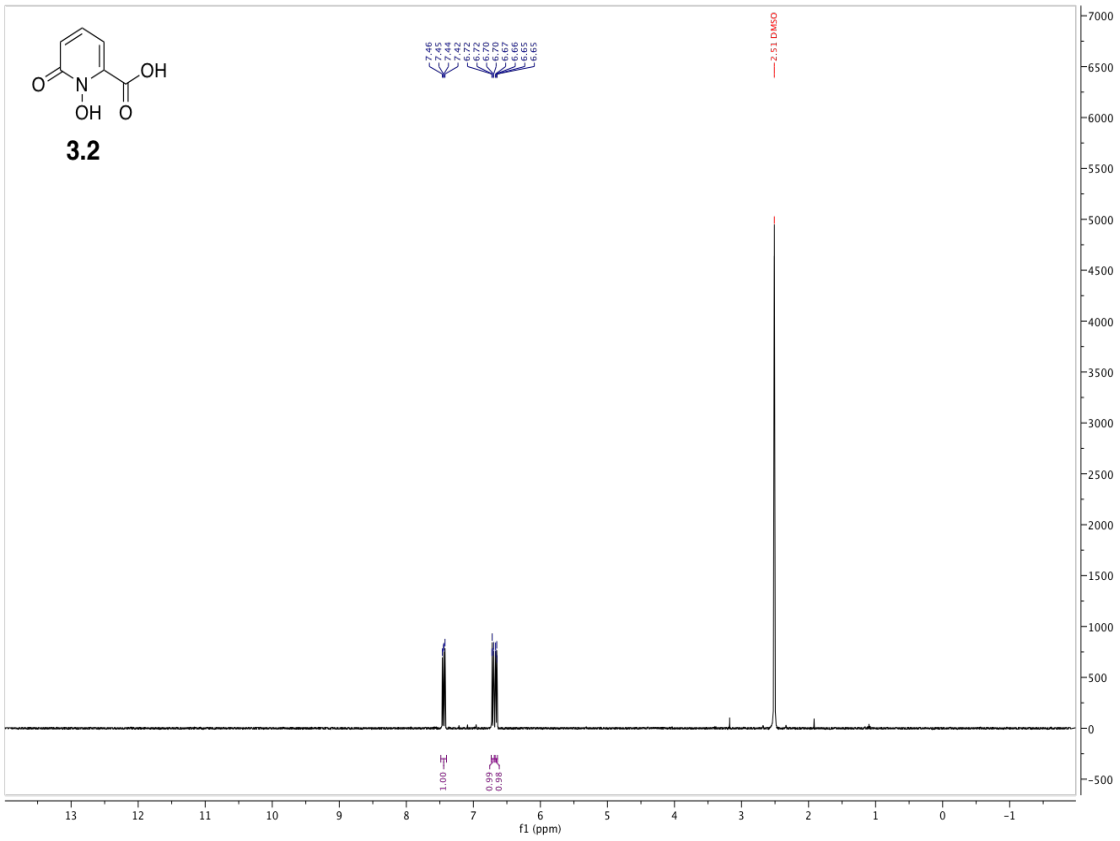

Figure A1: ^{1}H NMR (400 MHz, DMSO-d_6) of 1-hydroxy-6-oxo-1,6-dihydropyridine-2-carboxylic acid (1,2-HOPO-Acid, 3.2)

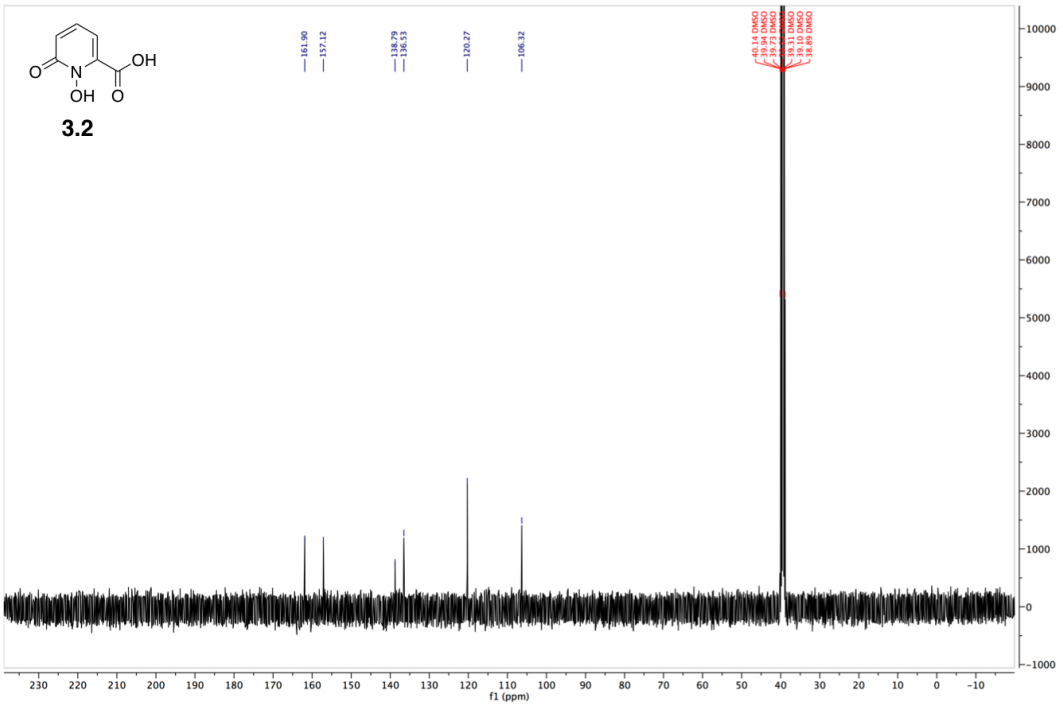

Figure A2: ^{13}C **NMR (101 MHz, DMSO-d$_6$) of 1-hydroxy-6-oxo-1,6-dihydropyridine-2-carboxylic acid (1,2-HOPO-Acid, 3.2)**

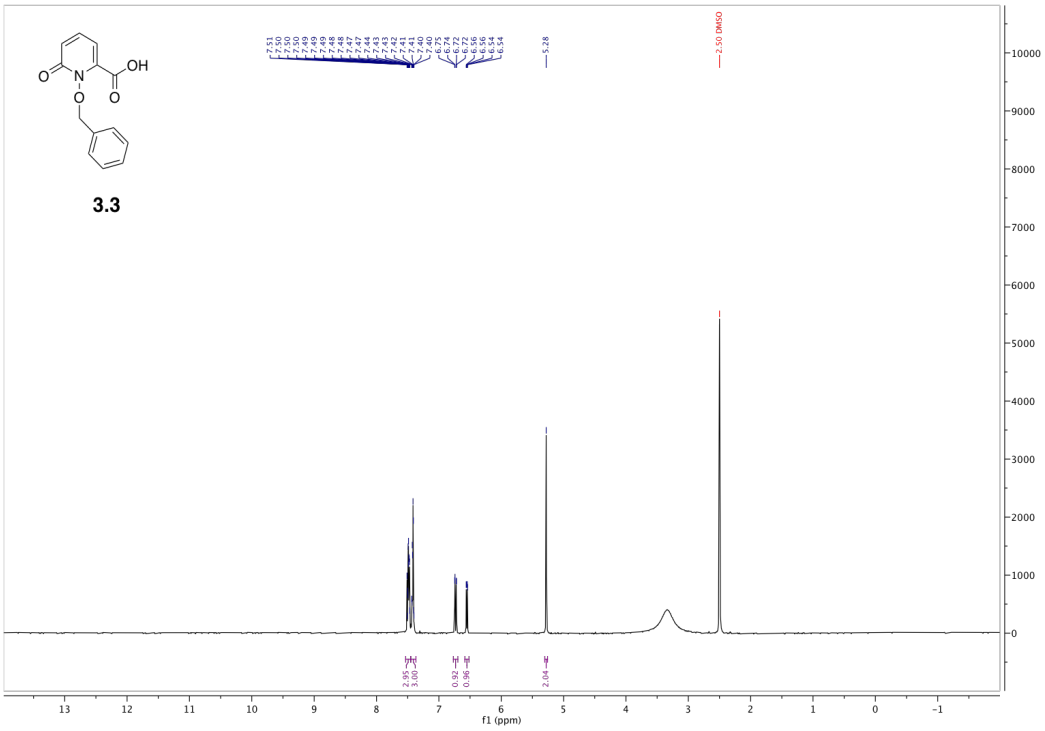

Figure A3: ^{1}H NMR (400 MHz, DMSO-d_6) of 1-(benzyloxy)-6-oxo-1,6-dihydropyridine-2-carboxylic acid (1,2-HOPO-OBn-Acid, 3.3)

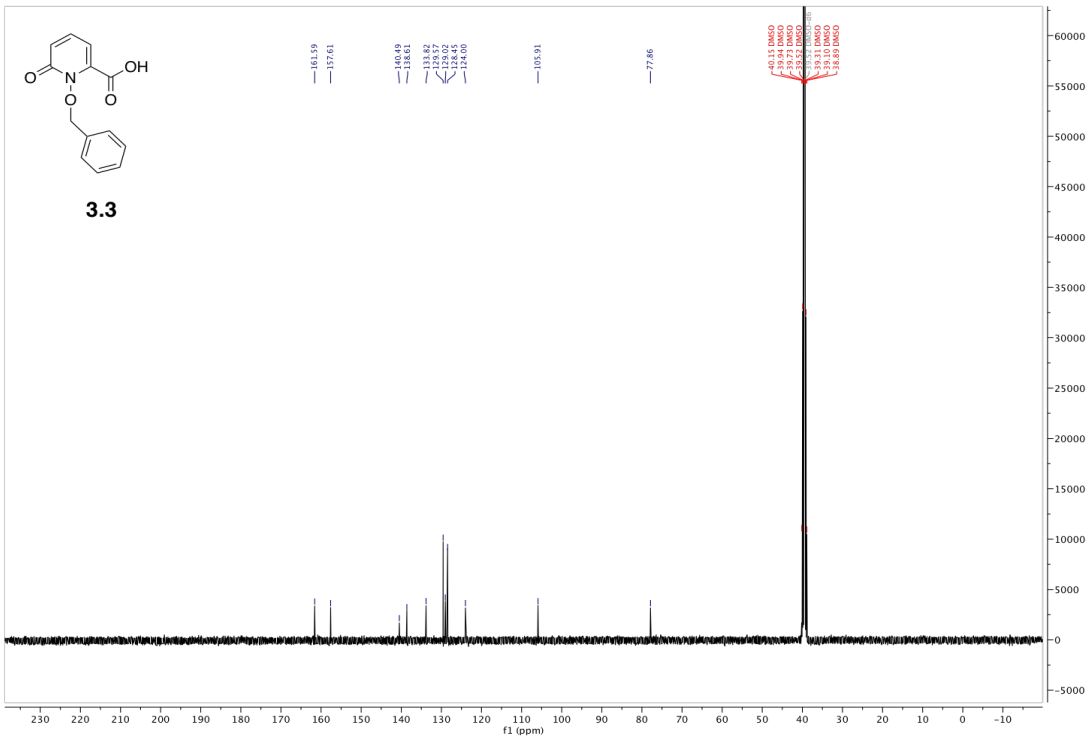

Figure A4: ^{13}C NMR (101 MHz, DMSO-d_6) of 1-(benzyloxy)-6-oxo-1,6-dihydropyridine-2-carboxylic acid (1,2-HOPO-OBn-Acid, 3.3)

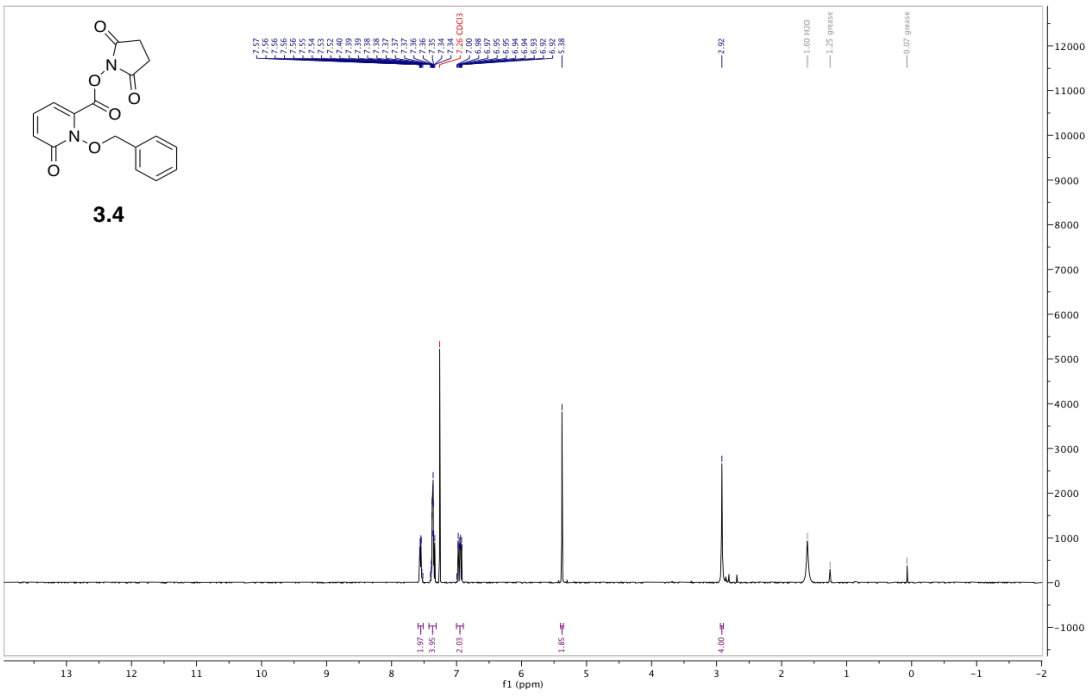

Figure A5: **^{1}H NMR (400 MHz, $CDCl_3$) of 2,5-dioxopyrrolidin-1-yl 1-(benzyloxy)-6-oxo-1,6-dihydropyridine-2-carboxylate (1,2-HOPO-OBn-Succ, 3.4)**

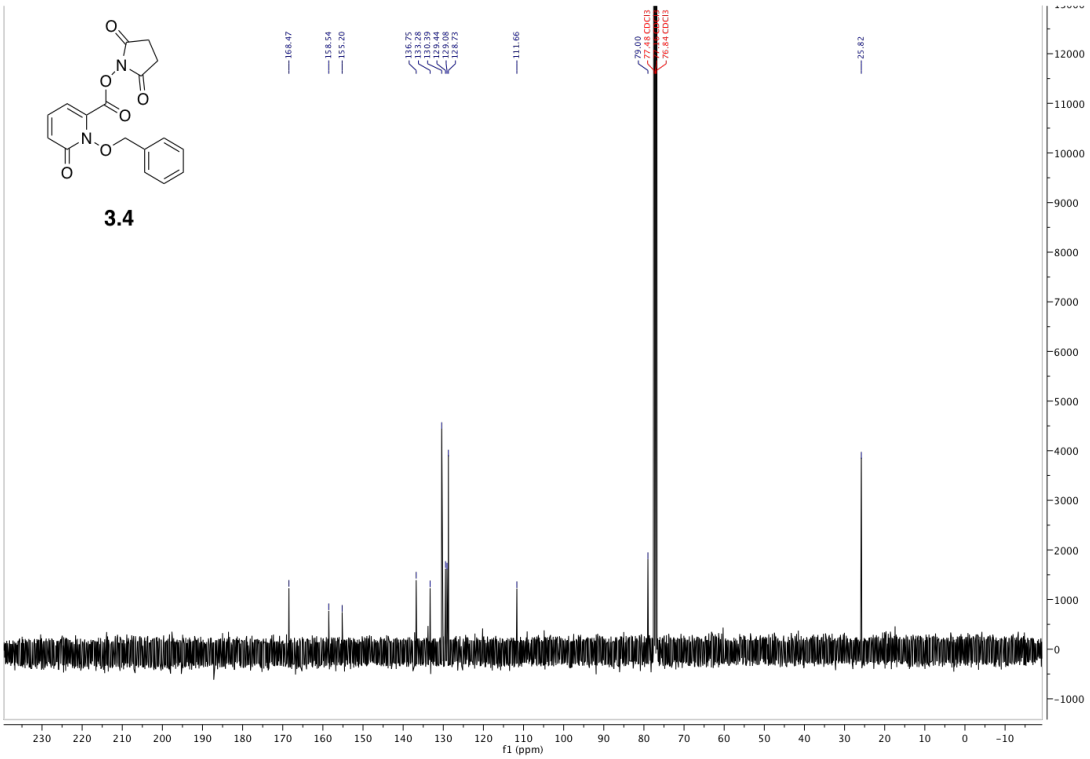

Figure A6: **^{13}C NMR (101 MHz, $CDCl_3$) of 2,5-dioxopyrrolidin-1-yl 1-(benzyloxy)-6-oxo-1,6-dihydropyridine-2-carboxylate (1,2-HOPO-OBn-Succ, 3.4)**

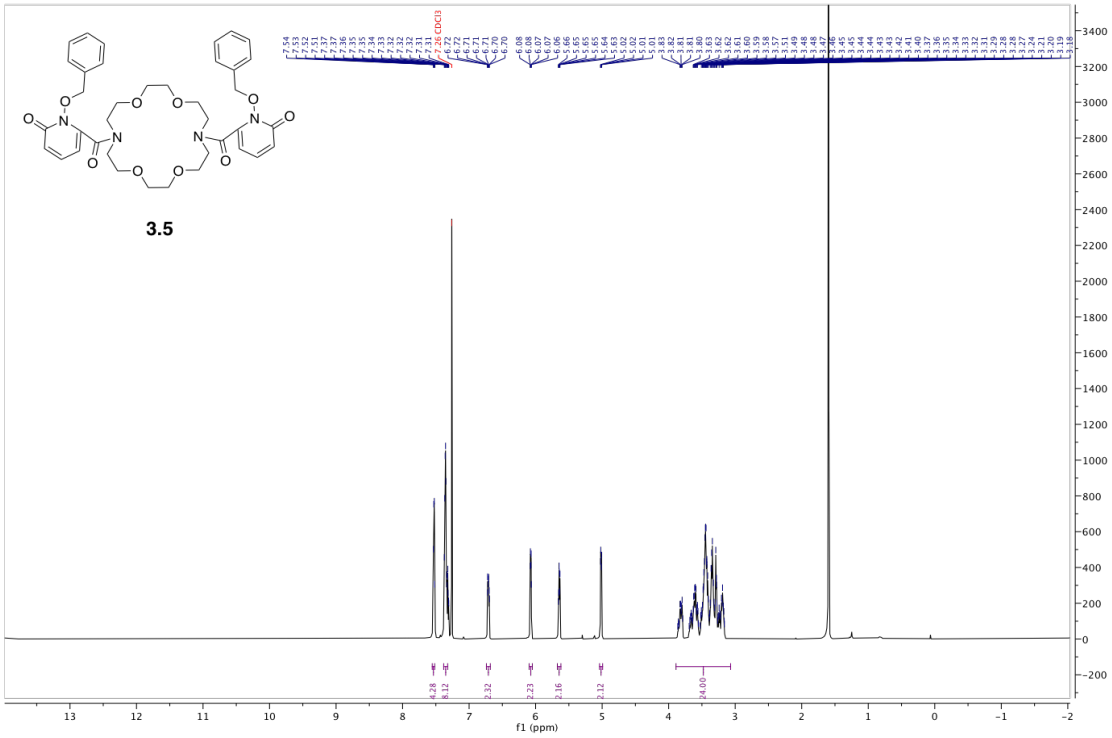

Figure A7: **^{1}H NMR (600 MHz, $CDCl_3$) of 6,6'-(1,4,10,13-tetraoxa-7,16-diazacyclooctadecane-7,16-dicarbonyl)bis(1-(benzyloxy)pyridin-2 (1H)-one)(1,2-HOPO-OBn-crown, 3.5)**

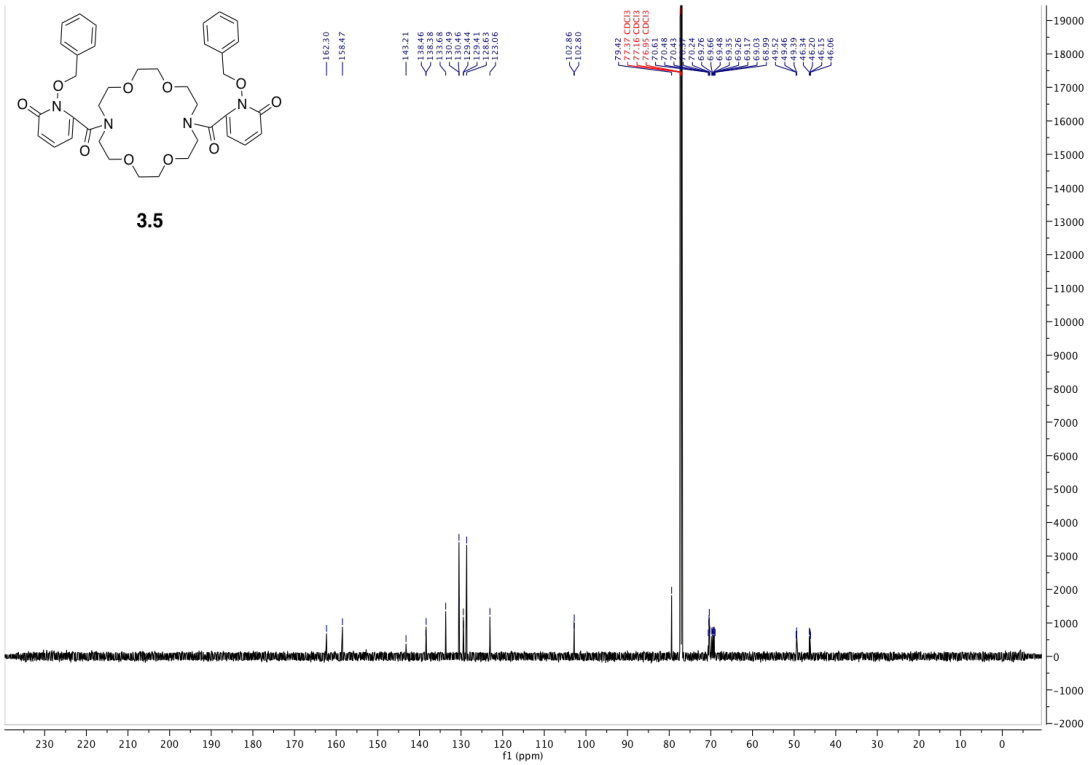

Figure A8: **^{13}C NMR (151 MHz, $CDCl_3$) of 6,6'-(1,4,10,13-tetraoxa-7,16-diazacyclooctadecane-7,16-dicarbonyl)bis(1-(benzyloxy)pyridin-2(1H)-one)(1,2-HOPO-OBn-crown, 3.5)**

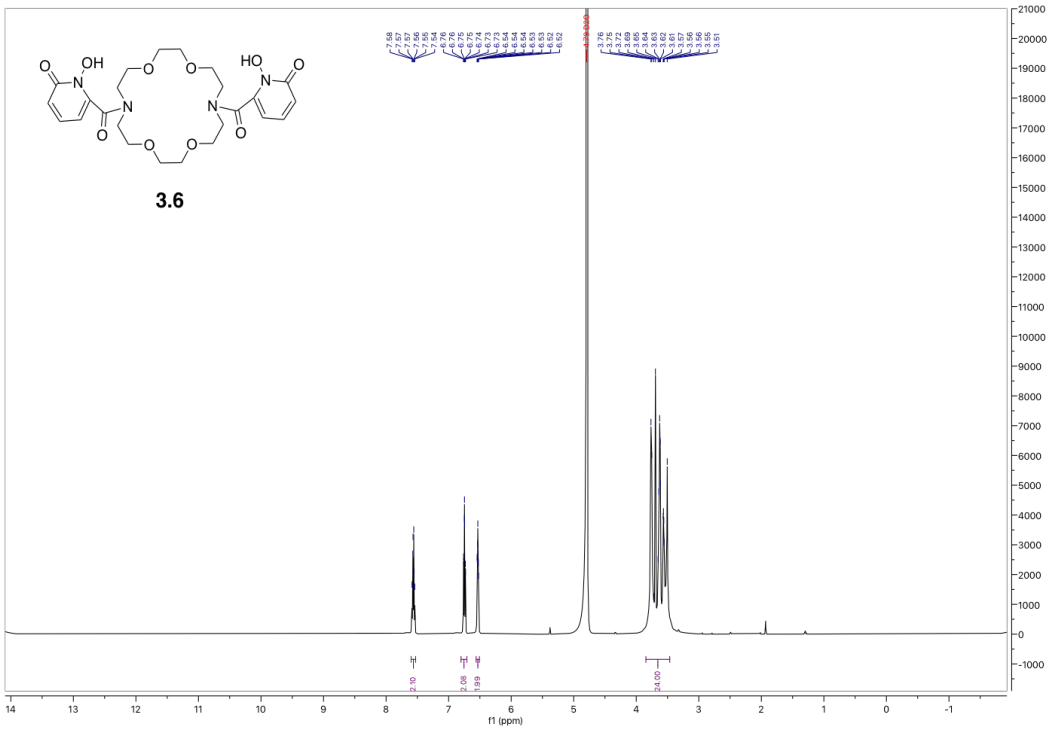

Figure A9: **^{1}H NMR (600 MHz, D_2O) of 6,6'-(1,4,10,13-tetraoxa-7,16-diazacyclooctadecane-7,16-dicarbonyl)bis(1-hydroxypyridin-2(1H)-one) (macrohopo, 3.6)**

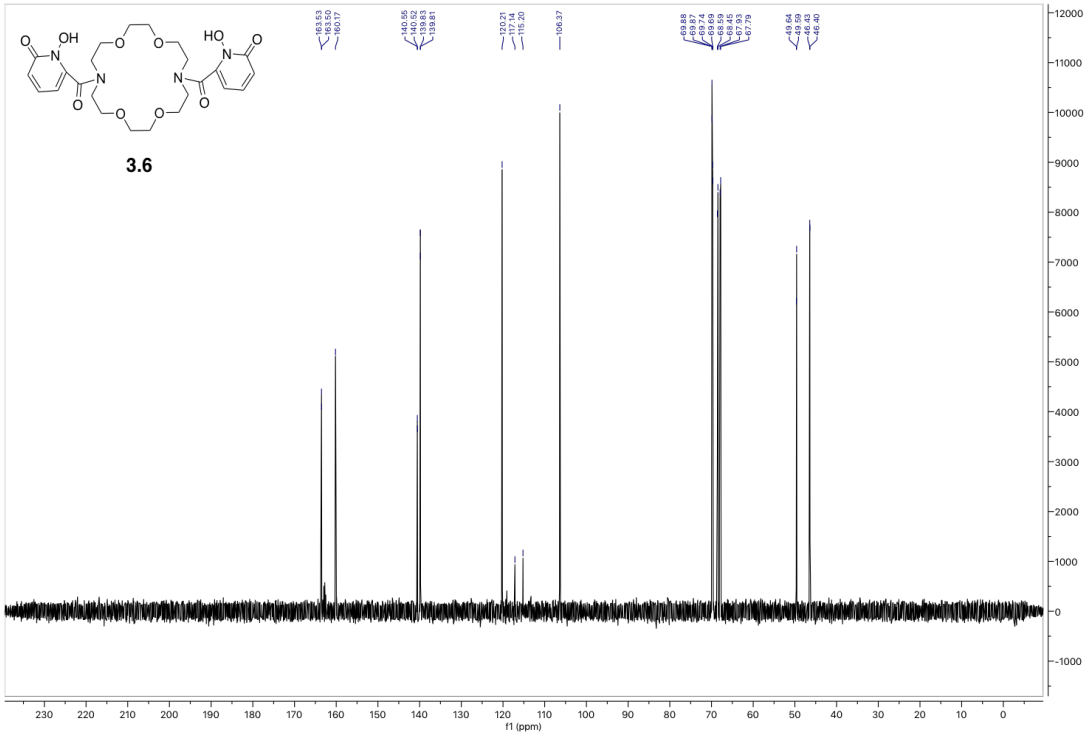

Figure A10: ^{13}C NMR (151 MHz, D_2O) of 6,6'-(1,4,10,13-tetraoxa-7,16-diazacyclooctadecane-7,16-dicarbonyl)bis(1-hydroxypyridin-2(1H)-one) (macrohopo, 3.6)

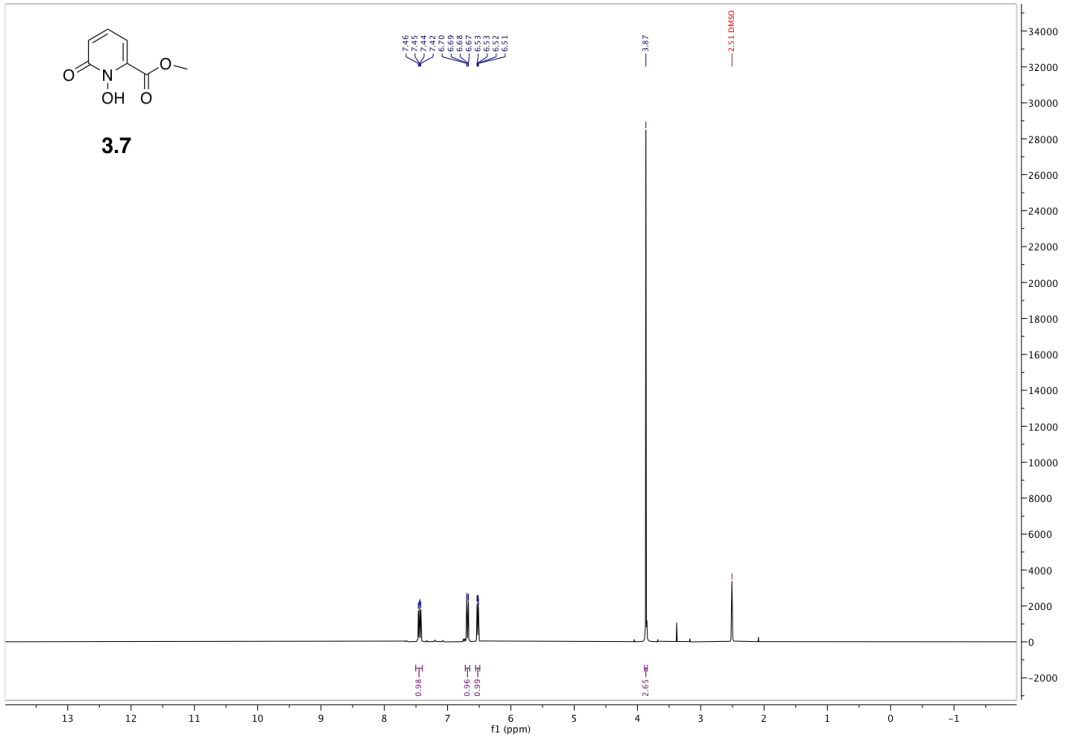

Figure A11: ^{1}H NMR (400 MHz, DMSO-d$_6$) of methyl 1-hydroxy-6-oxo-1,6-dihydropyridine-2-carboxylate, (1,2-HOPO-methylester, 3.7)

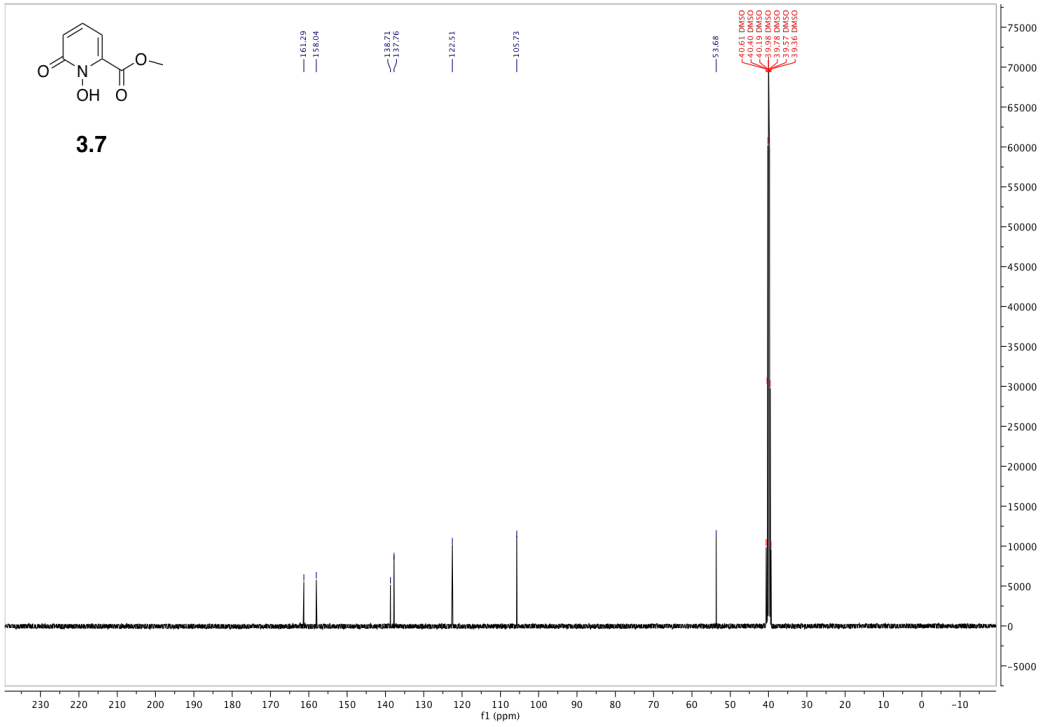

Figure A12: ^{13}C NMR (101 MHz, DMSO-d$_6$) of methyl 1-hydroxy-6-oxo-1,6-dihydropyridine-2-carboxylate, (1,2-HOPO-methylester, 3.7)

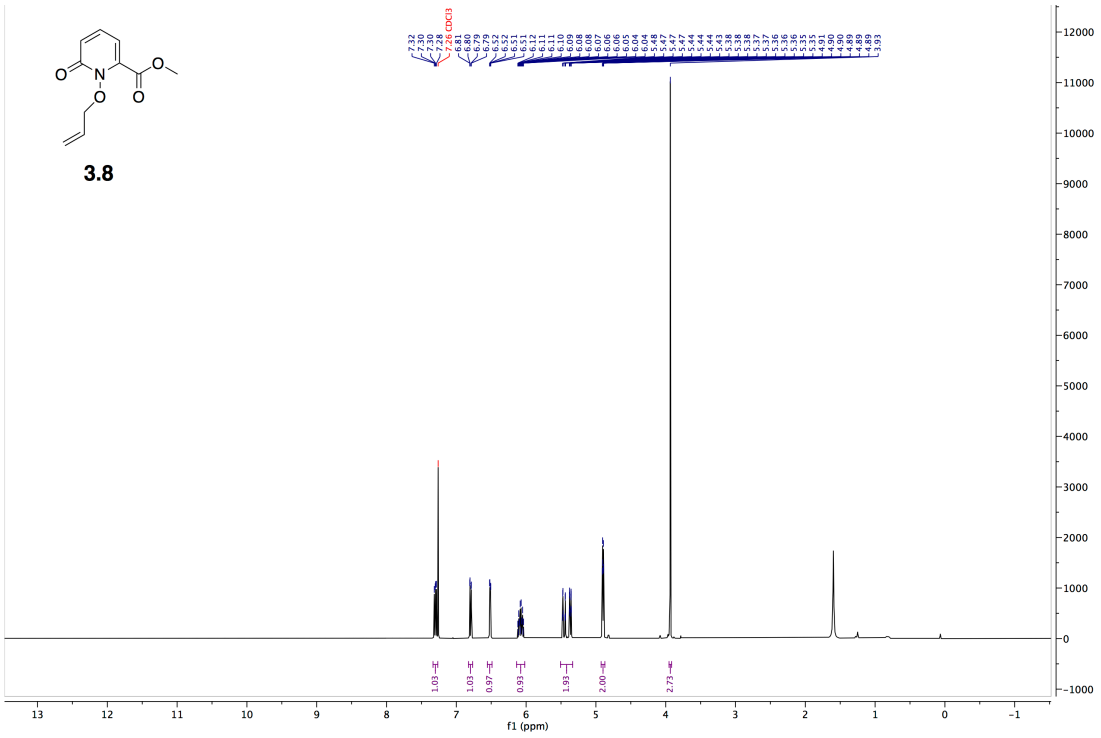

Figure A13: **^{1}H NMR (500 MHz, $CDCl_3$) of methyl-1-(allyloxy)-6-oxo-1,6-dihydropyridine-2-carboxylate (1,2-HOPO-allyl-methylester, 3.8)**

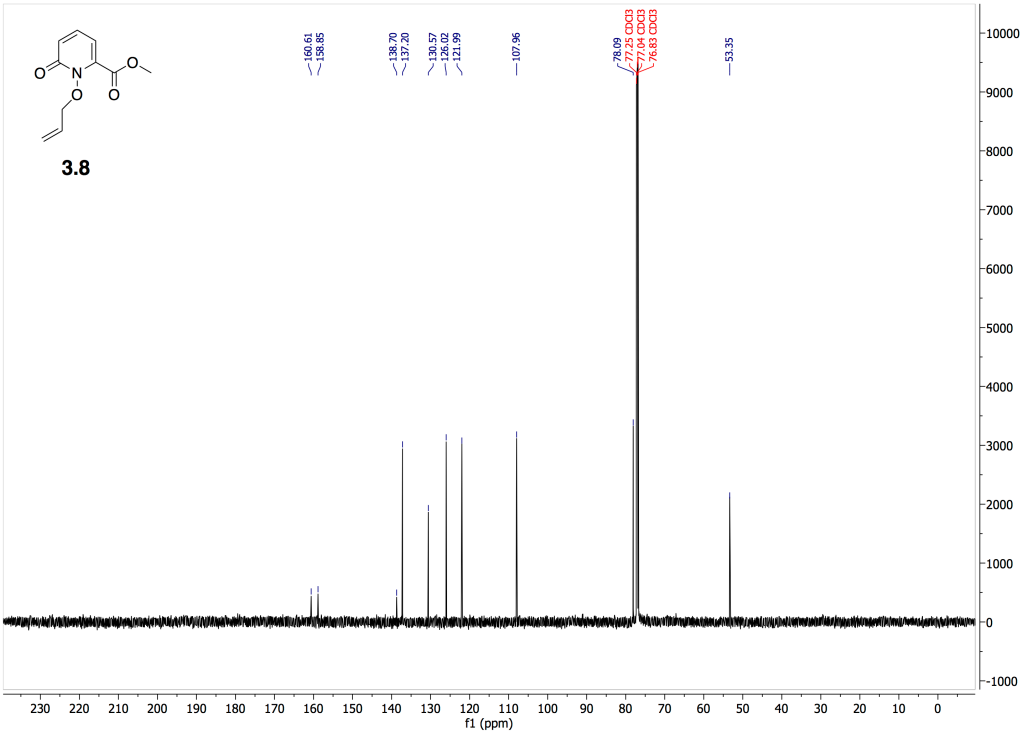

Figure A14: **^{13}C NMR (126 MHz, $CDCl_3$) of methyl-1-(allyloxy)-6-oxo-1,6-dihydropyridine-2-carboxylate (1,2-HOPO-allyl-methylester, 3.8)**

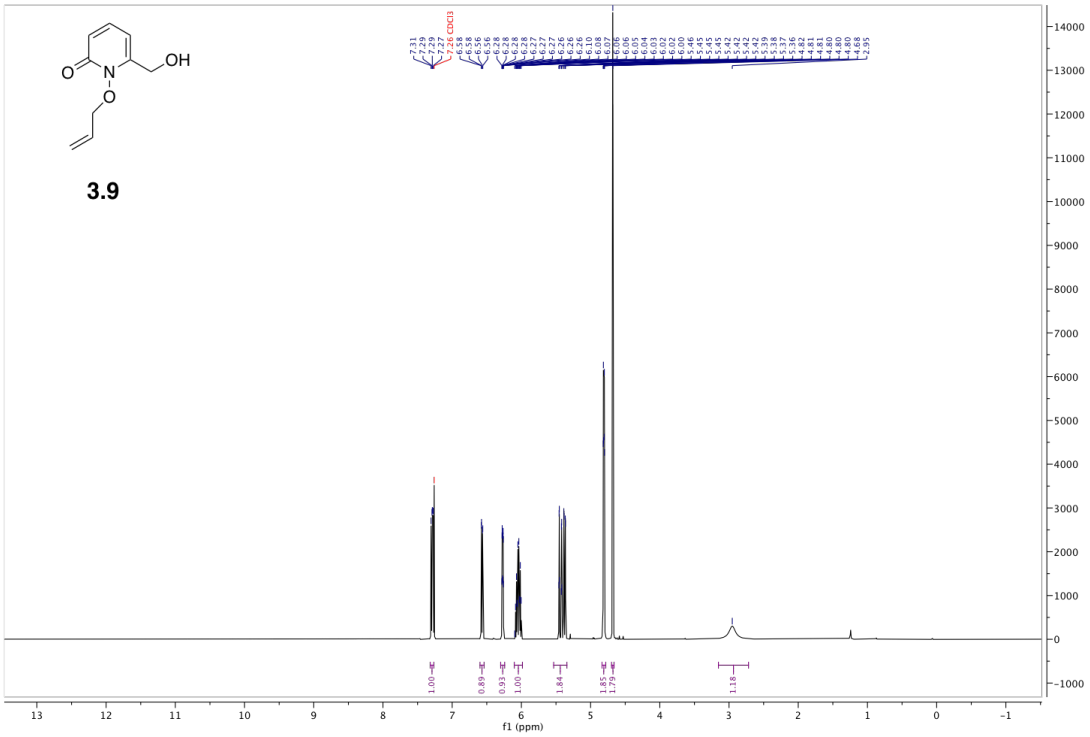

Figure A15: ^{1}H NMR (500 MHz, $CDCl_3$) of 1-(allyloxy)-6-(hydroxymethyl)pyridin-2(1H)-one (1,2-HOPO-allyl-hydroxide, 3.9)

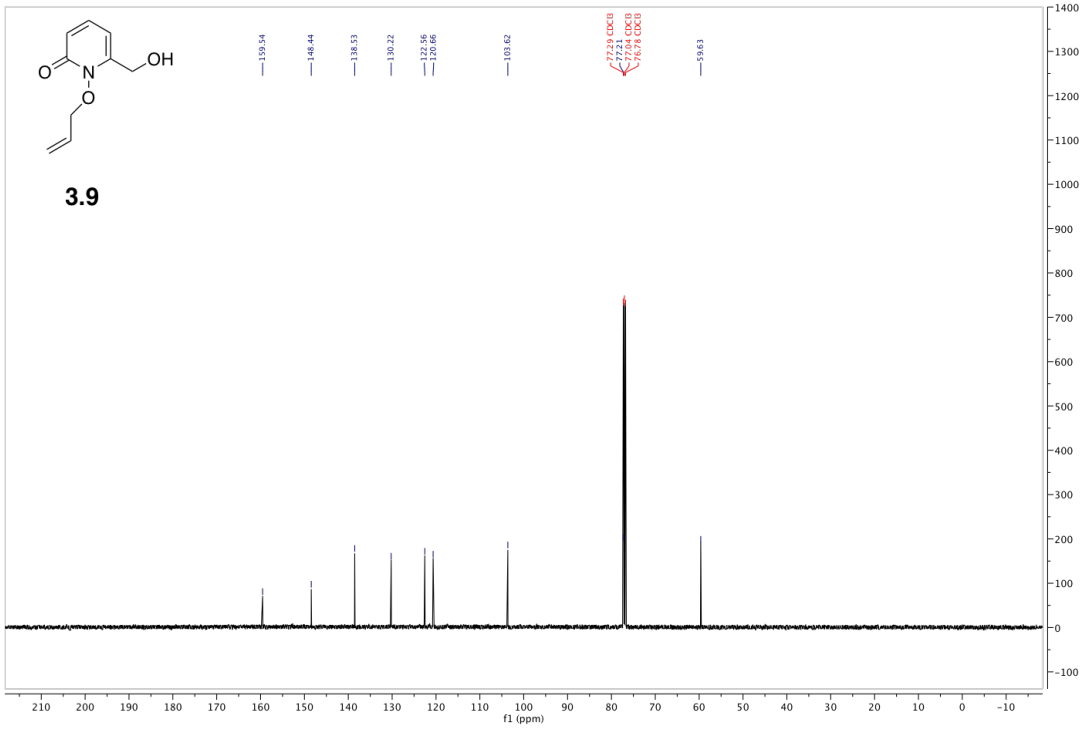

Figure A16: ^{13}C NMR (126 MHz, $CDCl_3$) of 1-(allyloxy)-6-(hydroxymethyl)pyridin-2(1H)-one (1,2-HOPO-allyl-hydroxide, 3.9)

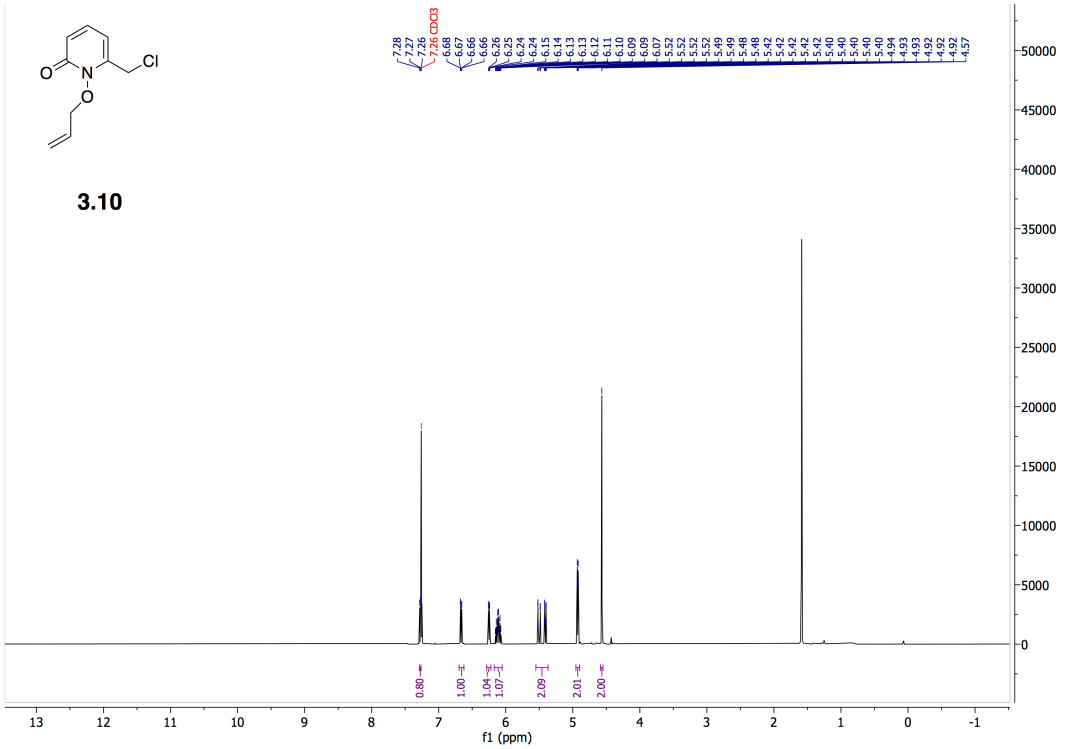

Figure A17: ^{1}H NMR (500 MHz, $CDCl_3$) of 1-(allyloxy)-6-(chloromethyl)pyridin-2(1H)-one (1,2-HOPO-allyl-chloride, 3.10)

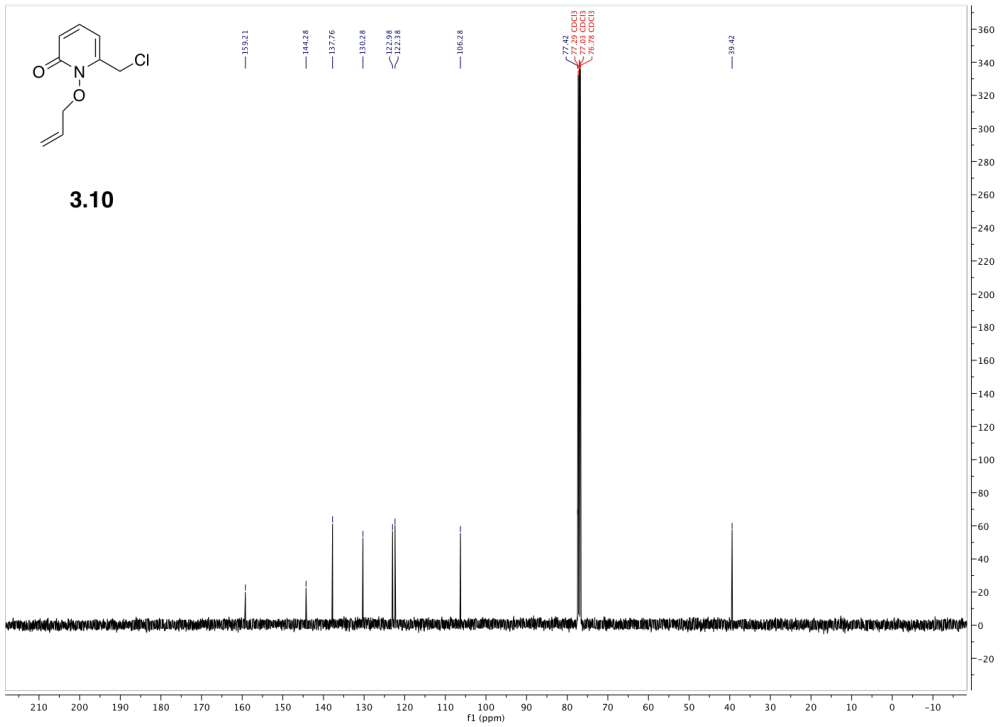

Figure A18: ^{13}C NMR (126 MHz, $CDCl_3$) of 1-(allyloxy)-6-(chloromethyl)pyridin-2(1H)-one (1,2-HOPO-allyl-chloride, 3.10)

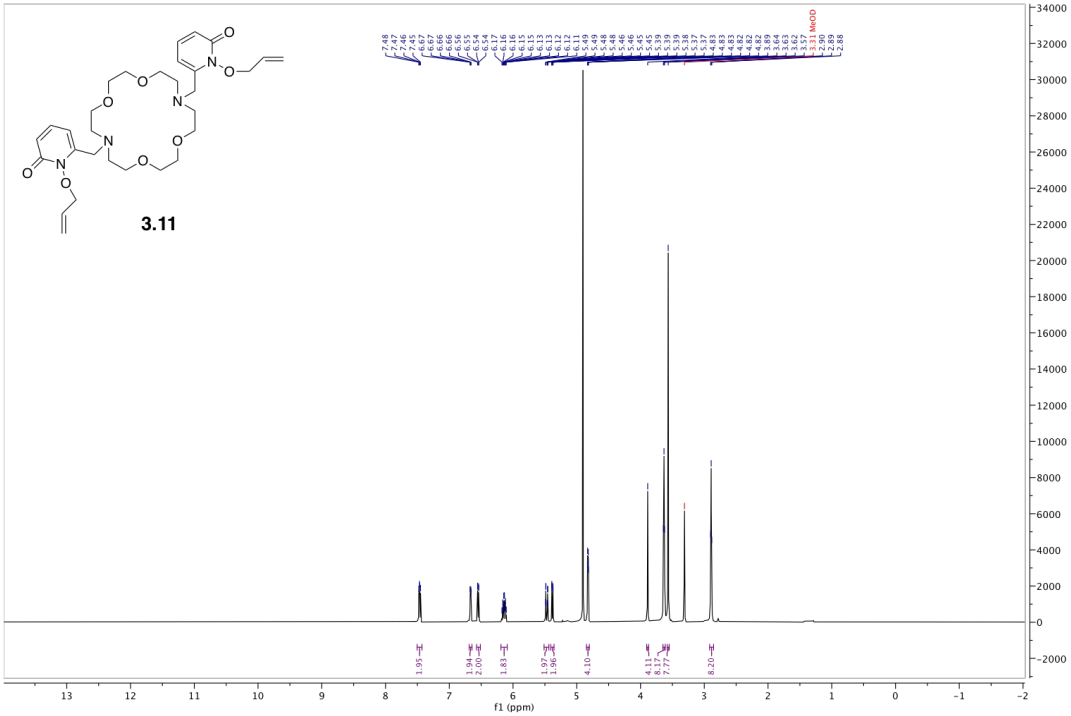

Figure A19: ^{1}H NMR (600 MHz, MeOD) of 6,6'-((1,4,10,13-tetraoxa-7,16-diazacyclooctadecane-7,16-diyl)bis(methylene))bis(1-(allyloxy)pyridin-2(1H)-one) (1,2-HOPO-allyl-crown, 3.11)

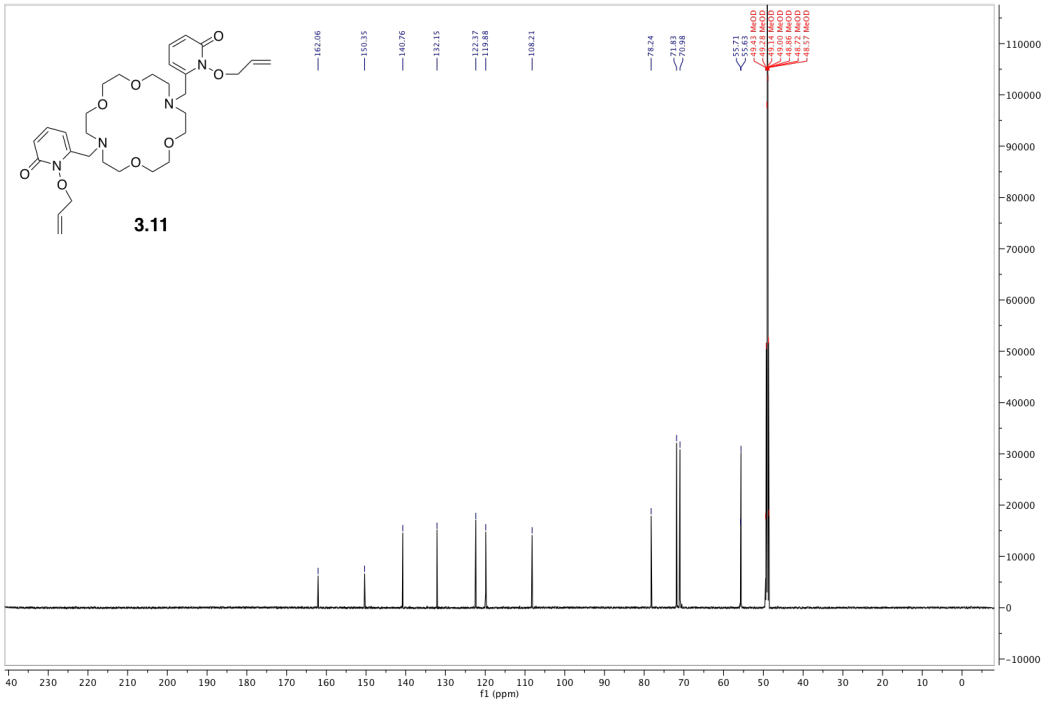

Figure A20: ^{13}C NMR (151 MHz, MeOD) of 6,6'-((1,4,10,13-tetraoxa-7,16-diazacyclooctadecane-7,16-diyl)bis(methylene))bis(1-(allyloxy)pyridin-2(1H)-one) (1,2-HOPO-allyl-crown, 3.11)

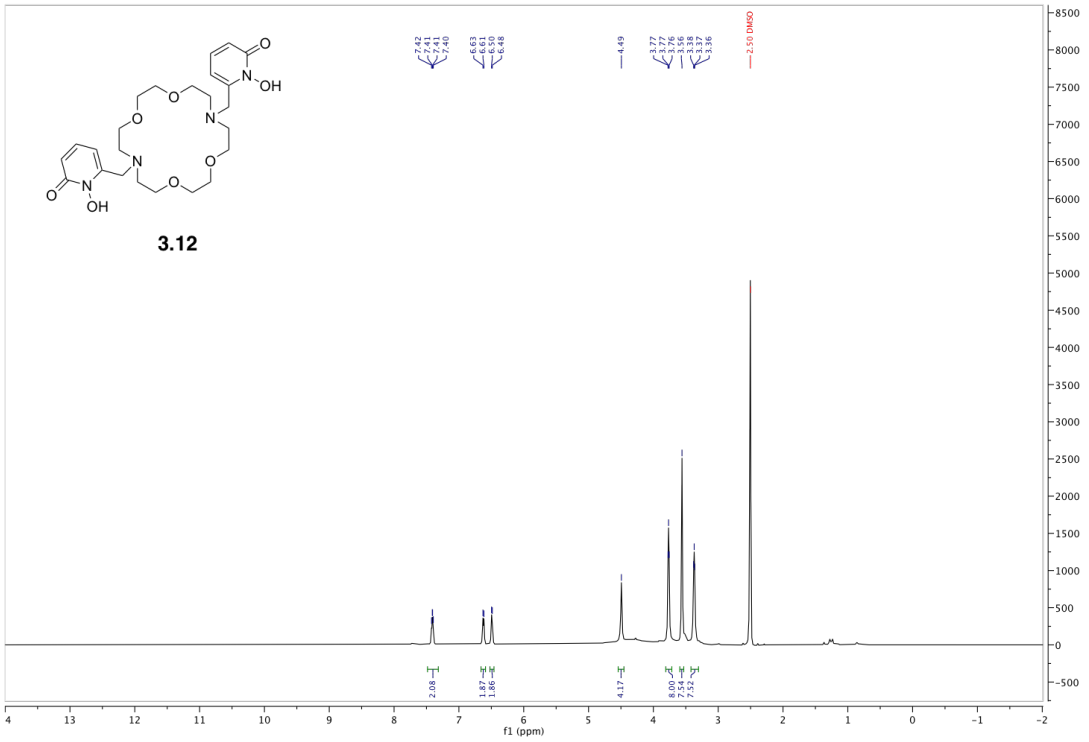

Figure A21: **^{1}H NMR (600 MHz, DMSO-d_6) of 6,6'-((1,4,10,13-tetraoxa-7,16-diazacyclooctadecane-7,16-diyl)bis(methylene))bis(1-hydroxypyridin-2(1H)-one) (macrohopo′, 3.12)**

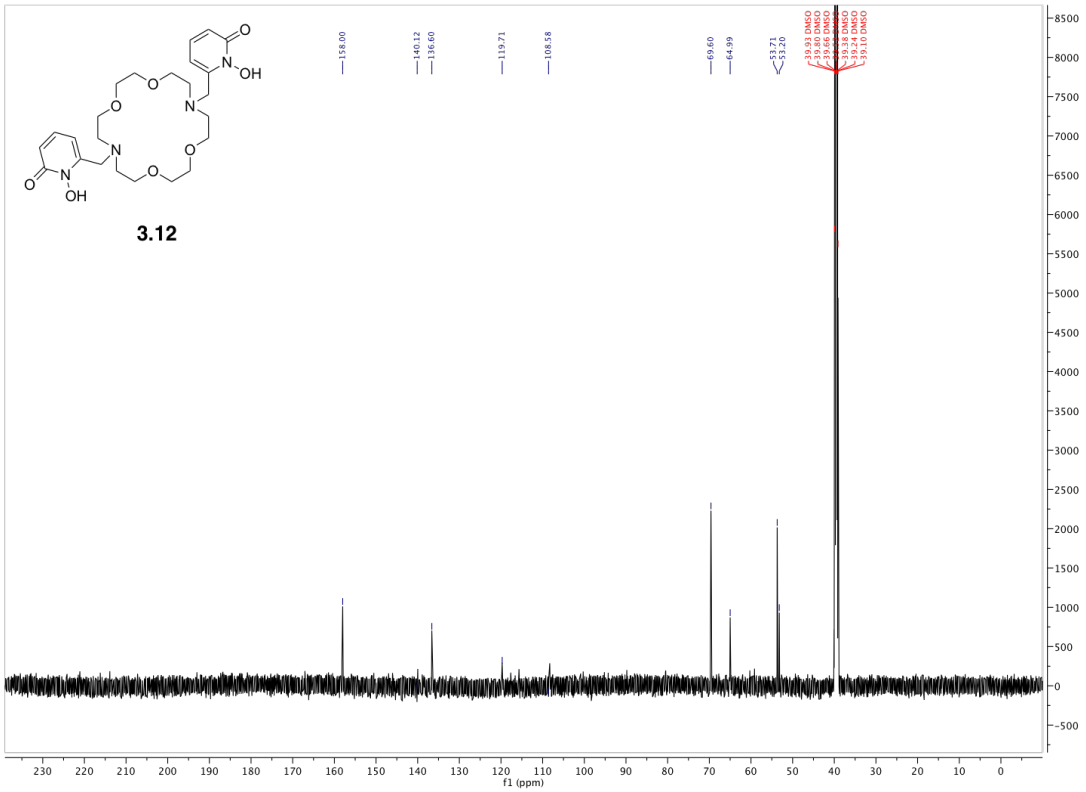

Figure A22: **^{13}C NMR (151 MHz, DMSO-d$_6$) of 6,6'-((1,4,10,13-tetraoxa-7,16-diazacyclooctadecane-7,16-diyl)bis(methylene))bis(1-hydroxypyridin-2(1H)-one) (macrohopo′, 3.12)**

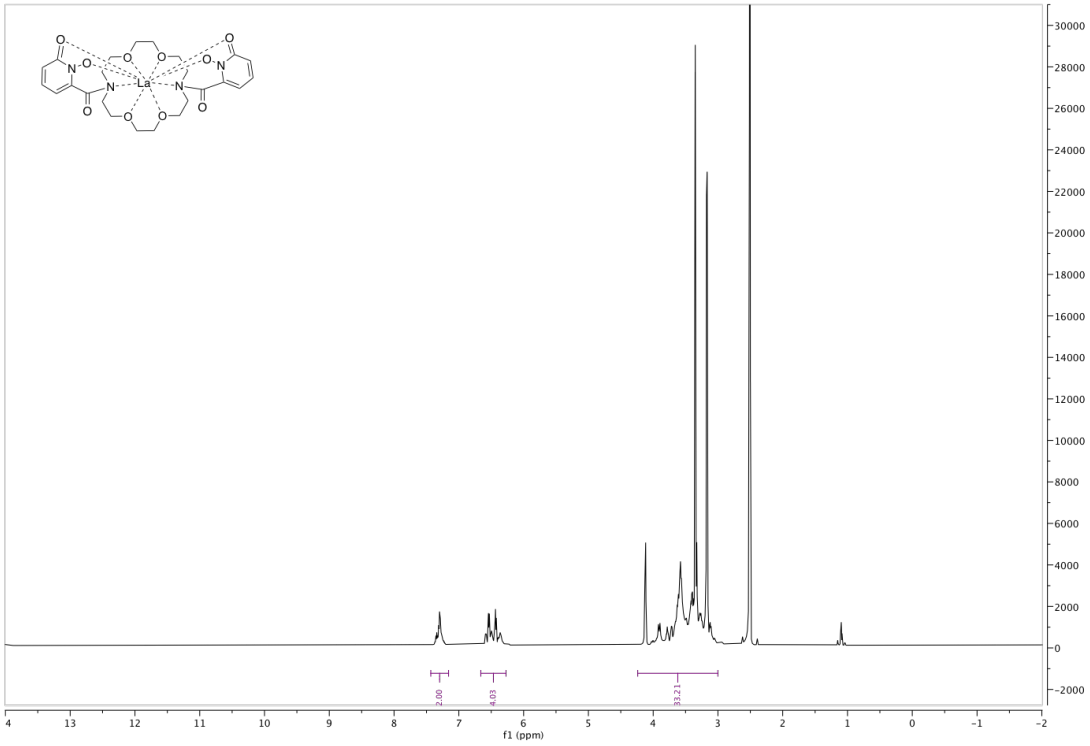

Figure A23: ^{1}H NMR (600 MHz, DMSO-d$_6$) of [La(macrohopo)][ClO$_4$]

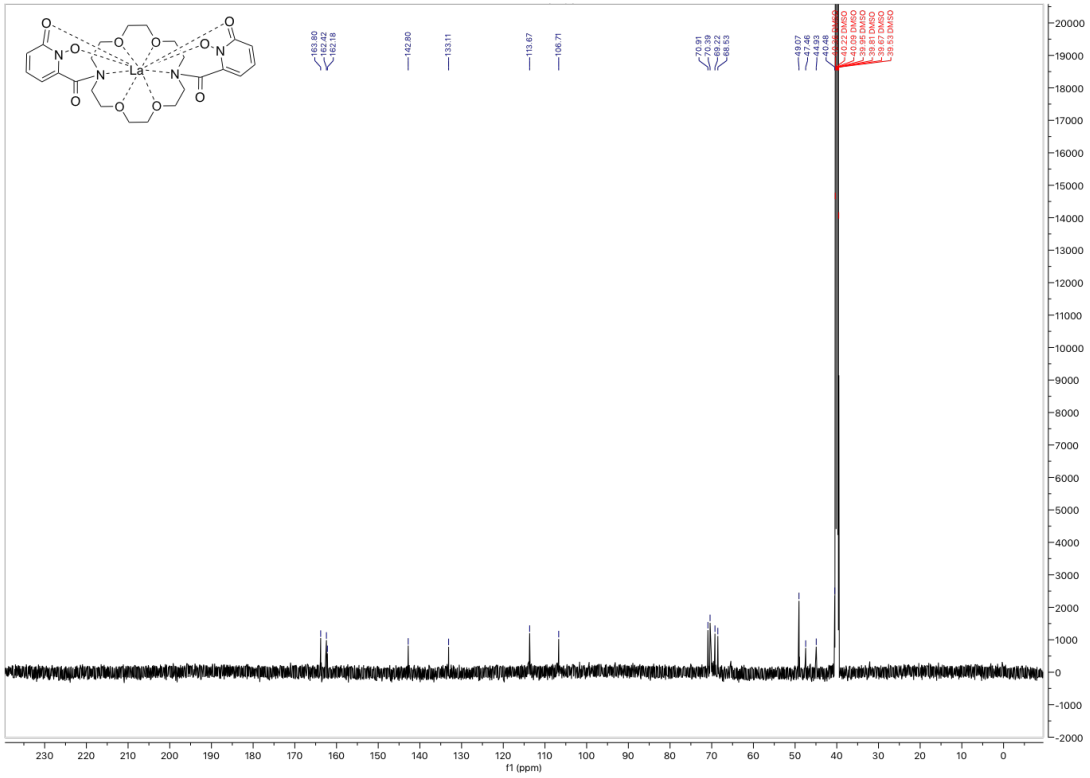

Figure A24: ^{13}C NMR (151 MHz, DMSO-d$_6$) of [La(macrohopo)][ClO$_4$]

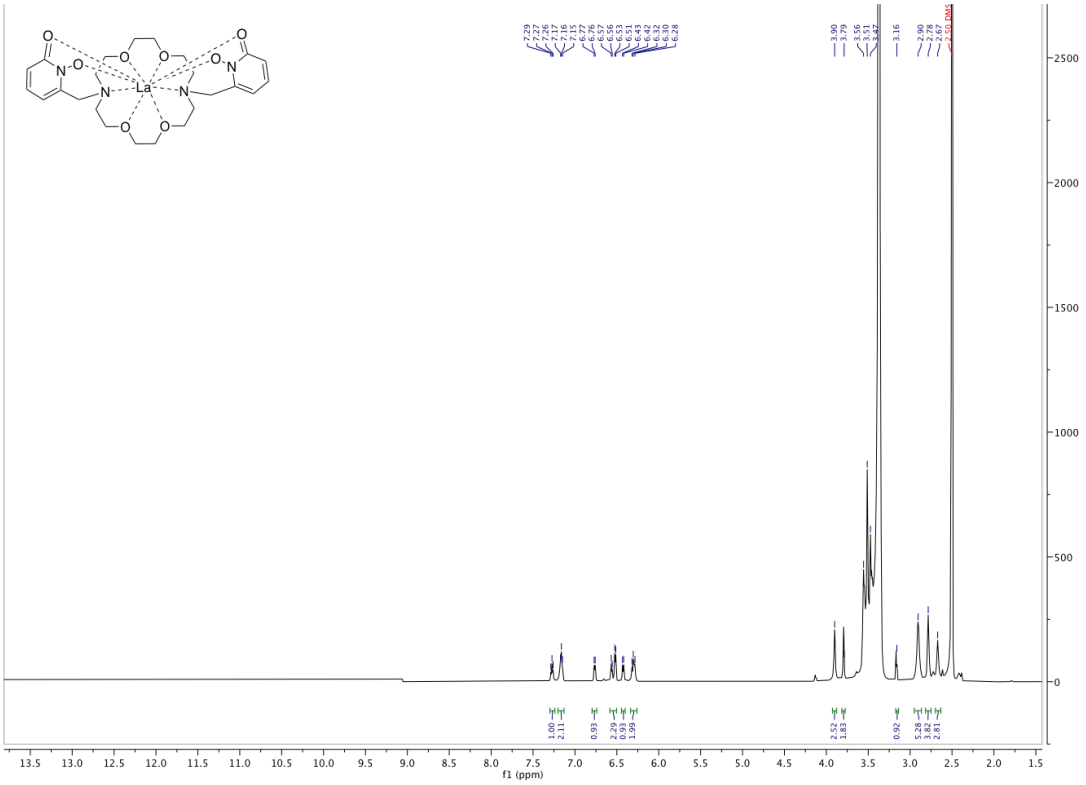

Figure A25: ^{1}H NMR (600 MHz, DMSO-d$_6$) of [La(macrohopo′)][ClO$_4$]

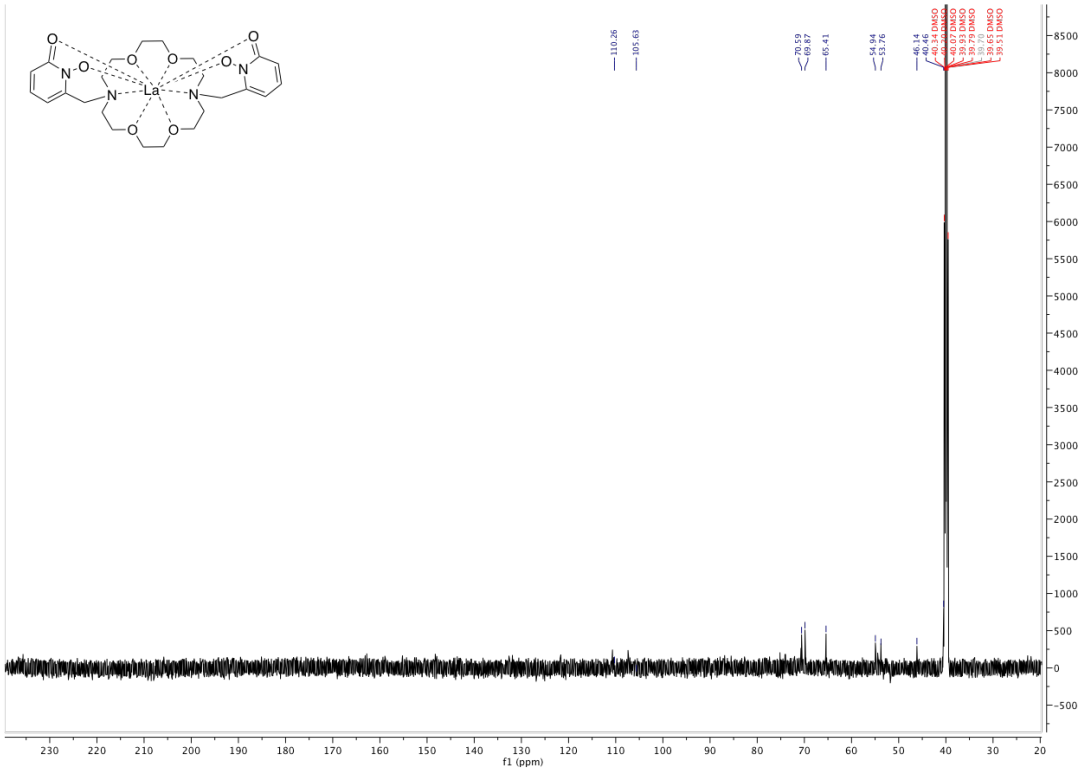

Figure A26: ^{13}C NMR (151 MHz, DMSO-d$_6$) of [La(macrohopo′)][ClO$_4$]

Additional NMR

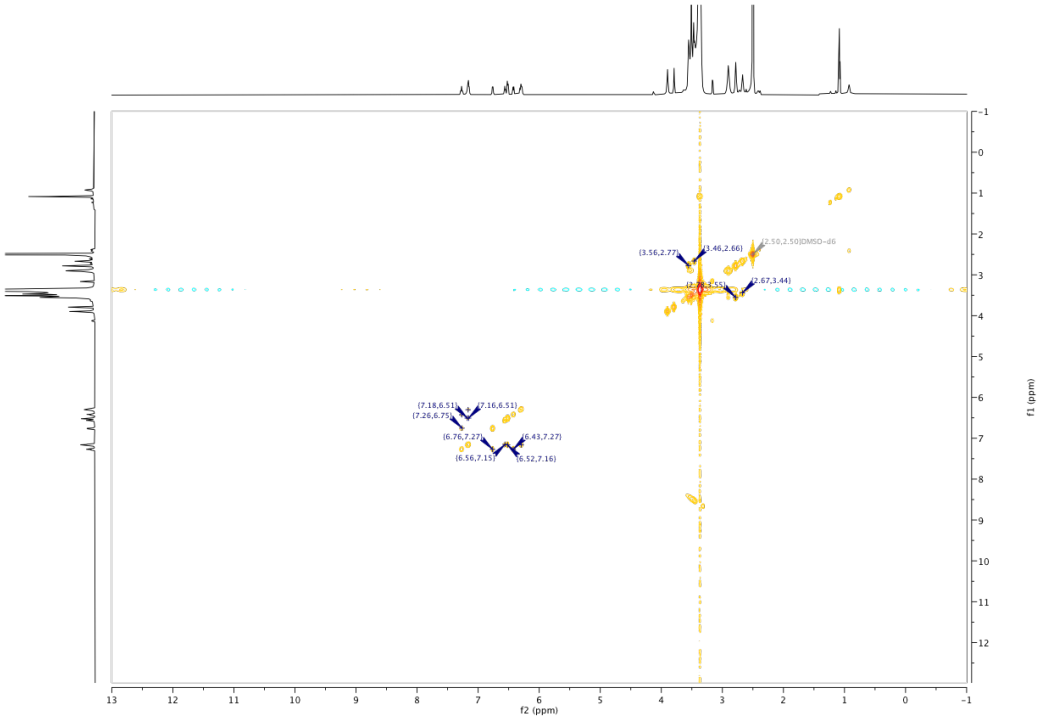

Figure A27: ^{1}H-^{1}H COSY NMR (600 MHz, DMSO-d_6) of [La(macrohopo′)][ClO_4]

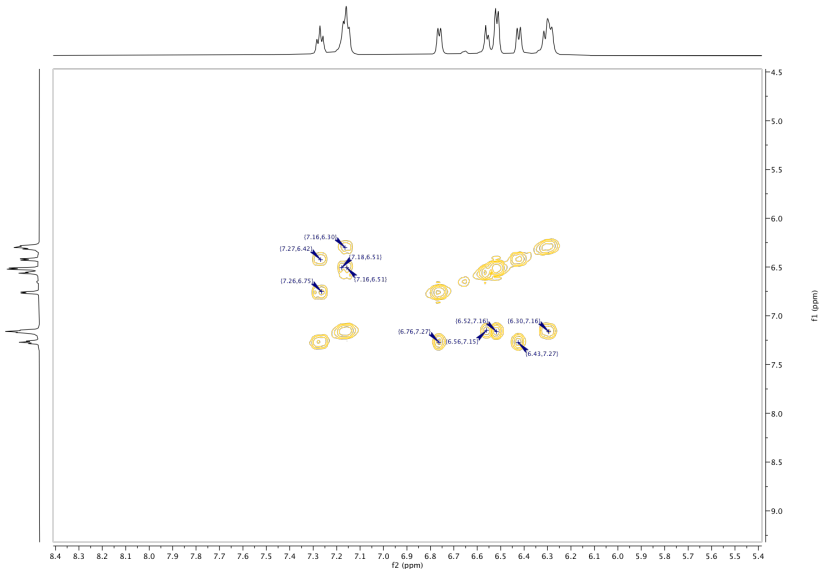

Figure A28: ^{1}H-^{1}H COSY NMR (600 MHz, DMSO-d_6) of [La(macrohopo′)][ClO_4] in pendant donor arm region

Variable Temperature NMR

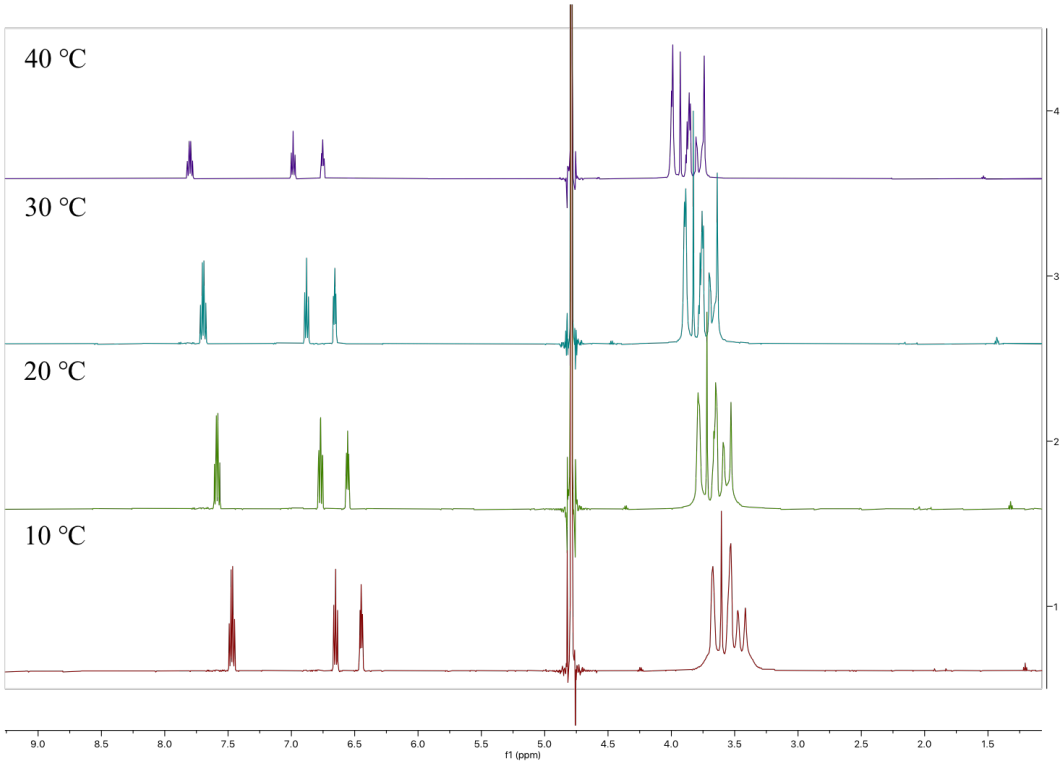

Figure A29: **^{1}H Varaible Temperature NMR (600 MHz, D_2O) of 6,6'-(1,4,10,13-tetraoxa-7,16-diazacyclooctadecane-7,16-dicarbonyl)bis(1-hydroxypyridin-2(1H)-one) (macrohopo, 3.6)**

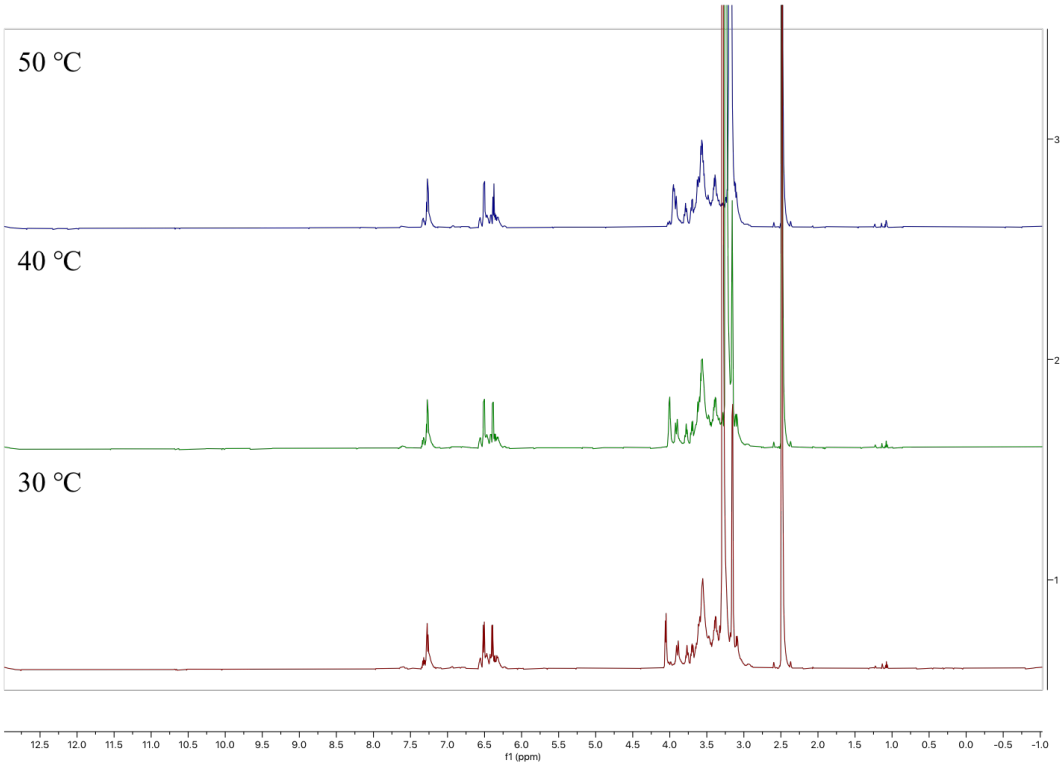

Figure A30: ^{1}H Varaible Temperature NMR (600 MHz, D_2O) of [La(macrohopo)][ClO_4]

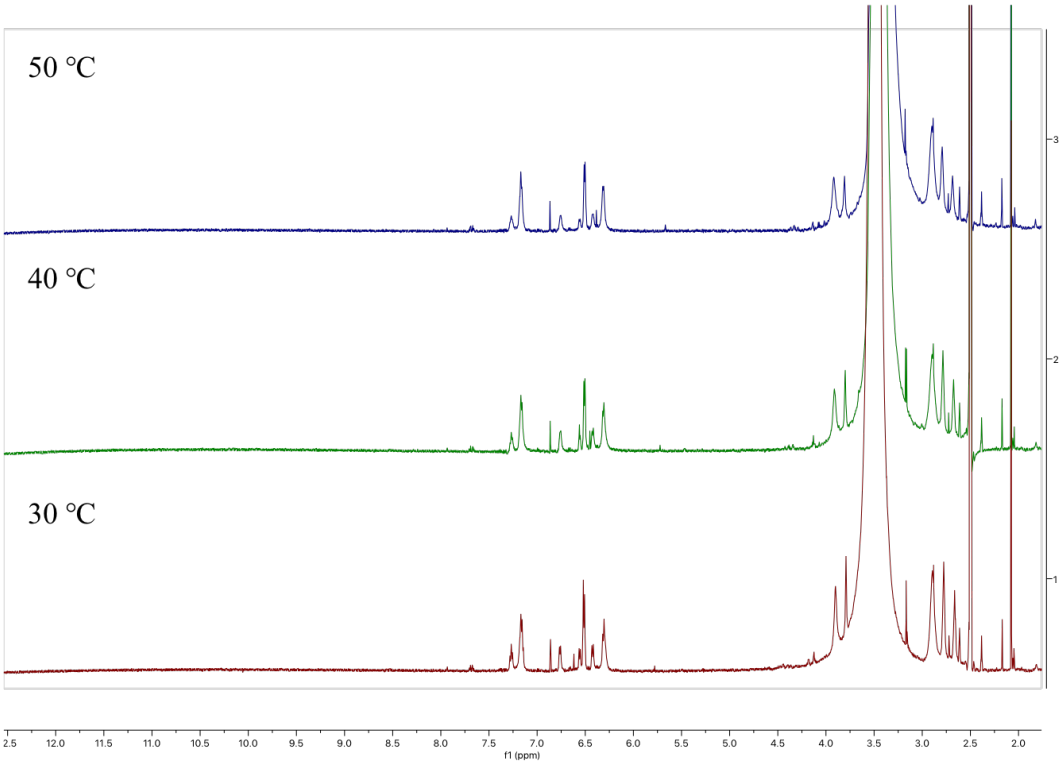

Figure A31: ^{1}H Varaible Temperature NMR (600 MHz, D_2O) of [La(macrohopo′)][ClO_4]

Protonation Constants

Table A1: Protonation Constants of macropa, macropaquin and macroquin-SO_3 determined by pH potentiometry

	Macropa	Macropaquin	Macroquin-SO_3
Log Ka_1	7.41	10.33	9.34
Log Ka_2	6.89	7.15	9.43
Log Ka_3	3.32	6.97	6.75
Log Ka_4	2.36	3.24	6.62
Log Ka_5	1.69		

All data was obtained from Thiele *et al.*,[80]

iTLC

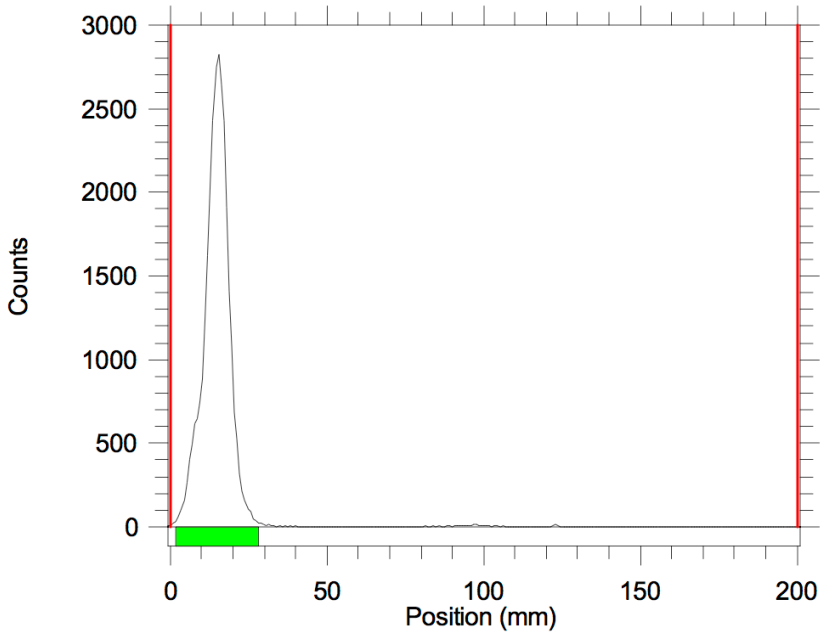

Figure A32: Represent the positive control iTLC radio-chromatogram for ^{225}Ac radiolabeling

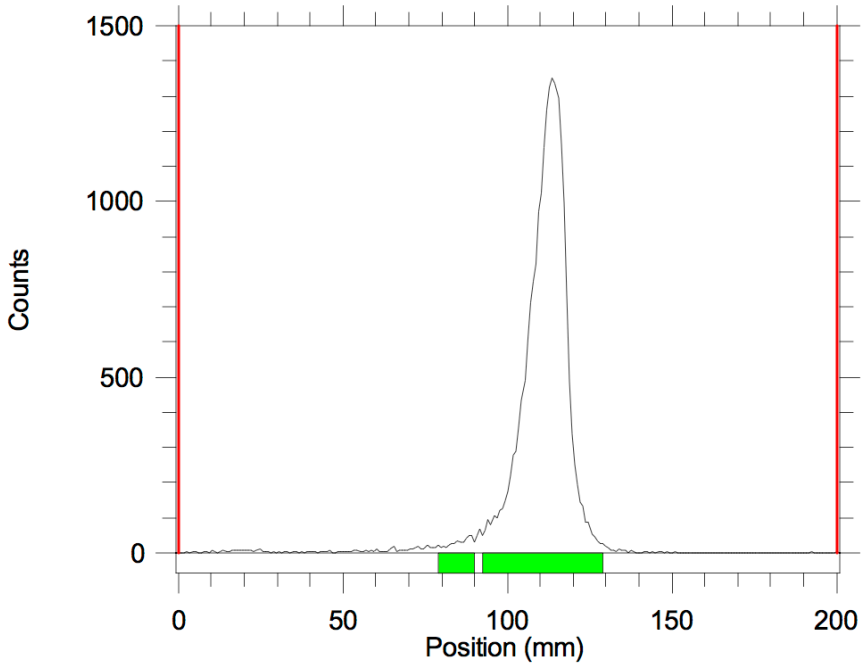

Figure A33: Represent the negative control iTLC radio-chromatogram for ^{225}Ac radiolabeling

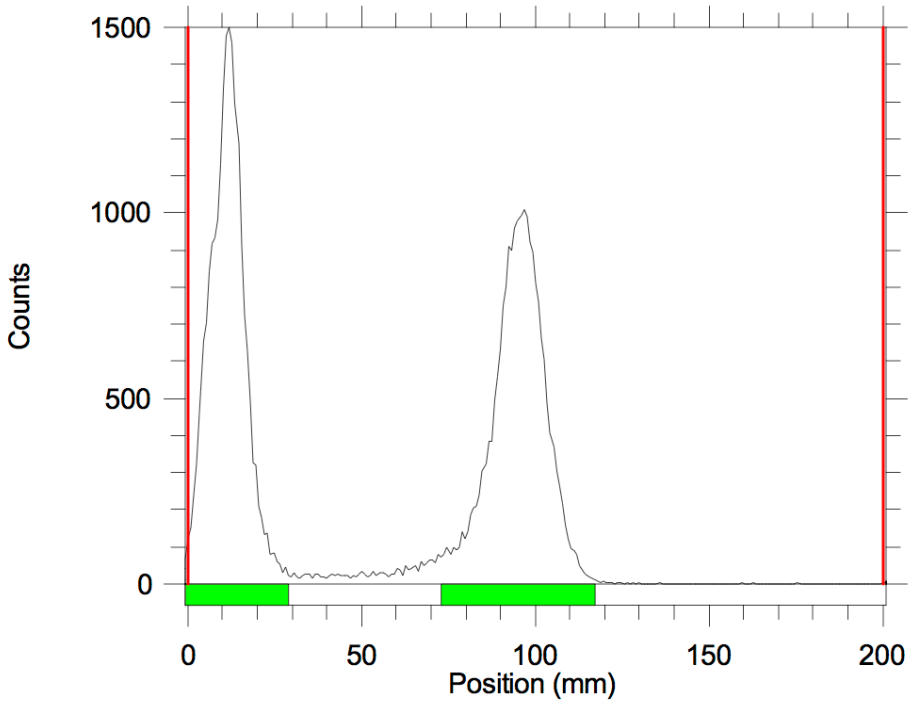

Figure A34: Represent a chelator with ~ 50% RCY iTLC radio-chromatogram for ^{225}Ac radiolabeling